Alma Mater Studiorum – Università di Bologna

DOTTORATO DI RICERCA IN

Chimica

Ciclo XXXIII

Settore Concorsuale: SC03/B1

Settore Scientifico Disciplinare: CHIM/03

USING LIGHT TO STUDY AND OPERATE SUPRAMOLECULAR SYSTEMS AND MOTORS

Presentata da: Martina Canton

Coordinatore Dottorato **Supervisore**

Domenica Tonelli **Alberto Credi**

Esame finale anno 2021

Table of contents

ABSTRACT

The topics presented in this thesis regard the developing of supramolecular assemblies and motors operated and characterized using optical techniques. The thesis work is organized in chapters each one corresponding to a different experimental project.

- In **Chapter 1** an introduction and significant examples from literature concerning the topics described in the following chapters are included. More specifically, the chapter starts with the "bottom up" approach towards supramolecular chemistry with specific referments to largely employed host-guests structures such as crown ethers and their properties. Successively, examples of molecular cages and containers are illustrated and the possible advantages of reactivity under confinement are described. Finally, the topic of molecular machines is discussed. Natural and artificial molecular machines are compared including the main adopted strategies regarding the energy sources and the regulation of the motion. As such, important ratchet mechanisms are introduced. Finally, interesting applications and materials based on molecular machines are described.

- In **Chapter 2** a light-activated molecular pump is illustrated. In the first part of the chapter the description of the properties and the operation of this motor is reported. Secondly, different optimization approaches are introduced, among them the substitution of the pseudostopper unit have been investigated. With this aim, a library of symmetric dibenzylammonium type axles was synthetized as guests for the DB24C8 ring and studied by means of UV-vis and NMR spectroscopy obtaining a precise evaluation of threading/dethreading processes. Furthermore, with the significant contribution of computational studies, two categories have been individuated within the group of studied axles one characterized by the effective formation of the complex and a second one in which the threading of the ring was not observed. From these guests a suitable pseudostopper unit was selected in order to be implemented in a second generation molecular pump.
  A new axle (13) was thus synthetized and characterized together with DN24C8 as a novel molecular motor. Having calculated all the necessary thermodynamic and kinetic parameters, the repeated cycling operation under continuous irradiation was examined by means of a dedicated NMR set-up. The behavior of the pump was distinguished into simple thermal relaxation, in dark conditions, and in an out of equilibrium dissipative regime under continuous luminous input.
  Finally, further undergoing projects involving the molecular pump unit such as the "molecular reservoir" are introduced.

- In **Chapter 3** a novel rotaxane (15) is described. Interestingly, this assembly presents both a point chiral element, due to the presence of an oxazoline moiety, and a mechanical one, intrinsic effect of the mechanical bond. Furthermore, the aim of this project is to exploit this structure as a switchable and possibly asymmetric catalyst, by using a pH-driven and a coordination-driven approach. For these reasons, UV-vis and CD spectroscopic titrations with a base and subsequently with

a metal ion are reported. This project is still ongoing, the specific coordination sites will be determined by means of NMR experiments, furthermore, alternative optimized molecular designs are being developed with the collaborators.

- In **Chapter 4** the encapsulation of the photochromic DHP unit within a coordination molecular cage is reported. The employed cage (16) presents four aromatic panels held together by six Pd^{2+} ions. This cage is fully soluble in water and is endowed with two large open "windows" which allow the entrance of suitable guests.
  Initially, the formation and characterization of the complex are reported. The cage, dissolved in water, was found to efficiently solubilize the guest by forming a 1:1 complex both with DHP and with its open form CPD. The stoichiometry and the arrangement of the guest within the cage cavity have been investigated by means of UV-vis and NMR spectroscopy. Moreover, the X-ray structure of the DHP complex have been reported and compared with the behavior of the assembly in solution. At this point to learn further about the binding strength of the complex, guests exchange experiments have been conducted with the MC (merocyanine) competitive guest by monitoring absorption and emission spectra. MC was selected among the already studied guests, as it presented similar structural features with the respect to DHP and, significantly, because its association constant with 16 was known. These experiments revealed a comparable equilibrium constant for the two species.
  Finally, as the hypothesized photoswitching mechanism of DHP includes a radical intermediate, the role of the cage in protecting and stabilizing the guest switching was investigated. The data showed a significant difference in the fatigue experienced by the encapsulated guest with the respect to the free DHP dissolved in organic solvents. Therefore, the improving contribution of the encapsulation was successfully proven. Future perspective includes the introduction of the same approach for other photochromic species or low yielding reactions.

1 INTRODUCTION

1.1 Nanotechnology, towards the bottom-up approach

Nanotechnology in our daily life is everywhere, is enough to think to our smartphones but also to our laptops and so on. These devices are projected end engineered by means of micrometrics components and during last decades we have seen the progressive miniaturization of them. This field historically, is based on a top-down production strategy this means that the starting materials are manipulated as a sculptor would do with a raw block of stone to obtain a detailed and refined statue.
Lithography is the most employed top-down production technique. In this process, required material is protected by a mask and the exposed material is etched away. It is possible to obtain different levels of resolution in the final product, depending on the etching technique and on the base material. This procedure can be done mechanically, using ultraviolet light, x-rays or electron beams but also chemically using acids. Moreover, this is the process applied in the fabrication of computer chips.
A completely new approach was proposed by the physic Richard Feynman during a famous lesson that he gave at the Caltech university in 1959 titled "There is plenty of room at the bottom"[1]. In a context where computers used to occupy whole rooms and nanotechnology was far to come, Feynman, with notable foresight asked to students and scientists to capsize their point of view and to start thinking about the idea of a "bottom-up" approach. Among his ideas, he talked about the possibility to write all the 24 volumes of Encyclopedia Britannica on the head of a pin and to have smaller and more powerful computers with atomic diameter wires or to build electronic microscopes with 100 times higher resolution. Moreover, he emphasized the absence of limitations from the laws of physics and he often referred to the ability of nature in creating complex systems able to write and store an incredible amount of information in a restricted space such as a cell.
His aim was to encourage the development of new devices and technologies not from bulk materials but starting from atoms, in other words, from "the bottom".
These concepts were actually not too far from being practically realized, in fact, in 1981 the scanning tunneling microscope was presented as well as, few years later in 1986, the atomic force microscope; both of these achievements were recognized by the Nobel prize in physic.

1.2 Supramolecular chemistry

Differently from Feynman mainly physic point of view, the developing of devices by means of an "atom-by-atom" bottom-up approach resulted not fully convincing from a chemical perspective[2]. In fact, the manipulation of such reactive and hard to handle species as atoms is indeed not trivial; molecules instead are much more stable as building blocks showing distinct shapes and properties. Some years later, in the 1970's, this idea gave rise to a completely new field, the field of supramolecular chemistry.
The definition of this branch was given by the Nobel laureate John Marie Lehn as the construction of highly complex, functional chemical systems from components held together by non-covalent intermolecular forces[3].

A fundamental concept for this approach is molecular self-recognition, this process is possible with the presence of a molecular receptor which requires selective binding features towards a molecular substrate through non covalent interactions. Several types of architectures have been designed exploiting different interaction pathways such as the combination of donor and acceptor groups, hydrogen bonding and metal ion coordination. Using these strategies, is possible to design the self-organization or, in better words, the self-assembly of molecular constituents leading to complex and organized supramolecular architectures.
Functionality is another key word, indeed, all the chosen components in the building process play a specific role and carry molecular information which is usually very far from the simple sum of the properties of the single constituents.
Contrarily from covalent bonds, which are usually fixed, static and require high amounts of energy to be broken; non-covalent interactions are labile and dynamic. Furthermore, dynamic, intended in traditional molecular chemistry, is mainly attributed to motional dynamics such as reorientations and reactional dynamics. Nevertheless, moving to supramolecular chemistry these concepts can be translated in the so called "constitutional dynamics". In other words, this feature provides the opportunity to supramolecular systems to assemble and dissemble upon proper external inputs in order to adapt and respond to different conditions.
Much inspiration comes from nature where many examples of organized biological molecular architectures are present. Among them, one of the most fascinating systems is certainly represented by DNA (deoxyribonucleic acid). Nature, with perfect engineering, has been able over long evolution periods to tailor such a complex structure which embodies all the features of a supramolecule explained before.
Week interactions, as hydrogen bonds, allow the connection and the self-assembling of the two strands of nucleotides forming the tree dimensional double helical structure (Figure 1) [4]. Hydrogen bonds confer to the whole structure a high dynamicity, the double helical system, in fact, is able to easily disassemble upon breaking these labile connections and to open the two nucleotide strands in order to be employed as replication templates upon suitable inputs. The order of the nucleotides sequence, in fact, constitutes the genetic information which is translated, by means of the genetic code, during the transcription process.

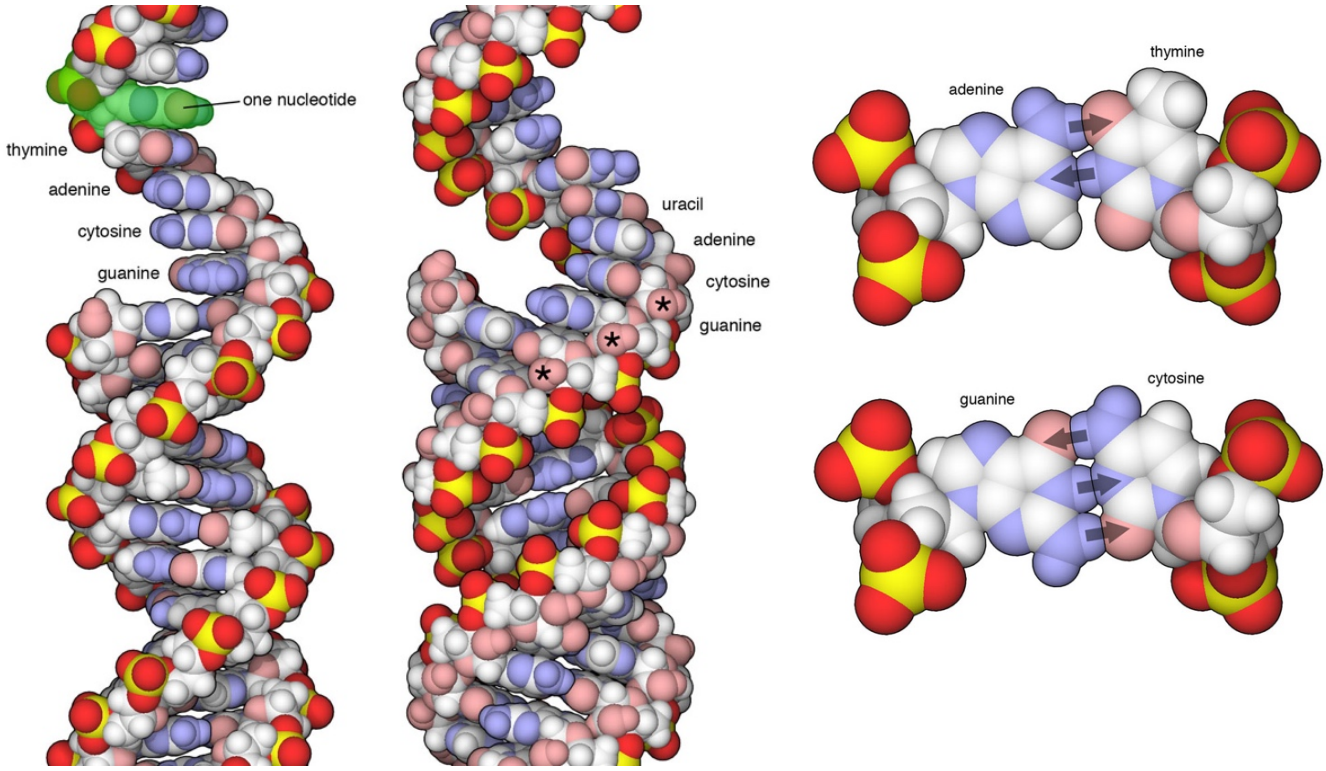

Figure 1 DNA double helical structure (left), bonds between couples of nucleotides (right). Adapted with permission[4].

The bottom-up developing of such complex and organized systems as the biological ones is indeed an extremely challenging task. Nevertheless, supramolecular chemistry is making remarkable progresses even by employing much simpler molecular constituents.
Concluding, the connection with the world of nanoscience and nanotechnology is evident by thinking for example about the possibility to create supramolecular polymers, liquid crystals or solid-state assembly, in other words, to design functional supramolecular materials.

1.3 Host-Guest systems

A typical example of supramolecule is represented by the host-guest complexes. Such assemblies are composed by two elements, a host which usually is a larger molecule or aggregate, characterized by the presence of a cavity or a hole which is endowed with one or multiple binding sites that allow non-covalent interactions with the guest. More specifically, the sites located on the guest, are defined by the Nobel laureate Donald Cram as convergent contrarily, the ones located on the host are called divergent[5]. The interaction between the molecular units can belong to various typologies such as hydrogen bonding, ion-ion or ion-dipole interactions, Van der Waals and so on.
The design of the host needs to be tailored on the target guest to obtain a selective recognition between the units. For instance, considering a metal ion guest, parameters such as size, shape and charge density are fundamental. Furthermore, binding sites should

be disposed far enough to minimize repulsions between each other but at the same time they need to be oriented as they can all interact simultaneously with the guest.
Depending on the desired level of stability of the complex, one can also modulate the binding strength over a large range. If an irreversible process is needed the binding should be projected not to have any unfavorable rearrangement or orientation that can decrease the total amount of free energy relative to the binding; in this case the host act as a "sink" and is perfect, for instance, in applications such as the removing of toxic metal ions from polluted air or water. On the contrary, for different purposes, a reversible binding is required. In this case, a relatively low association constant is necessary to allow the disassembling of the complex. This kind of features are useful for creating sensors or carrier which are projected to detect or transport a specific host and subsequently to release it.

1.3.1 Crown ethers and other macrocyclic hosts

Crown ethers are one of the most largely studied family of host-type molecules, they are derived from ethylene glycol and they are constituted by the unit -OCH_2CH_2 which is present as structural fundamental unit and repeated to form a closed ring.
They were presented for the first time by the Nobel laureate Charles J. Pedersen in 1967 who synthetized the dibenzo-18-crown-6 as a byproduct. However, he foresaw the possibility of innovative and useful applications and he decided to further characterize different type of crown ethers observing that they were able to solubilize alkaline metals salts in nonpolar organic solvents[6]. Such macrocycles, indeed, are characterized by a double nature, the external region is mainly nonpolar, allowing the solubility in organic solvents, on the contrary, the internal cavity provides a polar environment due to high electronic density derived from the oxygen atoms.
Because of these features, initially, such macrocycles have been employed as receptors for metal ions such as Li^+, K^+ or Na^+. The stability of the binding depends mainly on the match between the size of the cavity and the radius of the metal ion. For instance, Li^+ binds favorably with 12-Crown-4, while 18-crown-6 prefers K^+. (Figure 2)

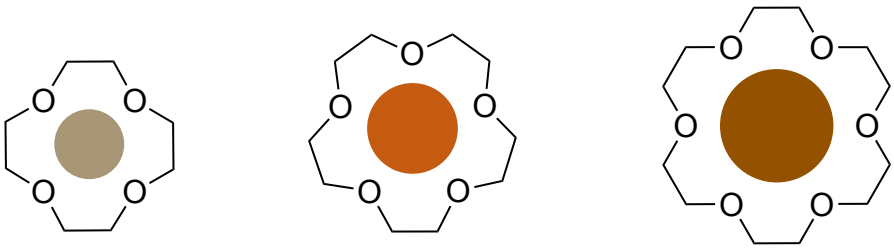

Figure 2 Representation of host-guest complexes involving crown ethers and metal ions as guests.

Heteroatoms in the macrocycles can also be substituted by halogenation or nitration reactions in order to obtain different features[7]. Moreover, they can be easily decomposed upon splitting of the ethers.
These macrocycles are often functionalized by connecting aromatic groups such as benzylic units but also larger units as naphthalene or anthracene. Furthermore, as crown

ethers are mostly colorless, another common strategy is the functionalization of the ring with a chromophore or a fluorophore unit. In this way, for example, a luminescent unit can be exploited to detect targets even at very low concentrations. In the field of electroanalytical chemistry, in fact, crown ethers are employed as sensing materials in the construction of potentiometric ion selective electrodes and many examples of sensors for cations and anions based on Schiff's bases and crown ethers have been developed[8].
Similarly, a liquid-liquid extraction can be achieved by using crown ethers because of their selective binding with metal ions. This procedure is convenient and flexible, moreover it can be applied in different solvents by modifying the structure of the macrocycle to render it water soluble. In fact, water-soluble crown ethers show effective masking effects for an increasing separation factor in the extraction of rare earth metal ions[9].
Concluding, crown ethers are employed in other supramolecular chemistry fields as well, one of the most important is molecular machines which will be discuss in chapter xx.
Cyclodextrins represent another well-known class of molecular hosts. These compounds are constituted of cyclic glucose oligomers linked by 1,4 glycosidic bonds. Depending on the number of glucose units, cyclodextrins can be distinguished in: α-cyclodextrins (6 units), β-cyclodextrins (7 units) and γ-cyclodextrins (8 units) (Figure 3)[10].

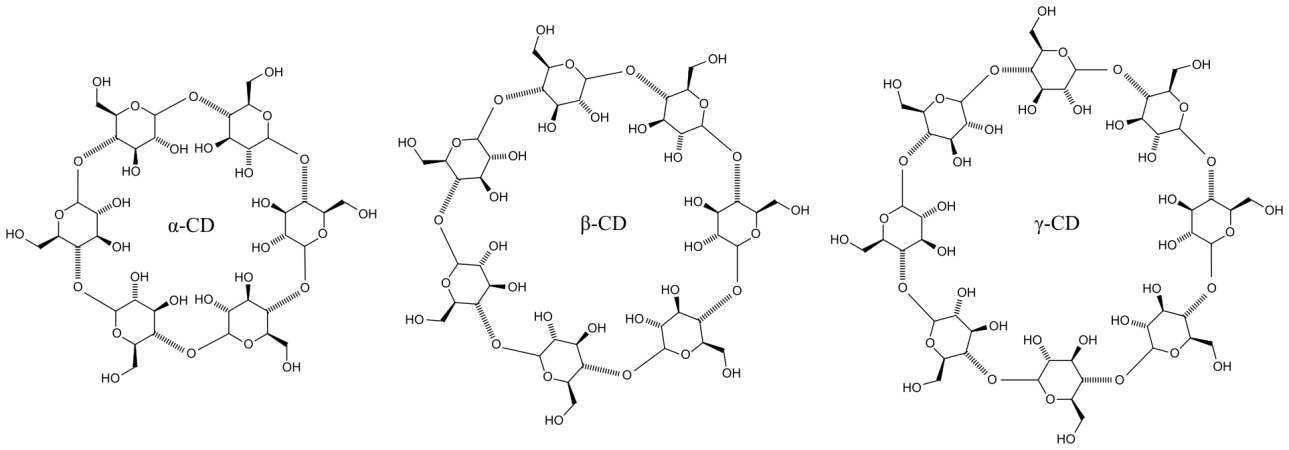

Figure 3 Structures of the 3 main cyclodextrins typologies.

These compounds are characterized by a toroidal 3D shape endowed of a larger and a smaller diameter opening which expose secondary and primary hydroxyl groups respectively. This configuration confers to the internal cavity a hydrophobic nature while the external hydroxyl units render the host soluble in polar solvents. Furthermore, other interesting features are their good stability over different conditions, and their simple preparation which is achieved by means of enzymatic treatment of starch that also render them cheap and biocompatible compounds. Among the common applications there are: drug delivery[11,12], liquid chromatography[13], preparation of polymers[14] and hydrogels[15].
Other important and commonly employed macrocyclic hosts are cucurbiturils[16,17,18] and calixarenes[19,20,21].

1.4 Molecular cages and containers

In the family of host-guest systems, another common assembly is represented by the so called molecular cages or molecular containers. This kind of hosts are able to encapsulate smaller molecules and act on the reactivity and features of the guests within their confined space. Many functional hosts with various dimensions and structure have been synthetized by exploiting the direct and modular strategy of self-assembly[22,23]. One of the most diffused structures are the octahedral coordination cages, presented by the group of Fujita in the early 90s. Such cages, are constitutes by ten molecules, four organic ligands held together by six metal ions[24]. This structure is based on the presence of coordination bonds; this type of bond is more robust with the respect to non-covalent interactions but still more flexible. Thanks to these features, the construction of different structures depending on the metal coordination geometry is possible. In particular, Fujita research group has exploited the 90° cis geometry relative to the square-planar Pd (II) or Pt (II). In this case the ligand is a rigid triangular 1,3,5-tris(4-pyridyl)triazine coordinated to Pd (II) ions endcapped with an ethylenediamine unit. The procedure introduced by Fujita is quite straightforward as it implies just the mixing in water of the two components in a ratio of 4:6 to obtain a self-assembled single component, in a quantitative yield. The final structure presents six Pd (II) ions placed at the vertexes of the octahedron and four triazine panels disposed in an alternate fashion on the faces of the octahedron. This arrangement provides a very large, hydrophobic cavity (Figure 4).

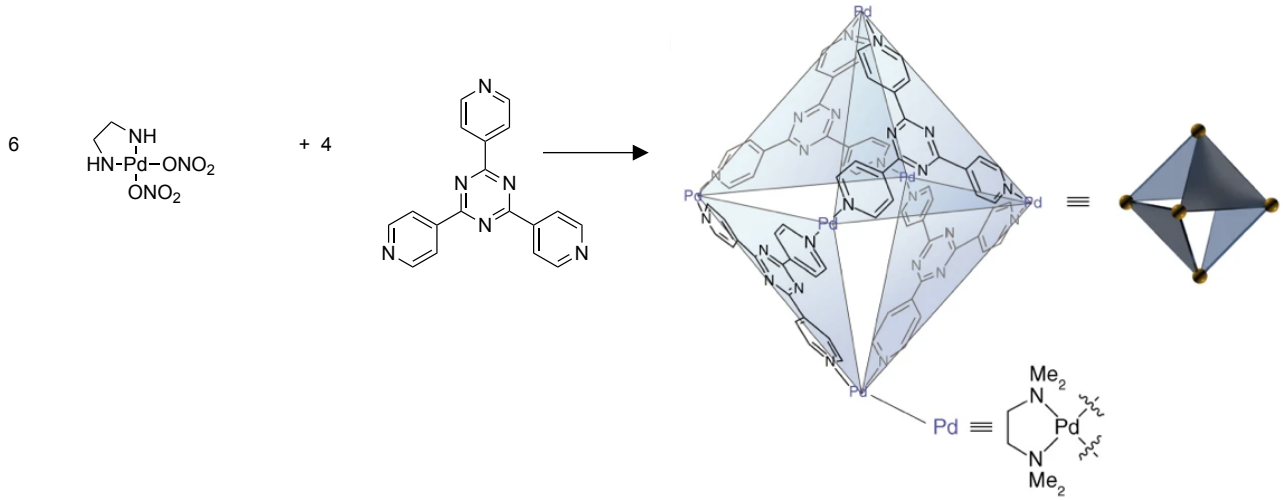

Figure 4 Scheme of the self-assembly of Fujita cage in water. Adapted with permission[25].

The presence of nitrate counterions confers to the cage high water solubility as well as an overall charge of 12^+ .The cage usually encapsulates favorably organic molecules as alkanes and planar aromatic molecules[26]. Furthermore, the Pd(II) ions are replaceable with other metal ions for instance with Pt(II) which form a more robust and rigid analogue of the previous cage; this host exhibits greater tolerance for acidic and basic conditions[27].
Hydrogen bonds are also extensively employed in the assembly of molecular containers, in this regards, a structure called "softball" capsule was presented by the group of Rebek[28].

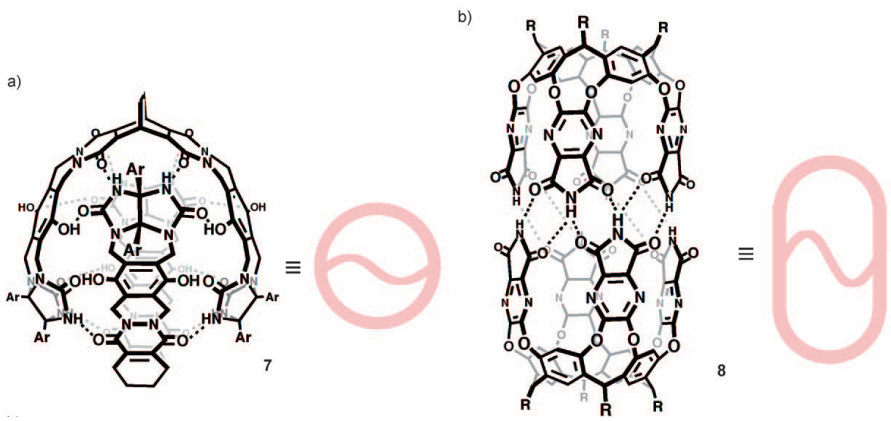

Figure 5 a) The hydrogen-bonding "softball" capsule 7 and b) cylindrical capsule 8 of Rebek and co-workers. Adapted with permission[29].

The image above represents the "softball" capsule (Ar=phenyl) and its derivative structure which is composed of two C-shaped parts, consisting of two glycoluril units associated by a linker (Figure 5a). Complementary hydrogen bonds, disposed along the circumference, allow the two molecular halves to form a stable container in the presence of smaller molecular guests. Capsule 7, for instance, shows a large cavity (ca. 400 A^3) which can possibly accommodate molecules such as adamantane or ferrocene carboxylic acid.
In addition, Rebek and collaborators developed as well the non-covalent calix[4]resorcinarene by linking aromatic units decorated with hydrogen bond donors and acceptors (Figure 5b)[30]. These features confer to the molecular container a cylindrical shape which is able to encapsulate two different guests at the same time.
Other types of interesting molecular flasks are: cryptands[31], molecular boxes[32], pillararenes[33], cavitands[34] and hemicarcerands, which consist in organic structure without the presence of metals, based on covalent bonds.

1.4.1 Reactivity under confinement

The previously described nano-containers are often called "molecular flasks" as they are able to modify and act on the reactivity of encapsulated guests in ways that normally are not possible for these compounds as free molecules. In the next paragraphs some important examples of the advantages of confined reactivity will be described.
A significant application in this context is the acceleration of chemical reactions, this can be achieved in many different methods that are summarized in the following figure (Figure 6).

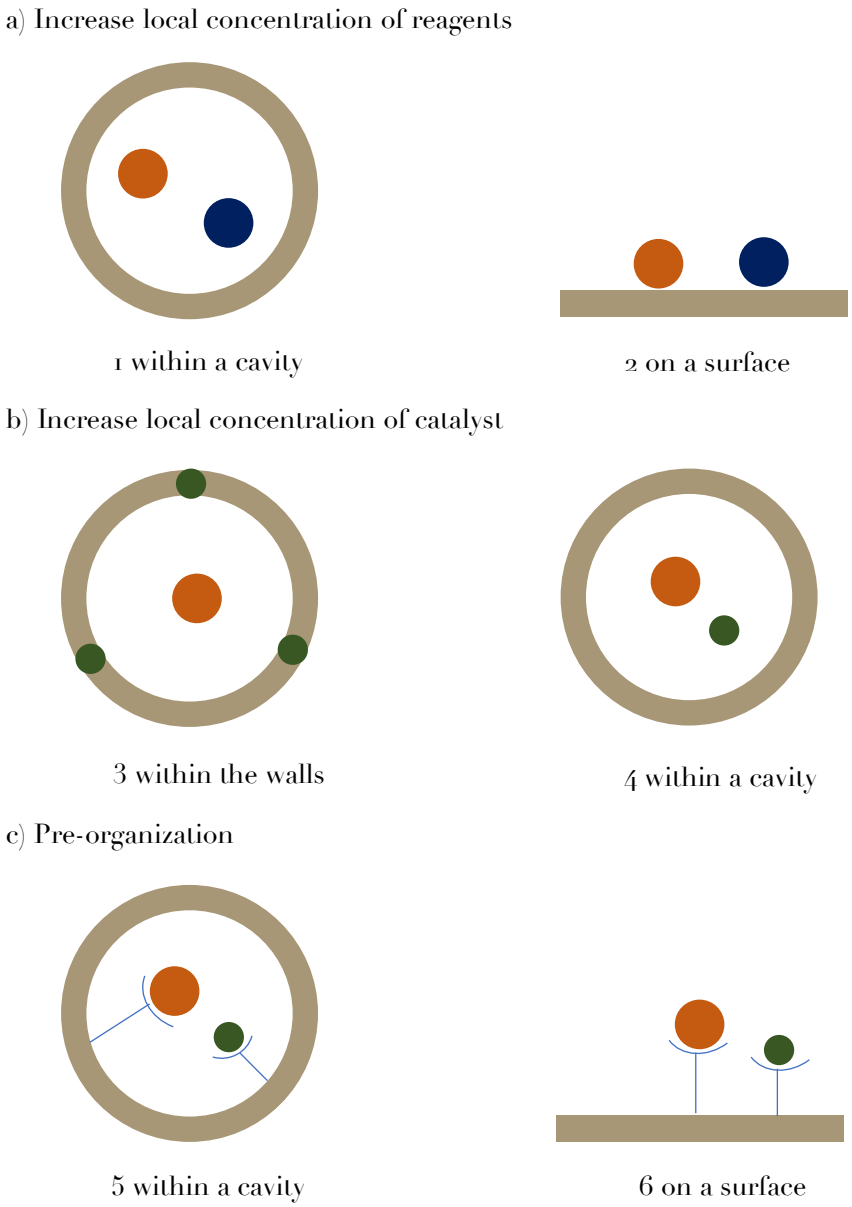

Figure 6. a) Increasing the local concentration of reagents (blue and orange) within a cavity (1) or on a surface (2). **b**) Increasing the local concentration of a catalyst (green) by embedding it within the walls of a cavity (3) or by co-encapsulating (4) it with a reagent (orange). **c**) Pre-organization of reagents (orange) and/or catalysts (green) within a cavity (5), or on a surface (6).

The first option consists in the increase of the local concentration of the reagents within a cavity or on a 2D surface, in this way a higher number of events leading to the reaction can be obtained. For instance, the acceleration of Diels-Alder reactions has been studied within coordination cage cavities[35] or in other self-assembled molecular capsules as well[36](example 1a in Figure 6). A gold surface has been similarly employed to improve the acceleration of silane alcoholysis[37] (example 2a in Figure 6).
A second approach is to act on the local concentration of the catalyst, by increasing this parameter the number of the effective encounters between catalyst and reagents will increase as well obtaining a more powerful and efficient catalysis. Significantly, the

catalyst can be incorporated within the walls of the considered molecular flask[38,39,40,41], this method was observed to favor intramolecular C O and C C bond-forming cyclization processes. Furthermore, trimeric macrocycles were found to assemble into supramolecular nanotubules that were then functionalized using palladium cations coordinated along the internal walls of these structures (example 3b in Figure 6). Such nanotubules were observed to catalyze C C coupling reactions[42].
Regarding last example (Figure 6c), in some cases the catalyst and the reagents con be co-encapsulated in order to be precisely placed to maximize efficient interactions. In other words, the involved species are favorably pre-organized under confinement. Coordination cages are suitable guests for this procedure as presented in this work where the host cavity have been functionalized with endohedral guanidinium binding sites[43]. A part of the binding sites is linked to a gold-based catalyst while others are connected to the reagent positioning it in the close proximity of the catalyst. Pre-organization was reported to increase the rate of cyclization of an acetylenic acid to the relative enol lactone.
Alternatively, pre-organization can be arranged on a surface as well (example 6c in figure 6). Gold nanoparticles, for instance, have been decorated with either oligo(ethylene glycol) as background ligands and ligands functionalized with azobenzene units[44]. Immobilization of ligands on the gold surface allows the OH groups from background ligand to reach in close proximity N=N bond of azobenzene. In this paper has been demonstrated that thermal relaxations from Z to E-azobenzene can be accelerated by a factor of ca. 6000 compared to similar systems. This effect can be attribute to the formation of hydrogen bonds between hydroxyl groups and nitrogen atoms in azobenzene.
A completely different application of molecular containers is the stabilization of chemical species. Molecular flasks are able to stabilize dynamic assemblies because of the ability to preserve intermolecular bonds from competition with other species, moreover the flask can provide further stabilization from interaction with internal walls or surfaces (Figure 7a). Furthermore, a molecular container can create a hermetic shell which minimize the activity of reactive species (Figure 7b). Other possibilities to render reactive species stable under confinement involve constriction which prevents, stabilize or trap transition states in order to increase the rate or the yield of a reaction (Figure 7c).

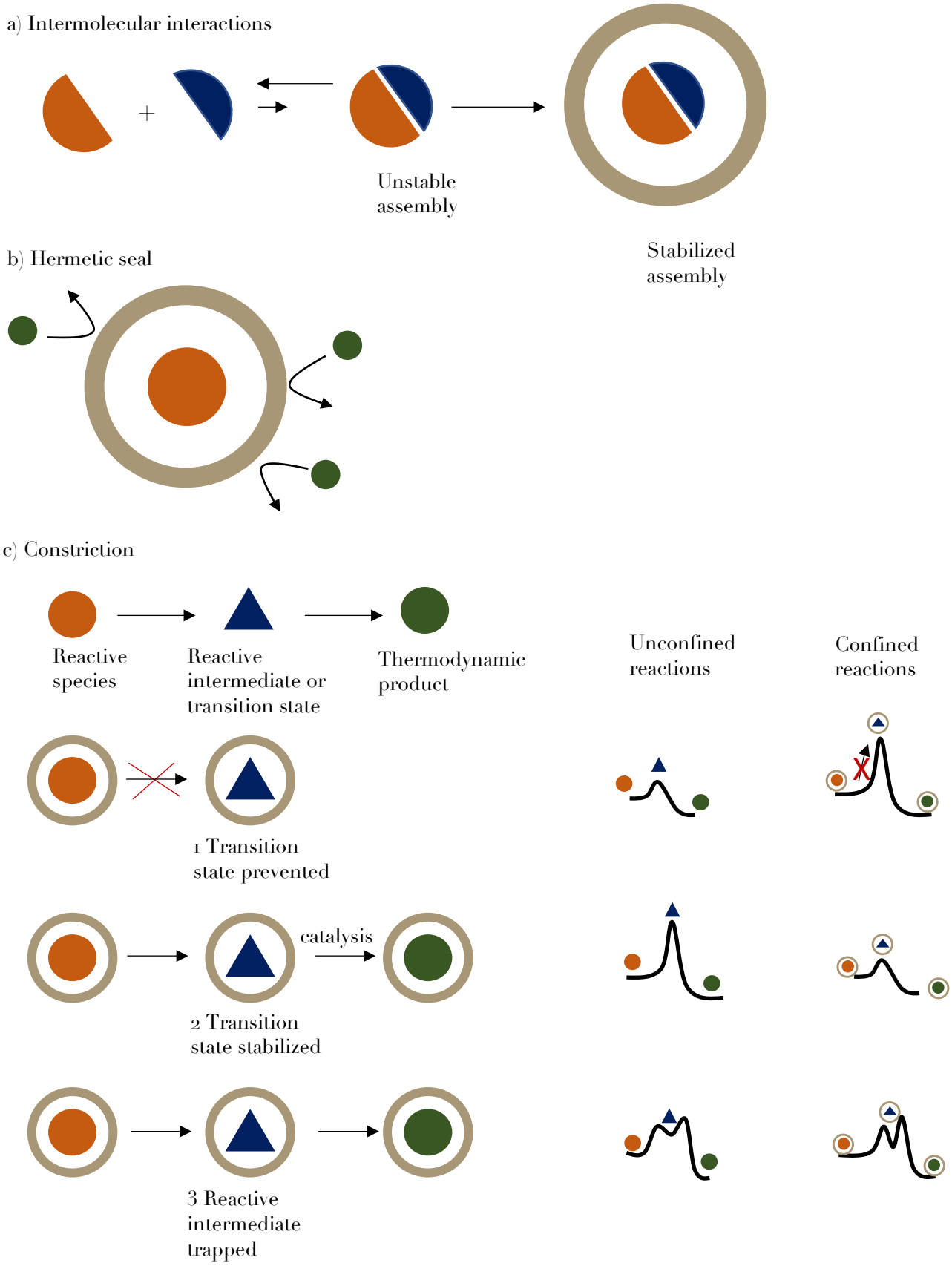

Figure 7. Principles controlling the stabilization of reactive species or unstable assemblies under confinement.

Self-assembled species can often be dynamic in solution thus, a confined space provides a stabilizing effect. For instance, a coordination cage has been shown to allow the formation of single A U base pair with optimal stability in water[45].
A similar strategy has been employed as well with fragments of double-stranded DNA which, if shorter than four base pairs, are hardly stable in water because they lack the cooperative forces typical of longer chains. Nevertheless, by using a confinement approach, single nucleotides adenosine monophosphate and uridine monophosphate were reported to bind by means of intermolecular hydrogen bonding (Figure 7a).
Another possibility is to create a hermetic seal exploiting a molecular container. This strategy provides an inert and isolated environment which minimizes the contact with other species or with the external environment (Figure 7b). This idea has been successfully applied by employing an hemicarcerand in order to stabilize cyclobutadene[46], such molecule tends strongly to dimerize, however, the limited size of the cavity does not allow the formation of the dimer stabilizing the monomer.
Alternatively, by exploiting the effect of confinement is possible to modify the energy level of an intermediate or a transition state (Figure 7c, 1). For instance, confinement can avoid the formation of transition states by leading a reactive specie to be inert. This procedure has been demonstrated by the encapsulation of P_4 (white phosphorous) in a coordination cage avoiding reactions with oxygen[47]. Besides oxygen can access the molecule of P_4 the cage cavity is not large enough to accommodate large transition state implied in oxidation, thus, white phosphors can be stable under atmospheric conditions.
A further method is to decrease the energy barrier of the transition state in order to increase the rate of the reaction[48,49,50] (Figure 7c, 2). This effect has been presented by performing the bowl-to-bowl inversion of etheylcorannulene[51]. In this work a molecular box was employed and a single molecule of etheylcorannulene was bound within the box cavity. The inversion reaction proceeds trough a planar transition state which, because of a good shape complementarity, is stabilized by the molecular box promoting an acceleration in the reaction rate.
The isolation of reactive intermediates can be often challenging[52], however, this task can be achieved by trapping these species by means of a molecular container (Figure 6c, 3). Cucurbituril was employed to confine a bicyclic azoalkane[53], the decomposition was monitored in the gas phase using mass spectrometry. By means of this technique several intermediates were individuated during the process.
Another interesting application regarding reactivity under confinement is the modulation of the selectivity of a reaction. For instance, constriction can limit the shape and the size of a product favoring the formation of a certain product over the others.[54,55,56]
Concluding, confinement can also modulate chemical features such as electrochemical properties [57,58] or in the case of chromophores encapsulation can also influence their absorption or emission features [57,59].

1.5 Molecular machines

1.5.1 Definitions and natural molecular machines

A molecular machine can be defined as an assembly of a discrete number of molecular constituents projected to perform a specific function[60]. Such device can include a molecular motor which is the unit able to convert an external energy input into directionally controlled motion[61].
Molecular machines exist in nature as well and constitute the base or our life. In the human body, in fact, we can find many examples of complex biomolecular assemblies from which the supramolecular chemistry field takes inspiration in the developing of artificial molecular devices. One of the most important bio-machine is the myosin protein family. These groups of proteins are involved in the process of muscular contraction and they can be considered as a supramolecular linear motor. The contractile units in muscles which are called sarcomeres are constitutes by several protein chains: two large "heavy" chains and four small "light" chains (Figure 8a).

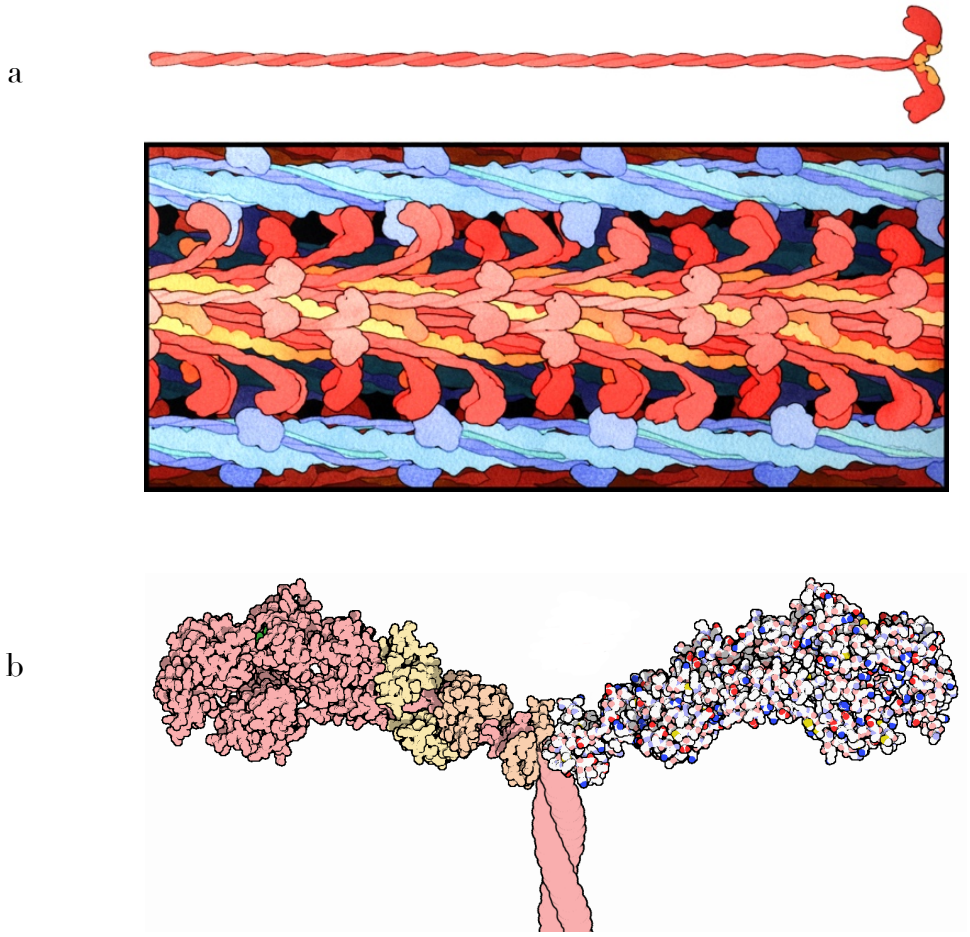

Figure 8 a) A short segment of a thick filament is shown in red, next to a scale drawing of a single myosin molecule. The many myosin heads extending from the thick filament then reach over to actin filaments, shown in blue and green. **b**) Molecular heads of myosin. Adapted with permission from (10.2210/rcsb_pdb/mom_2001_6).

The heads of myosin (Figure 8b) constitute the motor domain of this complex structure as they are able to move along the thins filaments causing a slide in both directions and consequently the muscle contraction. All the involved processes are coupled with specific phases in the hydrolysis cycle of ATP which provides the energy inputs.
Differently, another type of motion which is present as well in nature is the rotary motion which, for instance, is represented by the enzyme ATP synthase.

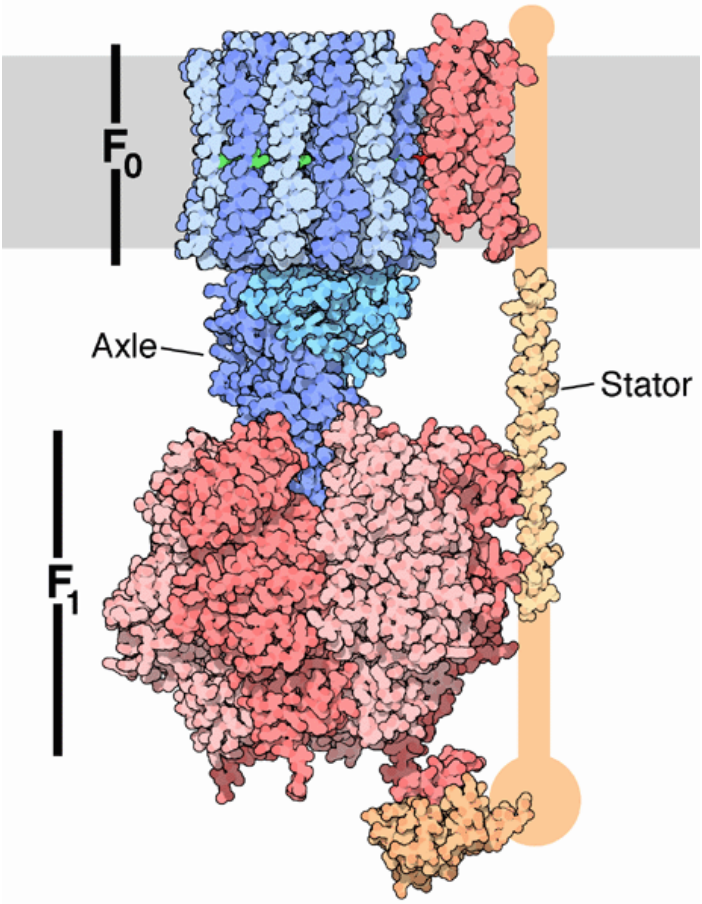

Figure 9 Schematic representation of ATP synthase: grey stripes symbolize the cellular membrane, Fo rotor (blue), F1 rotor (red), stator (yellow). Adapted with permission from (10.2210/rcsb_pdb/mom_2005_12).

ATP synthase is not only an enzyme but also a molecular motor, an ion pump, and a second molecular motor all combined in one complex bio-machine. It plays a fundamental role in human body cells, producing most of the ATP that is required for cellular processes as energy source. It is composed of the F_o and F_1 units: F_o is embedded in a membrane (shown schematically as a gray stripe), and is a rotary motor powered by the flow of hydrogen ions across the membrane (Figure 9). As the protons flow through the motor, they operate a circular motion (shown in blue). This rotor is linked to F_1, the second motor. F_1 is a chemical motor, activated by ATP. Furthermore, F_o and F_1 are connected by a stator, shown on the right in yellow that allows the coupled rotation of F_o and F_1.
All the described features render the biomolecules of myosin and ATP synthase perfect examples of natural machines. Their structure comprises motor units, linear and rotary, which convert an external energy supply into a controlled motion in order to perform specific tasks.

1.5.2 Artificial molecular machines

Regarding the artificial version of the sophisticated bio-machines developed by nature, the complexity of the molecular components decreases drastically.
Among the most employed systems we find interesting structures such as rotaxanes and catenanes. Starting from two simple molecular elements, such as a macrocycle and a linear molecule (Figure 10a), is possible to form a supramolecule called pseudorotaxane in which the linear shaped element is surrounded by the macrocycle upon the threading process (Figure 10b). At this point, two pathways can be followed, by terminating the axle with two bulky groups called stoppers a rotaxane is obtained (Figure 10c). Their function is to prevent the exit of the macrocycle and the consequent disassembly of the system. Alternatively, by performing a clipping reaction a catenanes can be assembled (Figure 10d). Rotaxanes and catenanes are defined MIMs (mechanically interlocked molecules) as one of the key features of these systems is the presence of a mechanical bond which is very common in the construction of molecular machines. [62]

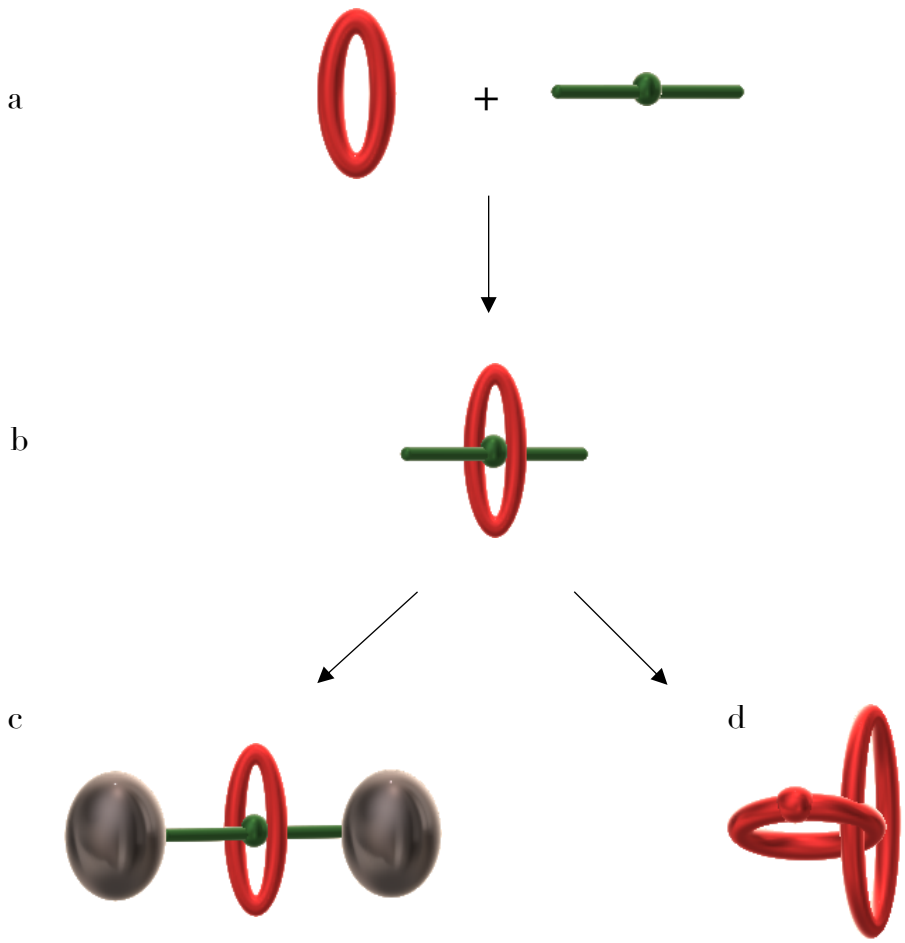

Figure 10 Schematic representation of two molecular components a macrocycle (a) and an axle (b) which can be associated forming a pseudorotaxane (b). Subsequently, upon capping of the axle a rotaxane (c) can be obtained or a catenane in the case of two interlocked rings (d).

In rotaxanes and catenanes complementary recognition sites are included in the molecular structure, these comprise hydrogen bonding, electronic donor-acceptor interactions, π–π stacking, columbic forces but also stronger interactions such as metal-ligand bonding. Molecular recognition is functional also for an effective template-directed synthetic strategy[63]. The most diffused types of rotaxanes and catenanes are structures based on N^+-$H^{\cdots}O$ hydrogen bonding between secondary ammonium functions (e.g., dibenzylammonium ions) and a suitable crown ether (e.g., dibenzo[24]crown-8). Alternatively, charge transfer interactions between π–electron donor (e.g., dioxyaromatic groups or tetrathiafulvalene units) and π–electron acceptor (e.g., 4,4'-bipyridinium derivative) are commonly adopted. In addition, the modulation of the interactions between molecular components needs to be projected in order to allow an external stimulus to operate on the assembly and activate a mechanical controlled movement.

1.5.3 Energy sources

The choice of a suitable energy input is of primary importance in the designing of a molecular device. The most adopted strategy by macroscopic machines is represented by exergonic processes as the ones occurring in the usual internal combustion engine. However, considering a molecular device or motor which needs to operate upon inputs of chemical energy, an addiction of fresh "fuel" (reactant) would be needed at every step in the working cycle. This implies the possible formation of waste products which can be accumulated over repeated cycles and consequently compromise the resulting efficiency of the device. All these considerations need to be taken into account as they can represent a significant limit.
For these reasons, endergonic and possibly reversible processes as isomerization or redox reactions are the mainly studied for the operation of molecular machines. Among the mainly employed energy sources we find light, which constitutes a widely available, renewable and clean energy source. Moreover, light is involved in many processes in nature, for instance it can induce the motion of retinal which is the chromophore at the base of the vision mechanism. Several categories of chemical processes involving organic and inorganic species such as dimerization, rearrangements and decomposition can be triggered by means of light energy[64]. Light can as well generate an excited state showing different properties with the respect to the ground state, such as redox or acid-base features which can lead to electron- and proton-transfer reactions. These processes can also lead to a change in the interactions of a multicomponent molecular structure.
Importantly, a photochemical stimulus can also induce large structural changes such as in isomerization processes. A common strategy is to include in the device a switchable double bond as C=C, N=N or C=N. Finally, an advantage of this approach is that by using optical techniques is possible both to operate and "read" the considered system.
Electrochemical energy is another extensively adopted source as it is also clean, easy to modulate and the associated redox processes are usually reversible.
In fact, an electrochemical input can be exploited in order to oxidate or reduce one or o more components of a molecular device[65,66]. In this case, an electrical potential can be externally applied to the system or a chemical redox reactant can be added leading to the desired motion. Electrochemical investigations can be performed to study the system in

solution or in different conditions, for instance, on solid surfaces by means of electron microscopy.
Finally, the most direct strategy is to use a chemical stimulus or in other words a chemical "fuel". A common example from biology in this case is represented by ATP-driven motor proteins which exploit the chemical energy derived from the metabolic processes of ATP to APD and AMP.
Differently from natural systems, where efficient recycling and modulation mechanism are present, in the case of artificial devices, upon the addiction of the fuel, the system reaches a new equilibrium state and subsequently a second reactant "antifuel" is needed to restore the system. Examples of a common fuel and antifuel are acids and bases indeed, a change of pH is often exploited to operate molecular devices (e.g. the deactivation of an ammonium recognition center in a rotaxane upon deprotonation).[67]
In conclusion one limit of this strategy is to include a method to recycle or remove waste products from the system without affecting the operation of the machine. This drawback renders such kind of systems often not autonomous as an alternated introduction of the fuel and antifuel reactants is needed in other words, the working cycle is defined "operator-dependent".

1.5.4 Motion at supramolecular level

Regarding the motion, scaling down to molecules implies dealing with different aspects. Contrarily to the macroscopic world, at the molecular scale the importance of Brownian motion becomes remarkable. This factor, which is not influent for macroscopic devices is indeed predominant in molecular motions. Nevertheless, from examples in nature and biology we know that is possible to overcome and modulate this random motion following a strategy called rectified Brownian motion (RBM).[68] Bio-machines, in fact, developed different mechanisms to control Brownian motion and to use external energy sources in order to render a certain direction more favored then others leading to a directional and controlled motion[69]. Similarly, regarding artificial machines two main types of motion are studied: linear and rotary motion.
A controlled linear motion can be achieved for instance by exploiting supramolecular structures such as rotaxanes. In principle, upon stimulation with an appropriate external input, a macrocycle (ring) can move in a linear fashion along a molecular axle. A system with these properties can be defined as a molecular shuttle or switch in which the ring is able to move between two stable states which usually corresponds to two different recognitions sites (stations) situated on the axle.
Initially, the ring occupies the station with the higher binding affinity (A) however, after an appropriate energy input can be transferred to the less efficient station (B) usually in a reversible way [70] (Figure 11).

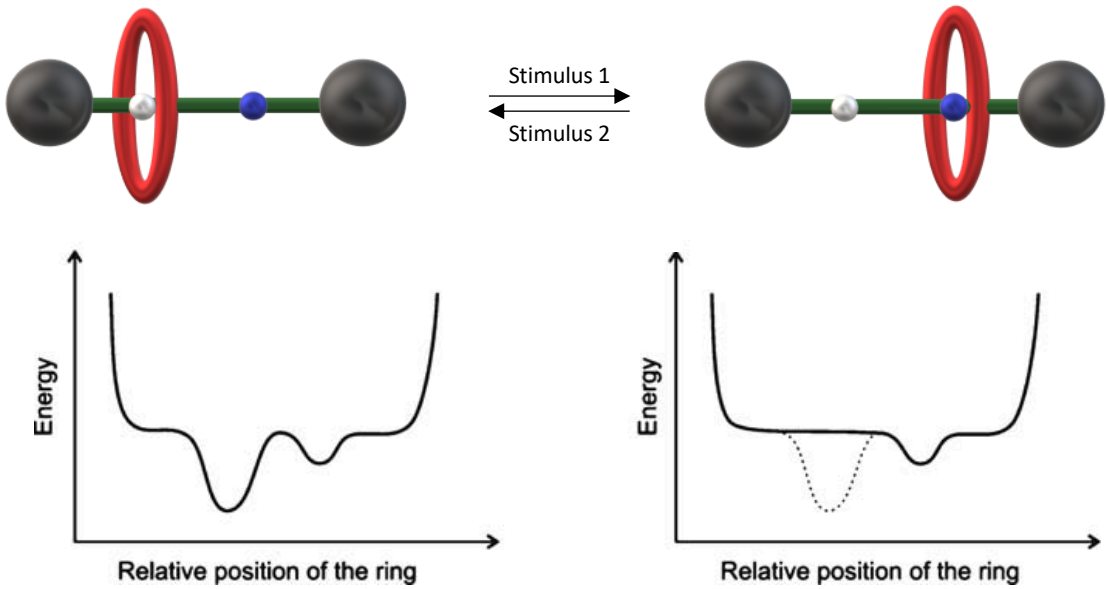

Figure 11 Schematic representation of a two-station rotaxane and its operation as a molecular switch. The graphs report a simplified representation of the potential energy of the system as a function of the position of the ring relative to the axle before (left) and after (right) switching off the station.

This strategy can be successfully employed in the projection of more complex molecular architectures. A well-known case is represented by the "molecular elevator"[71]. Significantly, in this work the authors presented a two-component molecular machine which can be described as a nanometric elevator.

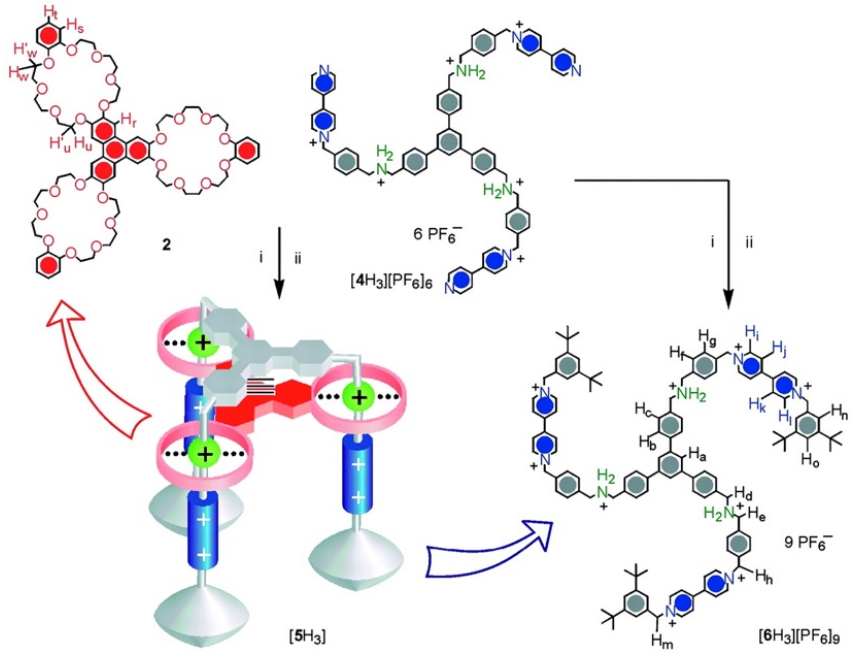

Figure 12 The trifurcated guest salt $[4H_3][PF_6]_6$ and the tritopic host 2 (each 6.6 mM) in a $CHCl_3$/MeCN solution (3.0 mL, 2 :1) form a 1:1 adduct (superbundle) that was, at elevated temperature (75°C), converted to the mechanically interlocked elevator $[5H_3][PF_6]_9$ in the reaction with (i) 3,5-di-tert-butylbenzylbromide(200 mM), followed by (ii) the counterion-exchange (NH_4PF_6/MeOH/H_2O). Adapted with permission[71].

This nanoactuator shows a 2.5 nm height and a diameter of ca. 3.5 nm. The assembly, synthesized by means of a template-directed methodology, is composed of a trifurcated rigid like guest salt that can bind with a 1:1 stoichiometry a tritopic host (Figure 12). Moreover, the guest has been functionalized with the bulky 3,5-di-tert-butylbenzyl stoppers in order to prevent the dissociation of the system.
The linear motion is achieved by means of a chemical external stimulus such as a change in pH. In fact, since strong hydrogen bonds are formed, in acidic conditions the favorable station is the ammonium group -NH^{2+}- however, upon the addition of a base the position of the host can be switched to the second station ($BIPY^{2+}$). The $BIPY^{2+}$ recognition site, differently from the ammonium group, is characterized by donor-acceptor interactions. Remarkably, such operation allows the lifting of the host from the one level to the upper one. This process is reversible as by protonating again the ammonium centers the host is observed to move back to the first level.
Another category of controlled motion is represented by rotary motion. A famous example is the rotary motor developed by the group of the Nobel laureate Ben Feringa.
Feringa and his collaborators published a remarkable work showing the first example of a novel supramolecular assembly able to perform an unidirectional controlled rotation[72].

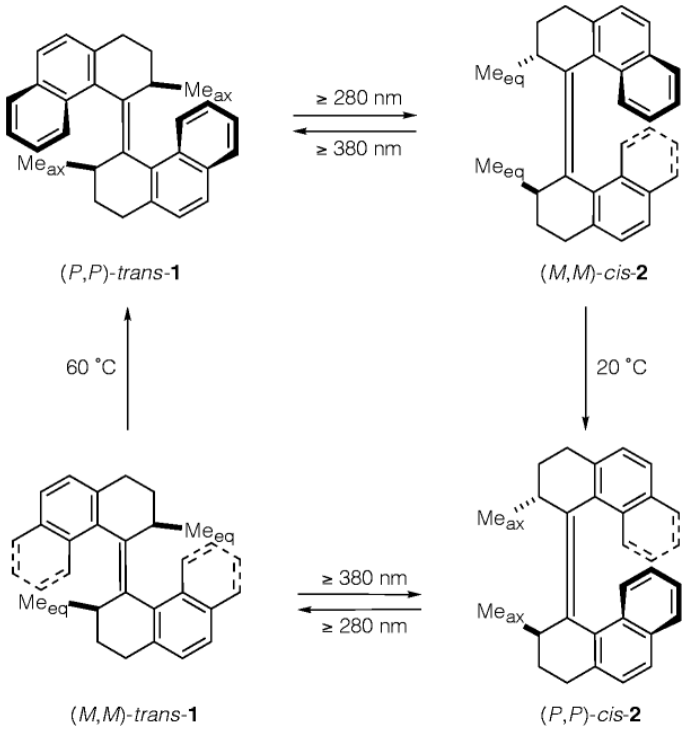

Figure. 13 Photochemical and thermal isomerization processes of (P,P)-trans-1. Adapted with permission[72].

The structure of (3R,3′R)-(P,P)-trans-1,1′,2,2′,3,3′,4,4′-octahydro-3,3′-dimethyl-4,4′-biphenanthrylidene, also called "overcrowded alkenes", is composed by 2 halves linked by the central C=C double bond. The rotary operation is controlled by means of alternated thermal and photochemical steps (Figure 13).
The first step is a low temperature endothermic photoisomerization of the trans (P,P) isomer to the cis (M,M) where P stands for the right-handed helix and M for the left-

handed helix. During this step, the two axial methyl groups are converted into two less sterically stable equatorial methyl groups. After increasing the temperature to 20 °C these methyl groups convert back exothermally to the (P,P) cis axial groups in a helix inversion. Since the axial isomer is more stable with the respect to the equatorial isomer, opposite rotation is prevented.
At this point, the second photoisomerization converts (P,P) cis into (M,M) trans, with the associated formation of sterically unfavorable equatorial methyl groups. Finally, a thermal isomerization process at 60 °C closes the 360° cycle back to the axial positions (Figure 13).
The systems described above are also proper examples in the clarification of another important concept in the field of molecular machines which is the difference between a molecular switch and a molecular motor.
A molecular switch, is usually defined as a device presenting two or multiple stable states which, after an appropriate external energy supply can be interconverted[73] (Figure 14a). Differently, a molecular motor is a device or the specific part of a molecular machine which is able to convert an external energy input into an unidirectional motion[61].

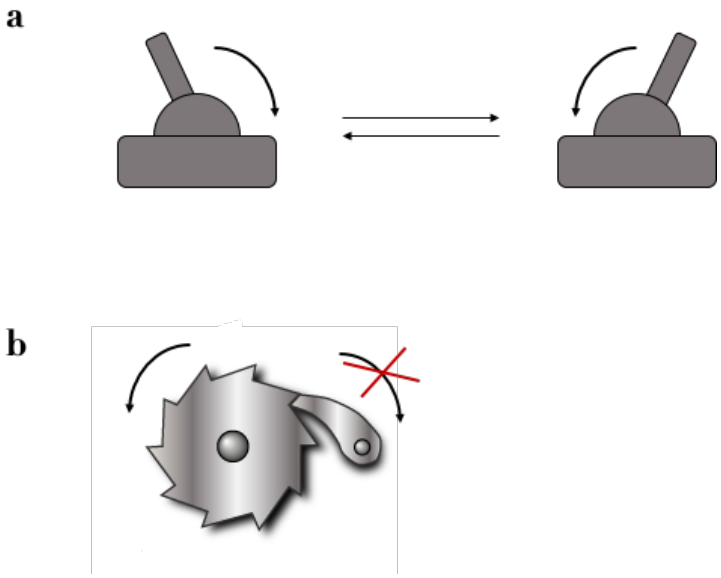

Figure. 14 Schematic representation of the operation of a switch device (a) and a ratchet mechanism (b).

The ability to perform unidirectional motion is actually the key point to obtain an effective production of work. In fact, the two states of a molecular switch are usually equal and opposite, this means that the work performed along one direction is canceled when the system resets to the initial state. Contrarily, this is typically prevented during the operation of a motor as it moves in a unique direction. Unidirectionality can be obtained by means of controlled ratchet mechanisms which can be visually represented in a simplified way by a gear mechanism (Figure 14b).
At the molecular scale, the control on the system becomes more complicated, in fact, in order to achieve unidirectionality, the potential energy surface needs to be carefully designed and controlled to have a right disposition of minima and maxima and to overcome Brownian random fluctuations. In this regards, two main ratchet strategies can be adopted.

The first consists in the energy ratchet mechanism[74]. To explain this process an asymmetric potential energy surface (presenting a series of minimally two different minima and two different maxima) along which a Brownian particle is directionally moved will be described (Figure 15 left).

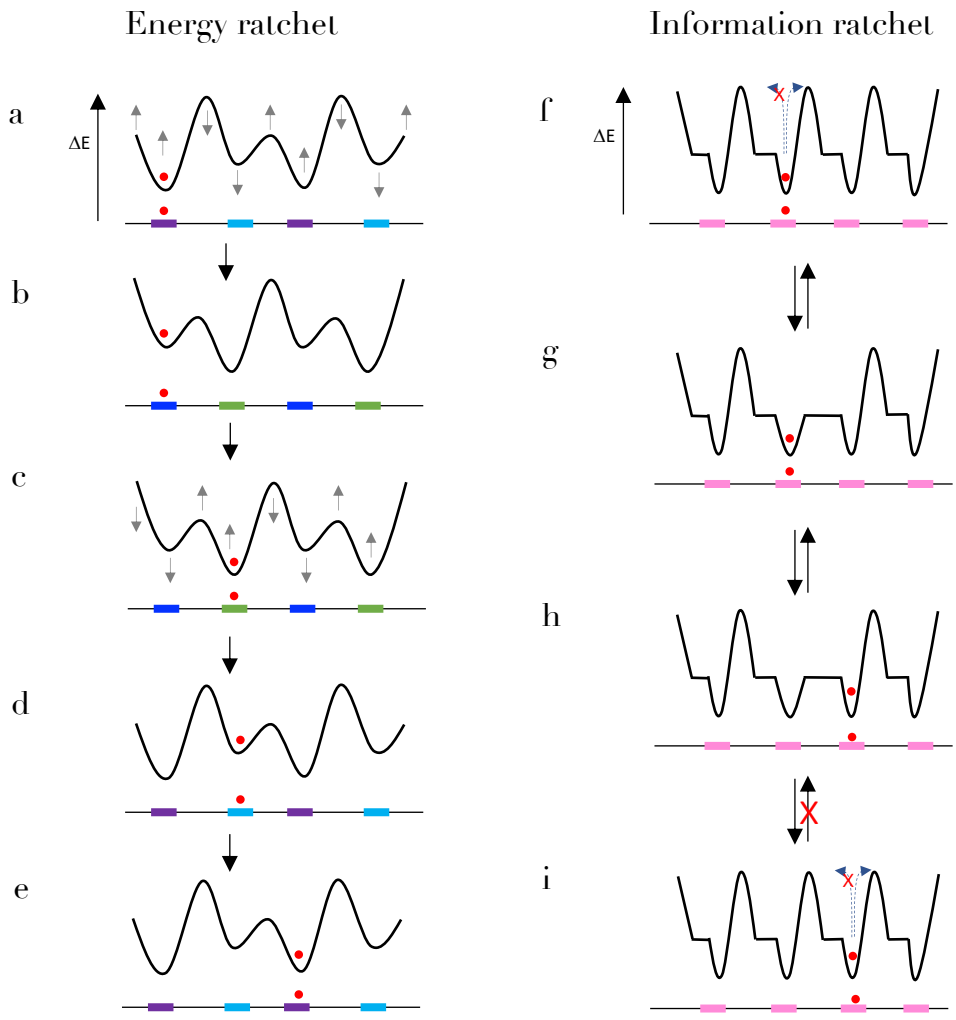

Figure. 15 Schematization of the operation of energy (left) and information (right) ratchet mechanisms.

The particle will initially occupy a global minimum well (Figure 15, a or c). At this point, the introduction of a suitable external stimulus (b→c or d→e) will raise the first minimum and, at same time, will lower the adjacent maximum allowing the particle to move forward in a directional fashion by means of Brownian motion (c). Significantly, the position of the particle along the surface has no influence and the switching has not to be necessarily regular. In addition, the particle will continue to move from left to right as long as the two sets of minima and maxima will be switched with the same order.
The second scheme represents the energy information ratchet[75] (Figure 15 left). Differently from the previously described mechanism, where the switching of the potential is applied globally with no dependence of the particle position, in this case the height of the maxima

changes according to the location of the particle. This implies that an information needs to be transmitted from the particle to the surface.
Also in this case, at the beginning, the particle will be located in one of the equal minima (Figure 15f) then, the particle position selectively lowers the adjacent kinetic barrier allowing the passage to the next right-hand well by Brownian motion (g→h). Notably, the minima depth does not necessarily need to be modified.
Upon the transfer of the particle (i) the barrier is restored and this avoids the movement in the back direction. Summarizing, the asymmetry in the particle position between two barriers provides the "information" which transports the particle directionally along the potential energy surface.
Another important point regarding a molecular motor is the possibility to achieve an autonomous operation. A molecular device can be defined autonomous if it can complete a working cycle by using a single input, in this way, as long as the stimulus is kept the machine will continue to repeat its operation. This feature is more difficult to be designed in fact, usually the output obtained upon a single stimulus move the system from one state to a second one and to reestablish the initial situation an opposite input have to be sent. Therefore, usually at least two different inputs need to be provided in order to perform a working cycle.

1.5.5 Applications and materials based on molecular machines

Applications including molecular machines and motors are various and in rapid evolution over the last years[76,77]. Among them, a remarkable goal is represented by the development of devices able to transport a molecular cargo. Examples of such devices are already present in nature, in fact, biomolecular machines as myosin and kinesin[78] show the ability to move in a controlled directional fashion along a path by exploiting their motor domains activated by ATP energy. Moreover, they can as well transport and release specific compounds. The design of similar artificial devices is still a challenging task in the molecular machines field; however, some simple structures have already been developed. For instance, is possible to project such operation by using common supramolecular assemblies as rotaxanes.
In a recent work, a rotaxane comprising a dibenzo[24]-crown-8 ring and a molecular axle including a dibenzylammonium and a 4,4'-bipyridinium stations was presented[79] (Figure 16). In such system, since the ammonium site shows a higher binding strength with the respect to the bipyridinium station, the ring is initially located on the ammonium. However, upon deprotonation of the latter the ring moves to the second station. By protonating again, the ammonium with an acid the initial situation can be restored. In this case, a reversible controlled shuttling of the ring can be achieved by means of a chemical input (Figure 16a). Furthermore, a short chain is linked to the ring with the function of binding site for the cargo. With this role, an $[Ru(tpy)(bpy)]L^{2+}$ complex in which tpy and bpy are chelating ligands (tpy = 2,2′;6′,2″-terpyridine, bpy = 2,2′-bipyridine and L is a monodentate ancillary ligand) was employed (Figure 16b).

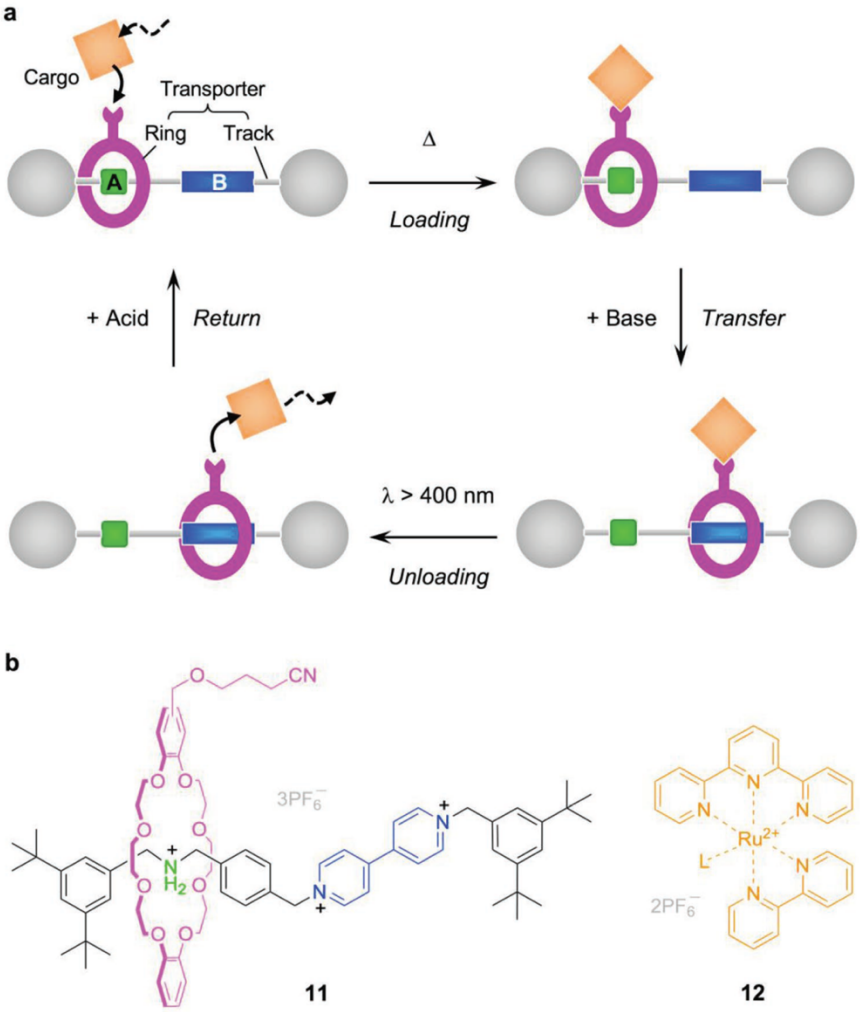

Figure 16 Schematization of a "molecular transporter" based on a controllable molecular shuttle and operated by two independent external stimuli (base/acid and dark/light). b) Structure formulas of the rotaxane transporter 11 and cargo 12. Adapted with permission[79].

The rotaxane was studied by means of several techniques such as electrochemical studies, ^{1}H NMR and UV-vis spectroscopy. The authors showed that, in suitable conditions the monodentate ligand of the Ru complex can be replaced by the nitrile group included in the rotaxane (Figure 16a). The cargo, connected to ring, is initially located in the station A however, after the addition of a base, the ring can be transferred to station B avoiding the detaching of the cargo which can occur upon irradiation with visible light. At this point, the ring, which is encircling the station B, can move to A after the reprotonation of the ammonium group. Interestingly, a similar strategy has been presented also by exploiting a rotary motor[80] however, in this case the cargo is never released from the "transporting arm" disabling the exchange with others species in solution. Both the described molecular designs report interesting results involving a precise spatial control of the motion by means of multiple stimulus. Nevertheless, in these cases the transport of the considered molecular cargo occurs in the same solution or intramolecularly making the operation unproductive.

MIMs such as rotaxanes can as well constitute an optimal solution for the design of artificial molecular pumps (AMPs). AMPs can be described as linear motors in which a molecular component is directionally moved with the respect to the motor unit[81].

Depending on the chemical design, pumps can, provided a sufficient external energy, transport materials against local concentration gradients, thus maintaining the system in a steady state far from thermodynamic equilibrium. In this regard natural machines represent an unlimited source of inspiration; many biomolecular pumps comprising transmembrane proteins, are able to connect the intra- and extra-cellular environments with precise mechanisms which overcomes the random Brownian motion. These proteins convert chemical energy to move ions or other molecules from low to high electrochemical potentials, i.e., in the direction opposite to that deriving solely from equilibrium thermodynamics. An important example is represented by the Na^+, K^+-ATPase which uses energy from ATP hydrolysis for creating and regulating gradients of Na^+ and K^+ ions across cell membranes[82].

Regarding the AMPs, despite the employing of much simpler chemical designs, remarkable devices able of operating out of equilibrium have been developed in the last years[83,84]. Among them in this recent work Stoddart[85] and collaborators show an alternative application of AMPs towards the design of controlled synthetic mechanisms. The authors presented a device composed of a linear component $PolyDB^{6+}$, and a ring $CBPQT^{4+}$. The $PolyDB^{6+}$ consists of two molecular pumps attached at both ends of the PEG chains by a pair of triazole rings, forming a collecting polymer chain located in the middle between the two pumps. (Figure 17a). This device is able, with a sequence of redox cycles applied chemically or electrochemically, to synthetize hexacationic polymer dumbbells incorporating two, four, six, eight, and 10 rings carrying 8^+, 16^+, 24^+, 32^+, and 40^+ charges, respectively. In the next figure (Figure 17b) the operating steps are described.

At first (I), the rings and the polymer dumbbell do not interact because of strong charge repulsions. Upon reduction (II), all $BIPY^{2+}$ groups are reduced to their radical cation ($BIPY^{+\bullet}$), allowing the threading of two $CBPQT^{2(+\bullet)}$ rings, one onto each side of $PolyDB^{4(+)2(\bullet)}$ with the formation of two trisradical tricationic complexes. After oxidation (III), the strong coulombic repulsions between the charged PY^+, $BIPY^{2+}$, and $CBPQT^{4+}$ units lead to the rings crossing the IPP steric barriers as a result of thermal energy and being kinetically trapped by the collecting polymer chain. At this point (IV), the poly[3]rotaxane is formed. The second reduction (V) causes the incorporation of two more rings from the bulk solution by an analogous mechanism. The two threaded reduced rings interactions are of radical-pairing type (indicated by a pair of triple vertical lines). The subsequent oxidation (VI) restores the $BIPY^{2+}$ units and the $CBPQT^{4+}$ rings and induces the second couple of rings to traverse the IPP barriers while the two reoxidized threaded rings are prevented from dethreading by these steric barriers, helped by the strong coulombic repulsions associated with both pumps. The second thermal relaxation results in the formation (VII) of the poly[5]rotaxane, and so on.

The key element that allows pumping to maintain a highly nonequilibrium structure is kinetic asymmetry[86] provided by the "pumping cassette", which comprises a switchable barrier (PY^+), a switchable recognition site ($BIPY^{2+}/BIPY^{+\bullet}$), and a fixed neutral steric barrier (IPP).

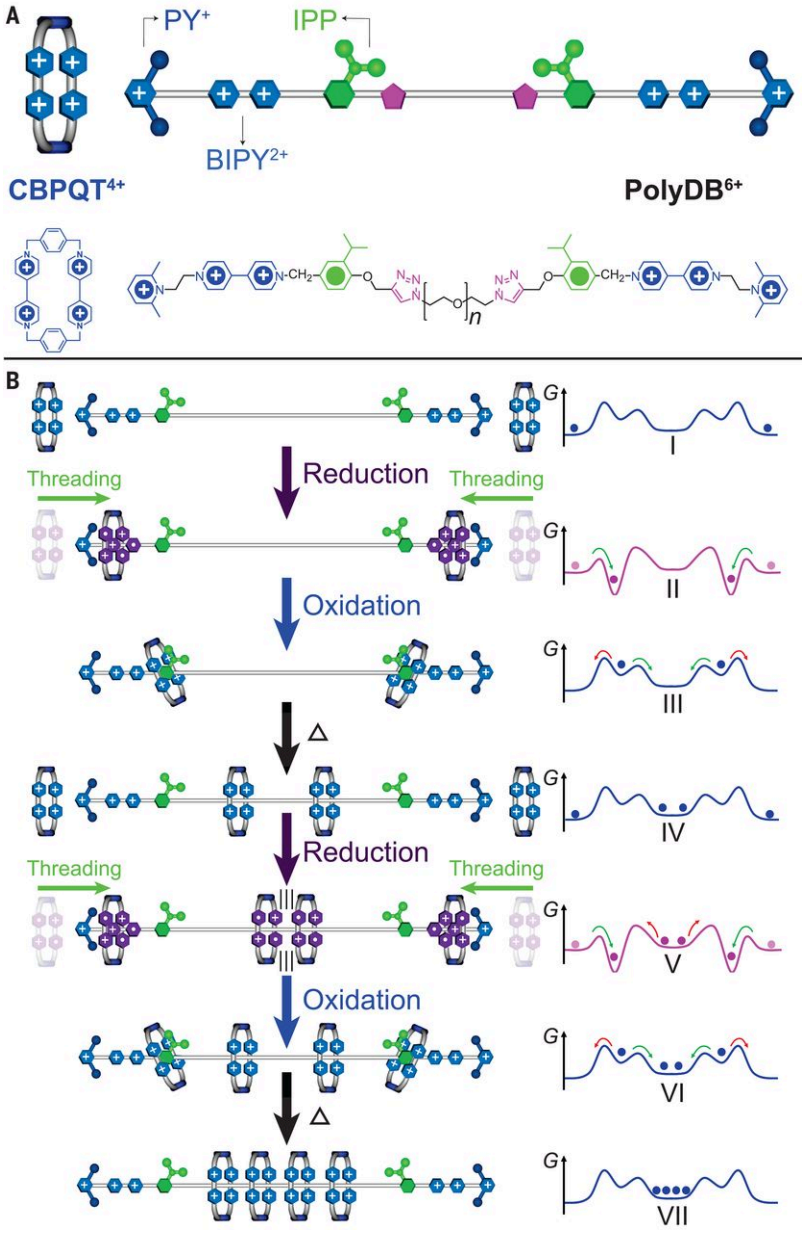

Figure 17 Graphical representations of the structural formulas for the $CBPQT^{4+}$ ring and $PolyDB^{6+}$ (a), The pumping mechanism for the redox-driven synthesis of the poly[5]rotaxane (b). Energy profiles representing the free energies of the system, as the rings are pumped in pairs onto the polymer dumbbell, are illustrated to the right of each intermediate in the reaction sequence. The curved arrows on the energy profiles represent reaction pathways that are either kinetically favored (green) or disfavored (red). The triazole rings (magenta) in each intermediate of the reaction are omitted for the sake of clarity. Adapted with permission[85].

Other interesting applications including molecular motors which operates out of equilibrium regard the incorporations of such devices within a bilayer membrane such as a cell membrane.

In this work a properly functionalized molecular rotary motor of the overcrowded alkene type (Section 1.5.4) was inserted in either synthetic lipid bilayers or cell membranes moreover, the behavior of the system was investigated under photochemical irradiation in order to test the membrane stability[87]. The motors are linked to dye units (cyanine, boron

dipyrromethene or BODIPY) or oligopeptide chains on the lower part. Significantly, the introduction of the dyes has no effect on the photoreactivity of the motor moiety.
Initially, the motor linked to cyanine and BODIPY were both inserted into large unilamellar vesicles (LUVs). By means of confocal fluorescence microscopy investigations, a decreasing of the BODIPY luminescence signal was observed upon exposition to light at 365 nm (Figure 18). The authors attributed this data to the destabilization of the membrane caused by the motion of the rotor triggered by light and to the consequent locking of the dye. In addition, the same rotor functionalized with cyanine and BODIPY was also tested in living cells by means of optical microscopy. After irradiation with UV light in control samples (carried out with derivatives that are either not photoactive or cannot rotate unidirectionally), negligible cell death was observed, this effect was thought to indicate that the unidirectional rotation of the molecular motors is necessary to have an efficient light-effected penetration through the membrane. Moreover, the membrane rupture and consequent pore formation were concluded to be an effect of a tangential mechanical force operated by the rotors (Figure 18).

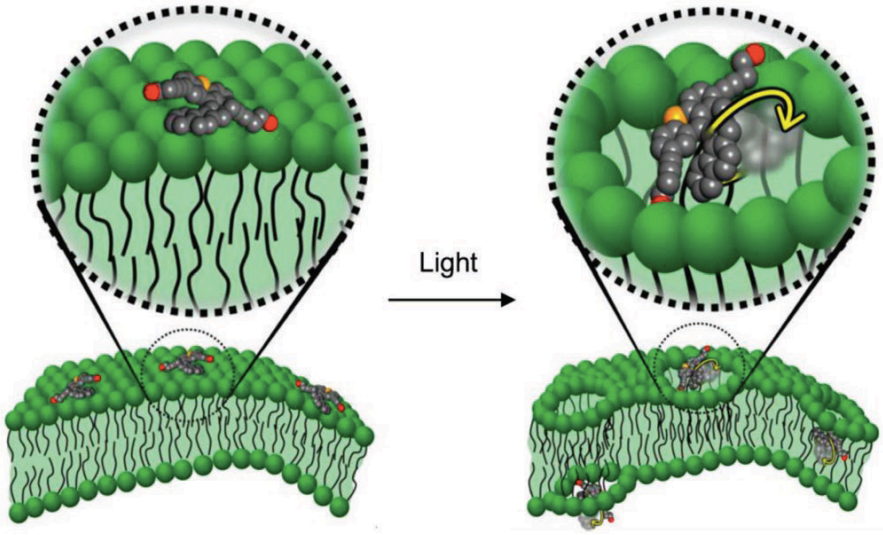

Figure 18 Schematic representation of molecular motors embedded in a cell membrane, and of their UV-induced rotation inducing membrane disruption and pore formation. Adapted with permission[87].

With a similar approach, molecular machines and motor can as well be implemented in macroscopic materials such as polymers in order to exploit specific motion features[88,89]. This option would give the possibility to scale-up and exploit the features projected at the nano-scale and to employ them for original purposes. In this regard, a remarkable work has been carried out by the group of Nicolas Giuseppone[90,91].
In these studies the authors presented an interesting combination of the rotary motor overcrowded alkene and a polymeric gel. The original molecular structure was modified in order to obtain compound 22 (Figure 19 a) by functionalizing the upper and lower part of the motor (highlighted in orange and in blue) with two azide terminated with

poly(ethylene glycol) chains and two alkyne-terminated oligo(ethylene glycol) chains, respectively. At this point a crosslinked polymer was synthetized by exploiting an alkyne-azide cycloaddition reaction Cu-catalyzed under high concentrations conditions. With this methodology the ethylene glycol chains were covalently linked to different rotary motors using triazole groups. The resulting polymer forms a gel in toluene 10% w/w.

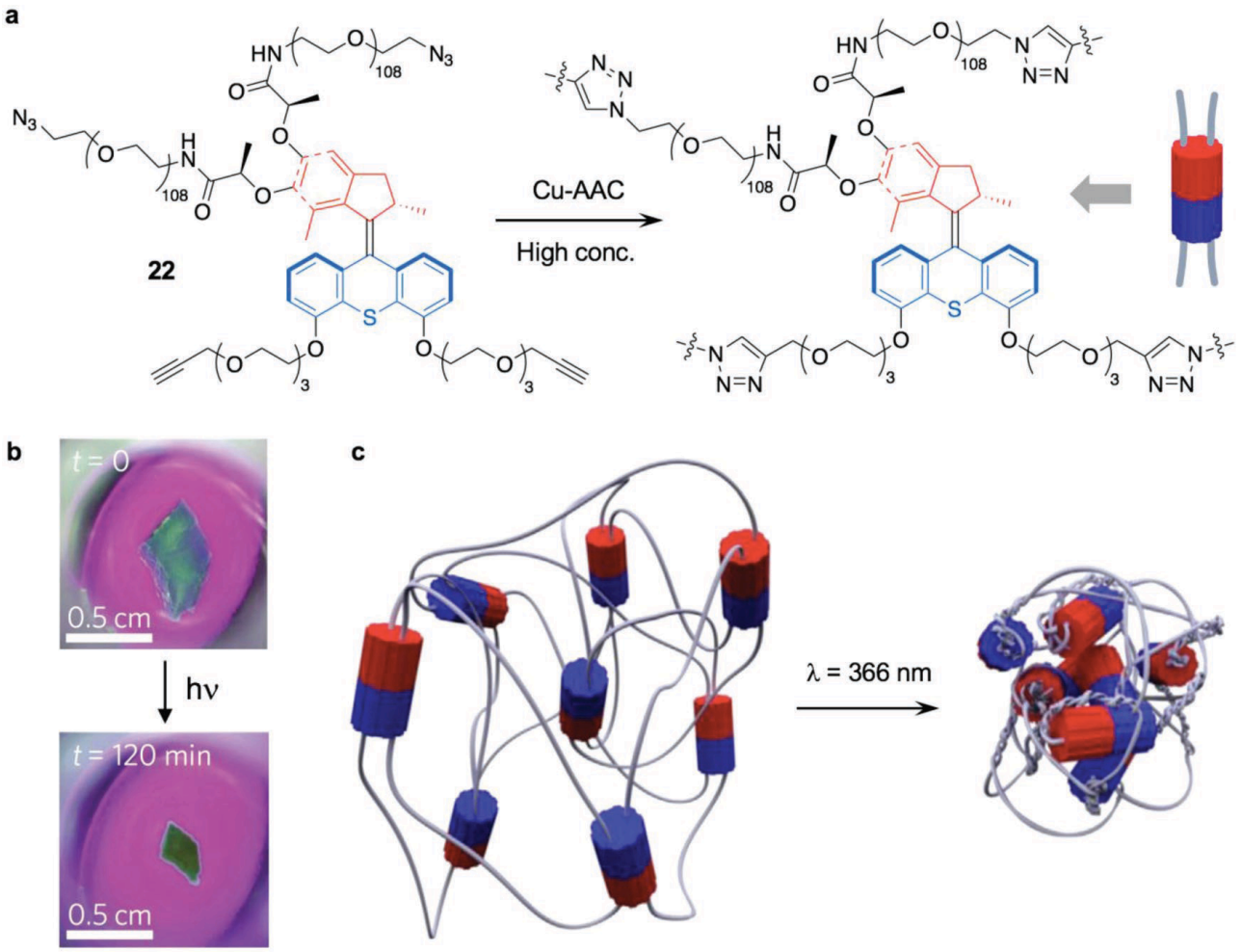

Figure 19 a) Structural formula of the molecular motor 22 functionalized with reactive chains, and its polymerization by Cu-AAC to generate a crosslinked polymer containing motor units. b) Photographic snapshots of a millimeter-sized piece of gel, obtained by swelling the polymer with toluene, evidencing the shrinking caused by UV irradiation. c) The photoinduced rotation of the molecular motor units at the branching points of the polymer determines the braiding of the chains, ultimately resulting in the contraction of the gel. Adapted with permission[76].

The material was then studied upon irradiation with UV light (366 nm) and, as the image shows, the photoinduced rotation effectively contracts the gel thanks to the twisting of the attached chains (Figure 19 b). This feature is based on a unique step conversion of luminous energy into free energy by the decreasing of entropy of the braided chains, nevertheless, a limitation consists in the irreversibility of the process. Contrarily from an optical switch which can be converted between two or more states, in this case an opposite step has not been developed in the context of this work.

To this aim, in a following study[92], the authors introduced in the molecular structure a "modulator" constituted by photoswitchable units, this component has the role of

controlling the twisting and untwisting of the chains. The new compound, resulting in structure 24 (Figure 20 b), was efficiently polymerized in a gel as the previous one.
This optimization gives to the systems the ability to respond in different ways upon irradiation at different wavelengths. More specifically, visible light unlocks the modulators to their open form while is not active in the operations of the motors. On the contrary, irradiation with UV light promotes the rotation of the motors whereas has no effect on the diarylethene units which retain a closed conformation (locked).
Since this polymeric gel can be irradiated with both visible and UV light, the braiding and unbraiding rates can be tuned by acting on the relative intensities of the irradiation sources defining the consequent contraction or expansion of the material.

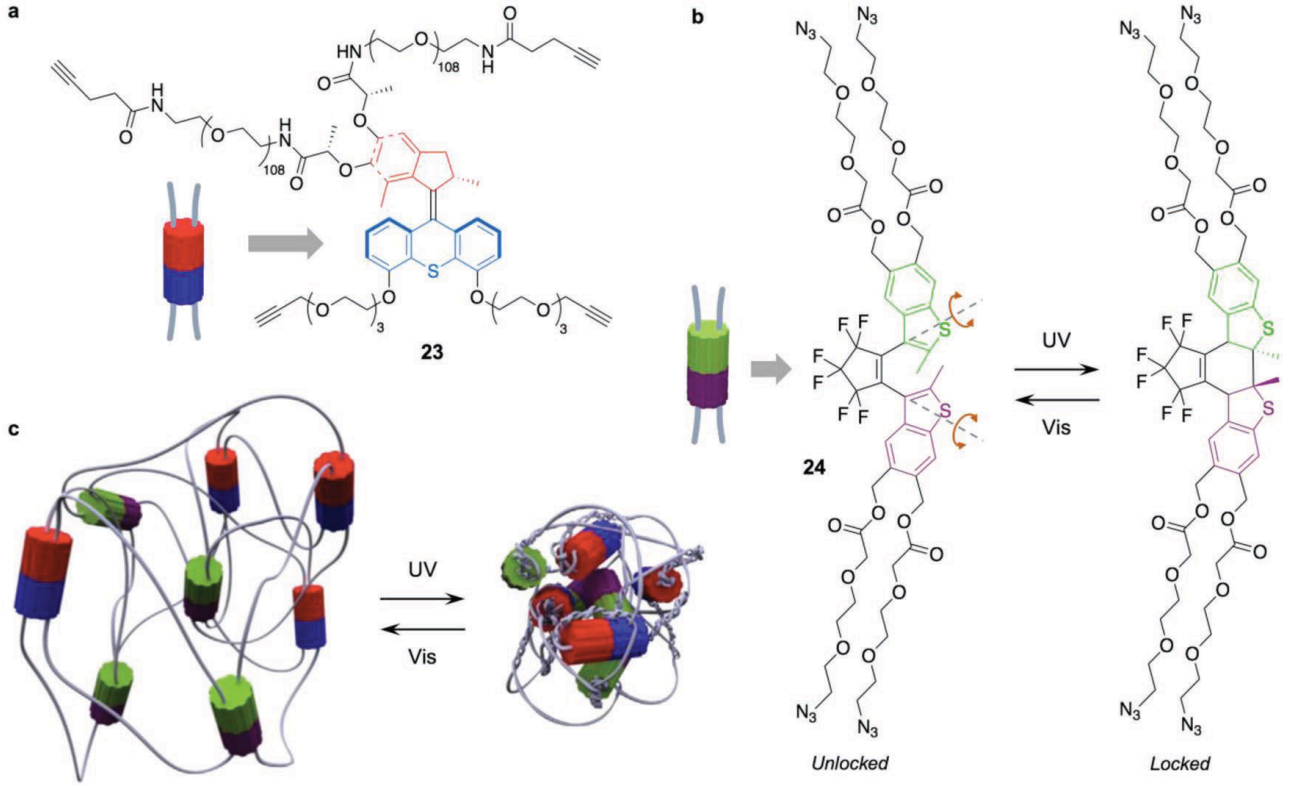

Figure 20. a) Structural formula and schematic cartoon of the molecular rotary motor 23 terminated with alkyne reactive groups. b) Structure formula of the diarylethene-based species 24 that, by a quadruple intermolecular Cu-AAC reaction with 23, affords a crosslinked polymer that contains both molecular motor and modulator units. The open (modulator unlocked; rotation axes shown in brown) and closed (modulator locked) forms can be interconverted by UV and visible light irradiation. c) Schematic representation of the gel obtained by copolymerization of 23 and 24, and of the braiding and unbraiding of its chains, induced respectively by UV and visible light irradiation. Adapted with permission[76].

This work constitutes a promising strategy to exploit the activity of molecular machines by projecting a functional and flexible material such as a polymer which could be employed in many different and innovative applications.
Regarding other possible employments of molecular switches and motors nowadays a lots of possibilities has been investigated, among them we find switchable catalysis[93,94,95], transmission of motion along molecular components[96,97], modification of surfaces[98] but also implementation in different materials such as crystals[99,100].

2 LIGHT EFFECTED SUPRAMOLECULAR PUMPS

2.1 Aim of the project and introduction

Molecular pumps are usually linear motors in which a molecular component is directionally transported with respect to the motor unit[81]. To render the transport active this should be intrinsically operated by the motor employing a suitable energy source with no effect from external concentration differences in other words, it should occur against a concentration gradient. As such, molecular pumps can be defined as energy transducers which are able to convert an energy input into a chemical potential leading to a nonequilibrium state[101]. These features are opposed to the ones of passive transporters, which basically help the system to relax and to reach equilibrium. An important inspiration comes from nature where controlled transport of molecular and ionic substrates across biological membranes delimits and separates compartments performing a fundamental task for living organisms.
The system developed in this project consists in a pseudorotaxane assembly in which a molecular ring moves unidirectionally along a molecular axle in response to an external photochemical stimulation[84]. The molecular pump is composed of a molecular ring (1) and a non-symmetric molecular axle (2) that comprises: a cyclopentyl unit as photoinactive stopper (β) at one end, an ammonium cation as central recognition site for the ring and an azobenzene stopper as bistable photoswitchable unit (α) at the other end (Figure 21a).

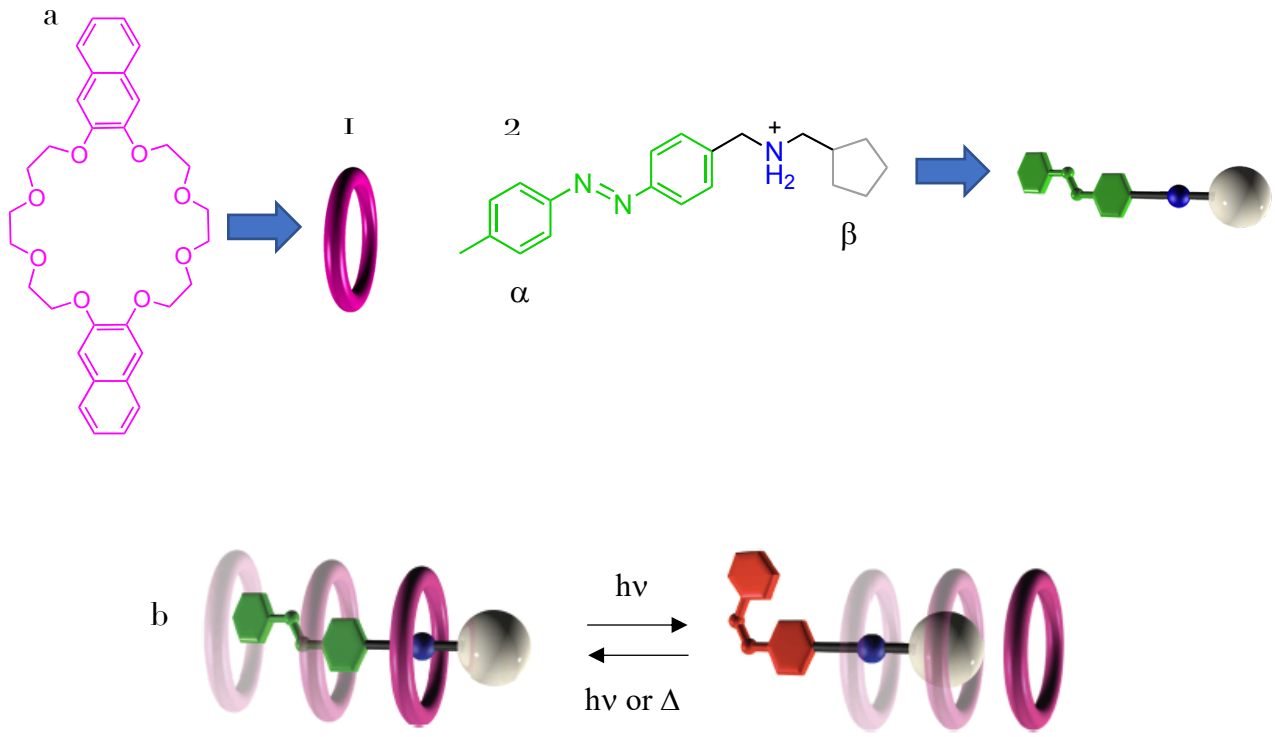

Figure 21 a) Structural formulas of the components. b) Schematic representation of the relative unidirectional translations of the ring and axle components triggered by light.

In the following figure a description of the pump operations step by step can be found (Figure 22). At first, the ring enters exclusively from the E-azobenzene side (α) of the axle for kinetic reasons, forming a pseudorotaxane in which the macrocycle encircles the recognition site on account of hydrogen-bonding interactions between the oxygen atoms and the ammonium center and, possibly, π-stacking forces involving the naphthalene and azobenzene units. Subsequently, light irradiation converts the E-azobenzene unit into the bulkier Z isomer, a process which causes a destabilization of the supramolecular complex and the dethreading of the components. The cyclopentyl unit β comprised in the axle can be defined as a pseudostopper because it shows a dual role: when the azobenzene is in the E configuration it acts as stopper since the kinetic barrier for the ring to enter from that side is significantly higher. On the contrary, when the azobenzene is on the Z configuration the dethreading of the ring is favored on that side. Finally, upon switching again the azobenzene photochemically or thermally, the reset of the system can be obtained in order to start a new cycle.

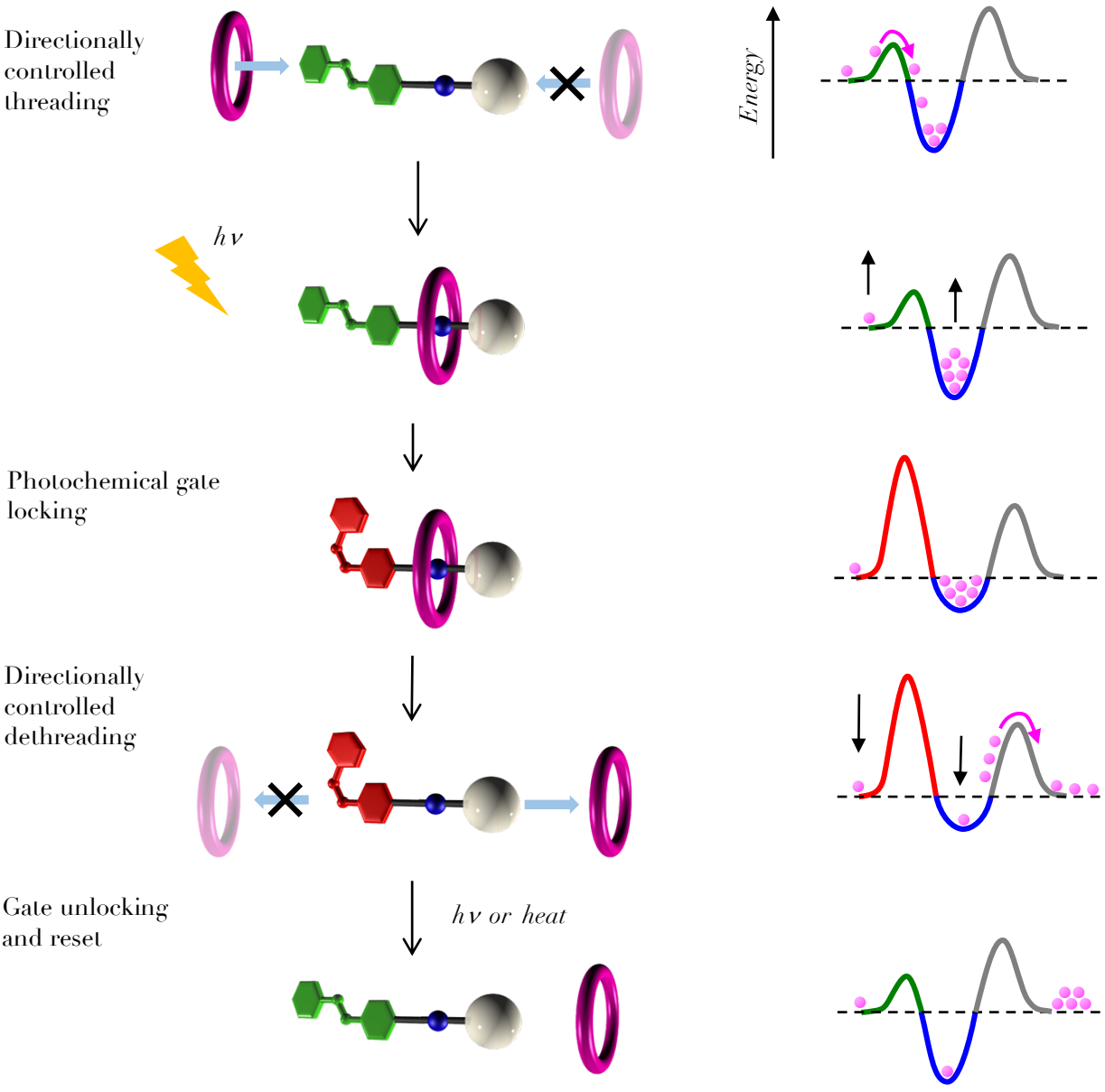

Figure 22 Stimuli-controlled unidirectional transit of the ring along the axle.

To summarize, regarding the thermodynamic point of view, the stability of the ring on the ammonium center is influenced mainly by the switching of the azobenzene, in fact, while E azobenzene favors the formation the complex, the Z isomer, because of his different geometry, leads to an increase of the steric hindrance on the axle causing a destabilization of the complex. To confirm this behavior titration experiments were performed which showed a higher binding constant for the E-axle with the respect of the Z-axle.
Similarly, when the azobenzene is in the Z configuration it behaves as a stopper causing a significant increase of the threading kinetic barrier[84]. As shown in the figure by the indicative energy profiles on the right (Figure 22), the unidirectional controlled transit of the ring along the axle and the ratchet of the system is achieved by means of a precise modulation of the energy surface and more specifically of the ratio between the kinetic and thermodynamic parameters relative to the trans and cis complex.
The presence of the azobenzene unit in the role of photoswtichable gate of this system, is very important as it allows to modify the configuration of the assembly without the introduction of any other chemical fuel. This approach is very smart as it avoids the production of chemical wastes which can be complicated to remove during the operation of the pump.
The steps sequence reported above, comprising the association/dissociation reactions and the photoisomerization processes, can be described as a cycle under continuous illumination conditions (Figure 23). The activity of the pump, in dark conditions, following the principle of detailed balance[102], reaches the chemical equilibrium. In this case the ratio of the horizontals processes constants is equal to the vertical one and all the rates are equal to zero (Figure 23, left green box). However, upon the introduction of a suitable light energy input in the two photoisomerization vertical steps of the cycles the equilibrium regime is not respected leading to a dissipative regime in which the rates tend to the same value correspondent to the obtained PSS state (Figure 23, right yellow box). In other words, by means of light irradiation an out-of-equilibrium[103 105] stationary state is reached, which determines a clockwise net flux of species along the square network of reactions that lasts as long as photons are absorbed. Therefore, in this device under continuous illumination, light energy activates and controls both the nanoscale directional transit of the ring (unidirectionality) and the macroscopic flux of the species along the closed reaction network (monodirectionality).

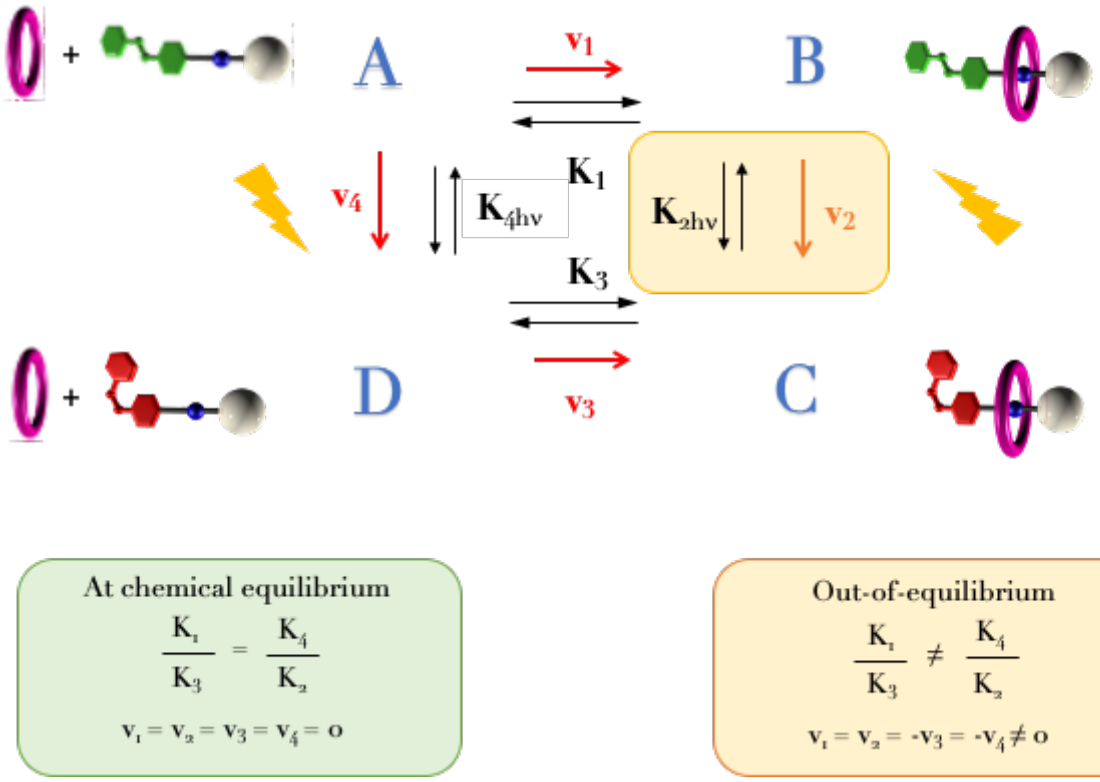

Figure 23 Top: Scheme of the pump operations cycle. Bottom: Equations describing the chemical equilibrium (left) and the out-of-equilibrium regimes (right)

Furthermore, a remarkable feature of this molecular pump is represented by its autonomous behavior. In fact, thanks to the overlap between the absorption spectra of E and Z azobenzene, both photoisomerizations can be triggered by means of a unique light stimulus or, in other words, by irradiating at a single wavelength.
The described molecular pump cycling operation can be activated by means of different irradiation wavelengths. Depending on the chosen wavelength different types of ratchet mechanism can be obtained, for instance by irradiating at 365 nm $K_{2h\nu}$ is higher than $K_{4h\nu}$ because the E-complex has a higher absorption with the respect of sum of the E-axle and the ring, for this reason the cycle tends to operate in a clockwise fashion. This is defined as information ratchet; for the same reason by irradiating at 287 nm an energy transfer from the ring to the E-axle selectively occurs and again $K_{2h\nu}$ is higher than $K_{4h\nu}$. Differently, when visible light is employed (436 nm), $K_{2h\nu}$ results equal to $K_{4h\nu}$ however, K_1 is still higher than K_3 thus, also in case (energy ratchet) the clockwise fashion is kept.

2.2 The role of the pseudostopper: precise modulation of the threading/dethreading

To optimize the chemical design of the molecular pump for different applications, several strategies can be adopted depending on which part of the axle or the ring is eventually modified (Figure 24). In a previous investigation the functionalization of the azobenzene unit was studied[106]. Moreover, the substitution of the PF_6^- counterion was studied by preparing several alternative threads. This study is important because it confirms the high influence of the ionic couple in the resulting binding stability of the ring. In fact, PF_6^- which is a non-coordinating ion gave the highest K_{ass} in the analyzed pseudorotaxane, however, other ions characterized by a stronger ionic as ClO_4^- lead to a lower K_{ass}.

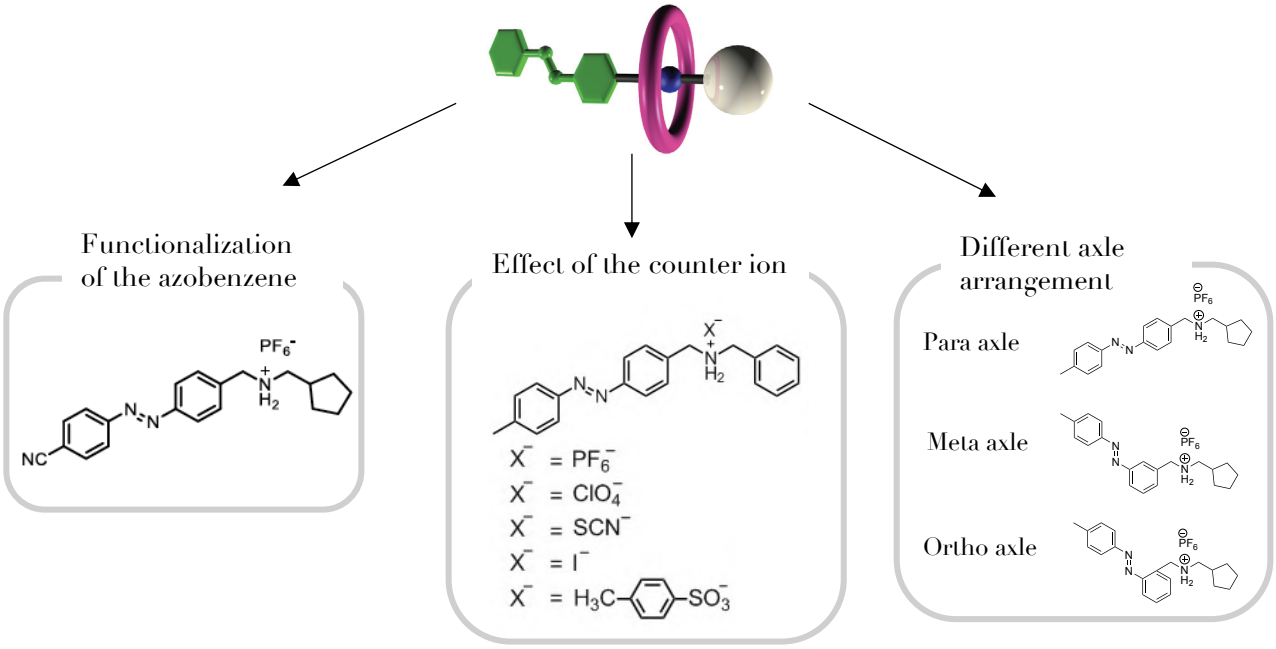

Figure 24 Schematic summary of the developed alternatives to the original molecular pump structure.

Furthermore, the original para configuration of the axle was also investigated in the meta and in the ortho substitutions. The effect of the overall configuration of the assembly on the kinetic and thermodynamic parameters is currently being evaluated.
The ring component represent a further important option in the modification of this structure. In fact, an interesting possibility is to functionalize the macrocycle with a fluorophore such as coumarin or naphthalene. In this way, the ring can become a "tool" to read the system. In previous studies it was seen that, upon association with the axle, the fluorescence signal of the ring is quenched. As such, the association percentage between the axle and the ring can possibly be correlated with the emission signal intensity.
Another direct approach is to replace the pseudostopper with a molecule or a group showing similar steric hinderance with the respect to the cyclopentyl unit (β). A suitable option in this case is an appropriately substituted phenyl ring, thus, a library of symmetric dibenzylammonium-type compounds was synthetized and investigated (Figure 25). The thermodynamic and kinetic features of the self-assembly of the new guests with the ring component 2,3-dibenzo[24]crown-8 ether (DB24C8) were evaluated by means of UV-vis and NMR spectroscopy [107].

This family of compounds was carefully selected because of their structural similarity which leads to a comparable binding affinity for the ring. Moreover, they represent a homogeneous group also in terms of solubility features. Another point is the direct synthetic strategy with the respect to the inclusion of cycloalkanes units as introduced in previous works[108].

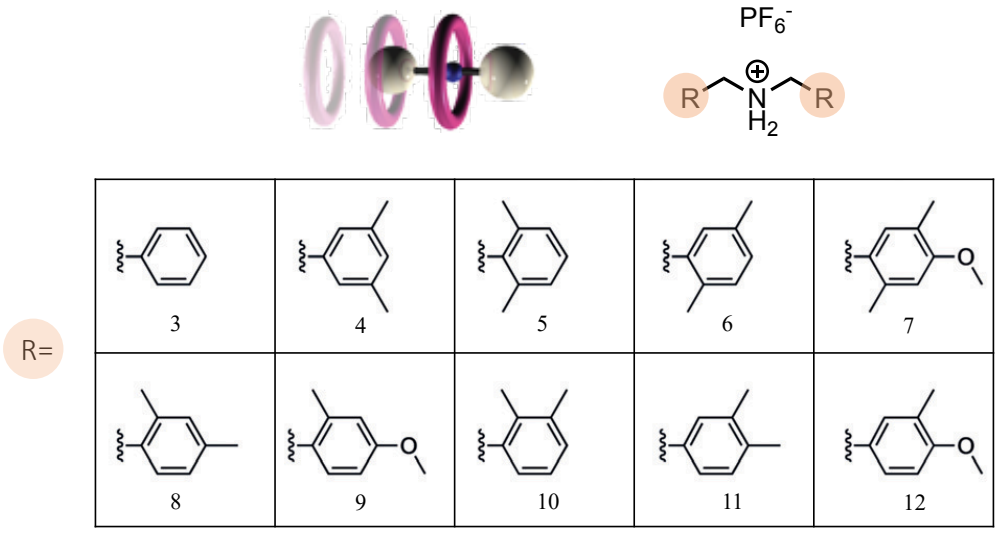

Figure 25 Structural formulas of symmetric dibenzylammonium salts investigated as guests for DB24C8.

Among the analyzed compounds 8 and 9 showed promising features to be implemented in the molecular pump. Having studied by means of NMR spectroscopy the formation of the complex in dichloromethane the corresponding UV-vis spectra were examined with a sum/mix experiment as well (Figure 26). The experiment consists in measuring the spectrum of the 2 separated compounds as the sum of the absorptions and afterwards to record the spectrum of the mixed species which is supposed to be different from the previous upon the association of the components.

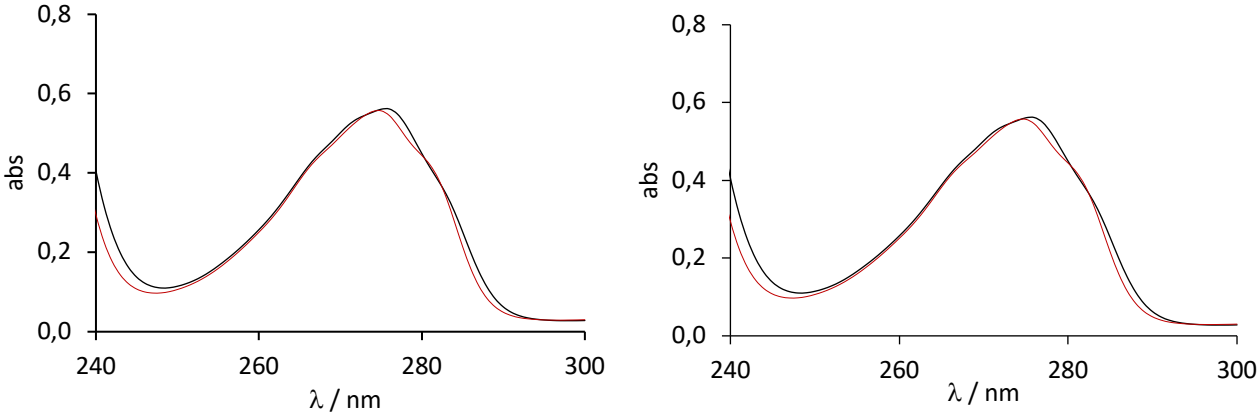

Figure 26 Sum of the absorption spectra of separated CH_2Cl_2 solutions of DB24C8 and 8 (left) and 9 (right) (black line) and absorption spectrum of the same solutions after mixing (red line). Concentrations in the mixture: [DB24C8] = [8] = 5.5 x 10^{-5} M (left) [DB24C8] = [9] = 1.84 x 10^{-4} M (right). The reported experiments were carried out by using dedicated spectrophotometric cells with divided sections.

The thermodynamic parameters of the investigated pseudorotaxanes were studied and the binding constant with DB24C8 was calculated from UV-vis titration experiments in CH_2Cl_2 by adding a concentrated solution of the axle to a more diluted (10^{-4} M ca.) solution of the ring. The changes in the spectrum correspondent to the formation of the pseudorotaxane were monitored and subsequently fitted at the selected wavelengths with a 1:1 binding model (Figure 27).

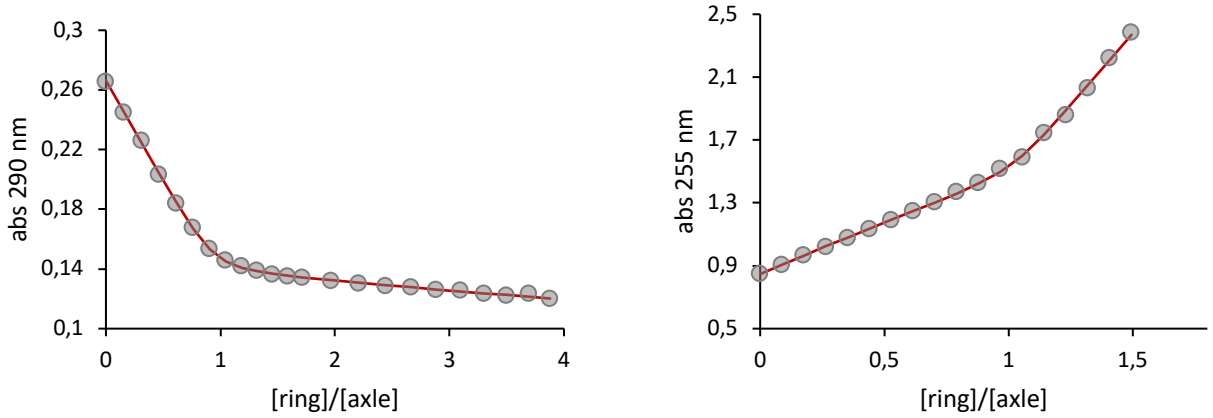

Figure 27. Absorption changes of a 4.5 x 10^{-4} M (left) and 2.5 x 10^{-4} M (right) solution of DB24C8 in CH_2Cl_2 upon addition of 8 (left) and of 9 (right), together with the fitted curve corresponding to a 1:1 binding model.

The calculated constants are 1.7 ± 0,7 (x 10^5 L mol^{-1}) for 8 and 7 ± 2 (x 10^5 L mol^{-1}) for 9; the results show a decrease of the binding constants with the respect of the unsubstituted dibenzylammonium 3 which has a constant of 22 ± 4 (x 10^5 L mol^{-1}). This difference, coherently with previous studies[109], could be caused to the presence of electron-donor substituents which lowers the hydrogen bond donor ability of the NH_2^+ unit and of the adjacent benzylic moieties and consequently the interactions with the crown ether.
The kinetic properties of 8 and 9 were examined as well in order to learn more about the threading process. The following experiments were performed by rapid mixing of the components in equimolar concentrations. After the addiction, the changes in the UV-vis spectrum associated with the formation of the complex were monitored and fitted with a second order kinetic model (Figure 28).

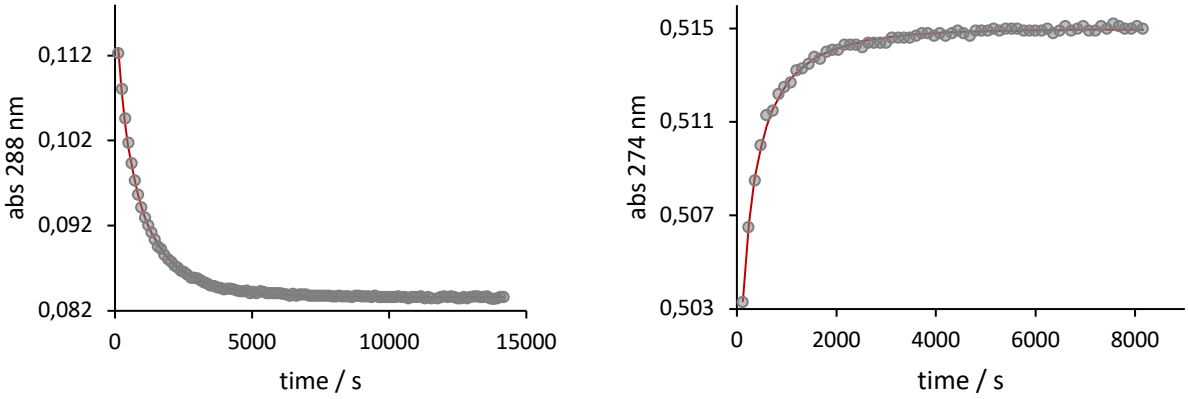

Figure 28 Time-dependent absorption changes at 288 nm (left) and 274 (right) recorded upon mixing DB24C8 and 8 (top) or 9 (bottom) in CH_2Cl_2 at 298 K. Concentrations after mixing: [DB24C8] = [8] = 1.0 x 10^{-4} M (left) and [DB24C8] = [9] = 7.8 x 10^{-5} M (right). The red solid line represents the data fitting.

The obtained constants for the threading process (K_{in}) are: 12 ± 1 ($L\,mol^{-1}\,s^{-1}$) for 8 and 34 ± 1 ($L\,mol^{-1}\,s^{-1}$) for 9. The results suggest that the replacement of a methyl group for a methoxy group in the 4-position has an accelerating effect on the threading process however, this conclusion is not always true for differently substituted axles.
In the following table the summary of all the obtained kinetic and thermodynamic values for the examined structures is reported. The dethreading constant is calculated from the fitting of the kinetic traces with an equilibrium model (second-order threading and first-order dethreading) in which the binding constant was fixed to the value obtained from the titrations (table 1).

Guest[a]	K [$x\ 10^5\ L\ mol^{-1}$][b]	k_{in} [$L\ mol^{-1}\ s^{-1}$][c]	k_{out} [s^{-1}][d]	$t_{1/2}$ [min][e]
3	22 ± 4	>2 x 10^7[f]	<9	<0.003
4	[h]	<7 x 10^{-5}[h,i]		
5	[h]	<7 x 10^{-5}[h,i]		
6	8 ± 3	37.9 ± 0.4	(4.7 ± 0.5) x 10^{-5}	246
7	[h]	<7 x 10^{-5}[h,i]		
8	1.7 ± 0.7	12 ± 1	(7.0 ± 0.7) x 10^{-5}	165
9	7 ± 2	34 ± 1	(4.9 ± 0.2) x 10^{-5}	236
10	[h]	< 7 x 10^{-5}[h,i]		
11	[j]	[j]		
12	[h]	<7 x 10^{-5}[h,i]		

Table 1. [a] Shaded entries highlight the axles that undergo fast threading. [b] Binding constant. [c] Threading rate constant. [d] Dethreading rate constant. [e] Half-life of the complex, calculated as $t_{1/2}=\ln 2/k_{out}$. [f] The process is faster than the time resolution of our stopped-flow spectrometer; lower limiting value of kin determined as described in the SI. [g] Estimated as $k_{out}=k_{in}/K$. [h] No complex is detected by ^{1}H NMR after 72 h. [i] Upper limiting value determined as described in the SI. [j] Data could not be obtained because of the poor solubility of axle 11 in CH_2Cl_2. Measurements performed in acetonitrile indicate that this axle belongs to the "threading" category.

Regarding the kinetic behavior of these pseudorotaxanes, differently from dibenzylammonium 3, which shows an instantaneous threading, upon the functionalization of the benzyl group with one or two methyl substituents the rate decreases consistently by at least five orders of magnitude.
Another significant conclusion is that by just modifying the relative position of the two methyl substituents on the phenyl ring (for example 4 and 5 in comparison with 6 and 8) the threading is allowed or completely prevented. This effect, observed in a precedent work[110], indicates that the threading relies on precise size complementary requirements, moreover, the conformational freedom of the components is important as well.
To gain further on the different properties of the analyzed complexes computational investigations were performed in collaboration with the group of Prof. Ettore Fois (University of Insubria). In particular, the complexes of DB24C8 respectively with 8 and 10 were modeled. These pseudorotaxanes, which differ only for the relative position of one methyl substituent, were chosen as two interesting examples of the "threading" and "non-threading" cases.

Initially, both the gas-phase structures were studied at the equilibrium and solvatated at 300 K. The data indicate that the assemblies are similar because of the presence of hydrogen bonds and π π stacking interactions of comparable strength. At this point the dethreading process was simulated by means of ab initio metadynamics calculations. The dethreading was chosen mainly because it results less affected by the solvent reorganization and provides the features of the pseudostopper unit in the role of "speed bump". For each structure, the displacement of the axle with respect to the ring was reported as a "reaction coordinate". The free energy changes observed during the transit of the axle through the macrocycle were monitored (Figure 29).

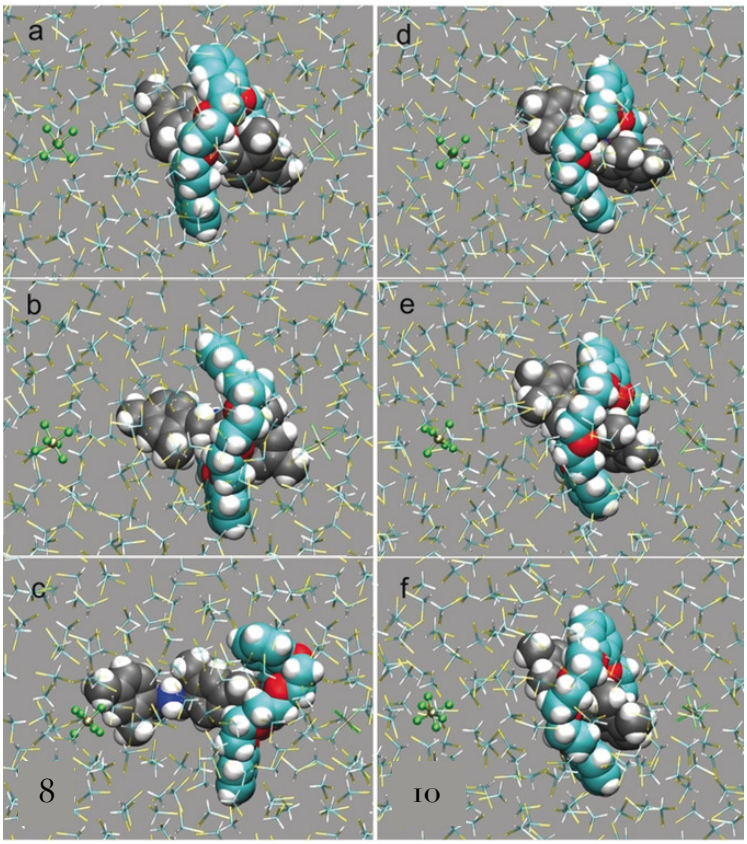

Figure 29 a c) Snapshots from the calculated dethreading path of the complex of DB24C8 with guest 8: a) initial state (threaded); b) transition state (partially dethreaded); c) final state (dethreaded). d f) Snapshots from the metadynamics simulation of the complex of DB24C8 with guest 10, which predicted no dethreading. The atoms belonging to the complex are shown in a space-filling representation; color codes: C (ring)=cyan spheres; C (guest)=grey spheres; O=red; N: blue; H=white. Atoms of the solvent (CH_2Cl_2) and counterion (PF_6^-) are shown in a stick and ball-and-stick representation; respectively; color codes: C=cyan, Cl=yellow, H=white, P=light grey, F=green. Adapted with permission[107].

The data reveal an evident difference between 8 and 10; while the exit of 8 only need about 20 kcal mol^{-1}, the same process for 10 occurs with not less than 100 kcal mol^{-1} (Figure 30). Moreover, the larger displacement of 10 is observed when both phenyl rings are still located within the ring cavity (Figure 29 e, f). Differently, considering the same profile for 8, one phenyl unit is already outside the ring at the free energy maximum (Figure 29 b)

and the dethreading is essentially completed at the end of the simulation. The exit profile of 8 and 10 indicate that both the axles are stably hydrogen bonded to the ring furthermore, 8 is observed to bind different oxygen atoms in the macrocycle. This difference can also confirm the role of the hydrogen bond in the overcoming of the dethreading barrier. The distortion of the ring during the process was also compared in the two complexes. While for 8 this effect is not pronounced, during the exit of 10 the ring elongates significantly. However, this rearrangement is still not sufficient to allow the guest exit (Figure 30).

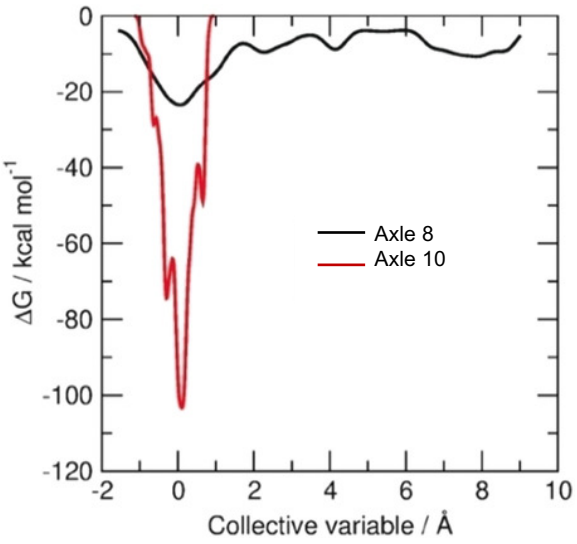

Figure 30 Free energy profile for the dethreading of the complexes of DB24C8 with guest **8** (black line) and **10** (red line) as a function of the displacement of the axle, defined by the collective variable. The latter is selected as the displacement of the 9 carbon atoms of one phenyl unit of the axle (including the C atoms of its two methyl substituents and of the methylene group) with respect to the 10 oxygen atoms of the macrocycle. The free energy cost associated to dethreading of **8** is 19.8 kcal mol^{-1}, while no dethreading can occur for $\mathbf{8}^{+}$ (free energy barrier above 100 kcal mol^{-1}). Adapted with permission[107].

Concluding, after an extensive study of the kinetic and thermodynamic features of these guests by means UV-vis and NMR spectroscopy and with the support of computational studies, the behavior of the different complexes could be distinguished in two categories depending on the relative position of the substituents. The first class is characterized by an effective formation of the complex (guests 8, 11, 6), and the second one by the absence of the threading process (guests 4, 5, 10) (Figure 31).

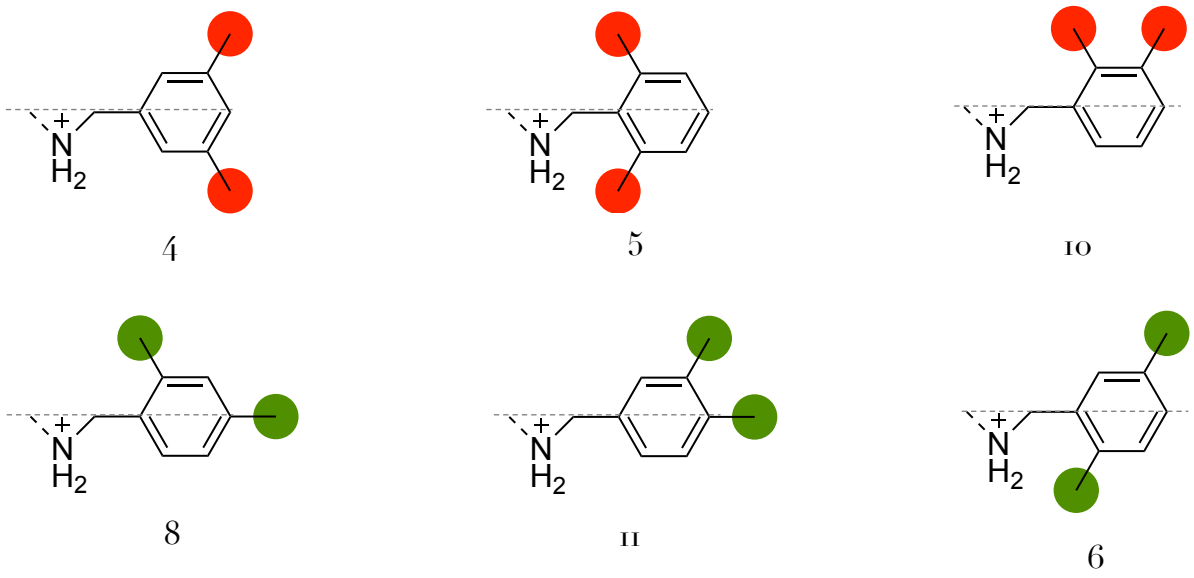

Figure 31 Correlation between the substitution pattern and the kinetic behavior of DB24C8 threading for symmetric dibenzylammonium type guest with two methyl substituents in each phenyl ring. (4, 5, 10) "Non-threading" category, methyl indicated in red. (8, 11, 6) "Threading" category, methyl indicated in green. The gray dashed line represents the axis correspondent to the transit direction.

In light of these results the implementation of a new pseudostopper in the axle 2 structure (described above) was investigated. The right candidate for this role was chosen in order to maintain a high equilibrium constant with the ring ($K > 10^5$) and moreover, proper kinetic features. In other words, a suitable pseudostopper needs to have a lower kinetic value with the respect of E azobenzene threading and, at the same time, a higher threading rate when the azobenzene is switched to the Z configuration. This balance between the kinetic and thermodynamic properties of the system is necessary to obtain a controlled and unidirectional transit of the ring along the axle.

2.3 Second generation molecular pumps

The pseudostopper which was selected for the incorporation in the axle component of the molecular pump (Figure 32b) is the 2,4 dimethyl-phenyl unit (Figure 32a) which showed suitable kinetic and thermodynamic properties.

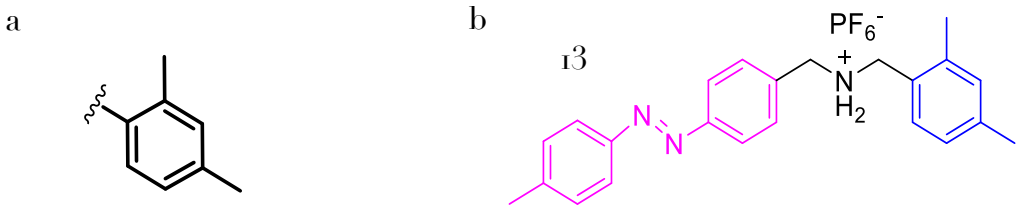

Figure 32 Structural formulas of the selected pseudostopper (a) and of the new molecular axle 13.(b)

The association properties of the axle 13 were studied with dinaphtho-[24]crown-8 (DN24C8) in CH_2Cl_2 by NMR and UV-vis spectroscopy. In the following figure the absorption spectra of DN24C8 and of the axle are reported (Figure 33).
In the spectrum of the E-axle (green line) the typical azobenzene unit signals are present: the first stronger band is relative to the π–π* transition band centered at 332 nm while the second one between 390 nm and 550 nm corresponds to the weaker n-π* transiotion band. The axle can be photoisomerized to the Z configuration by irradiating at 365 nm, the red spectrum corresponds to the Z-axle. More details about the photoisomerization processes will be given in the next paragraphs.

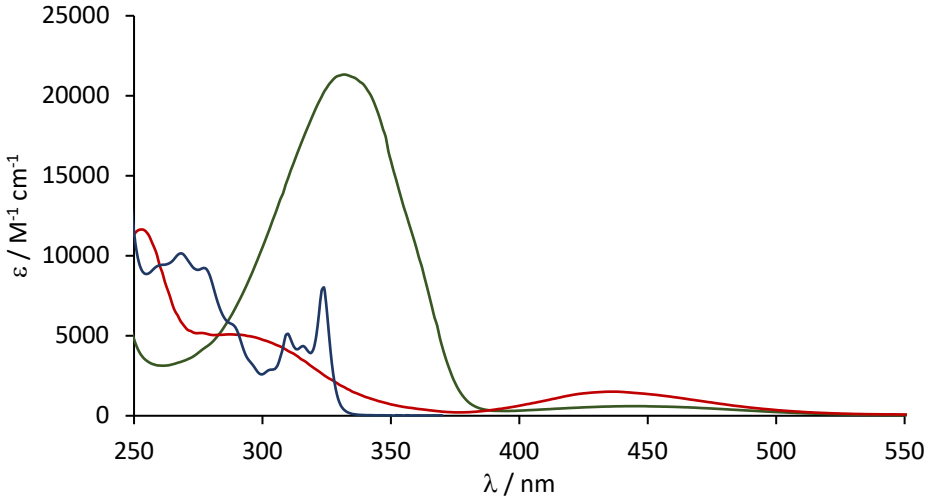

Figure 33 Absorption spectra of the E-axle (green line), Z-axle (red line), DN24C8 (blue line) (CH_2Cl_2, r.t.).

In the next figure the sum/mix experiments for the E-axle and for the Z-axle are reported (Figure 34).

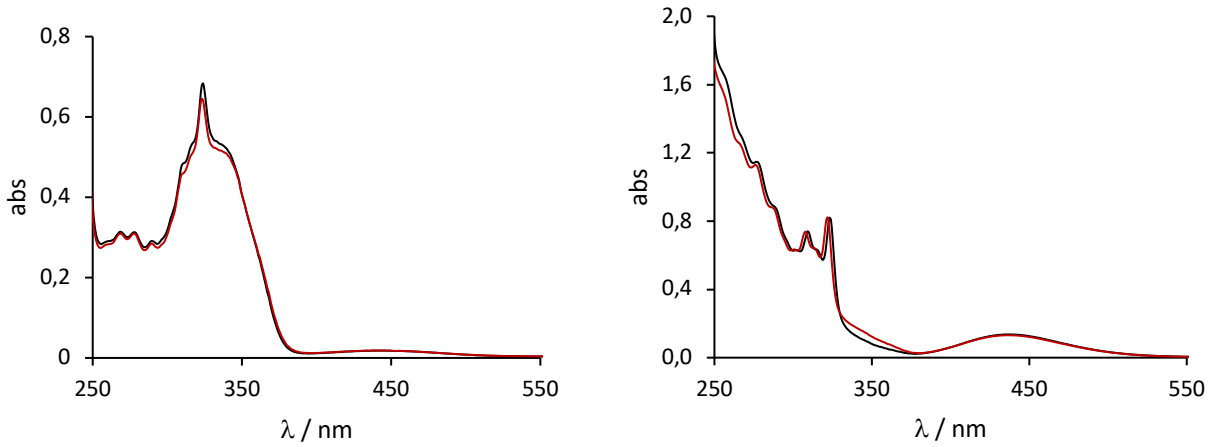

Figure 34 Sum of the absorption spectra of 86 µM DN24C8 and E-axle (left), and of 200 µM DN24C8 and Z-axle (right), and absorption spectrum of the mixture of the two compounds (red line) (CH_2Cl_2, r.t.).

The results indicate that the formation of the complex occurs in both cases, in fact, the spectrum of the sum of the components where there is no interaction between the reagents present several differences with the respect to the relative complex both for the E and for the Z axle.

Furthermore, the threading kinetics have been measured by means of UV-vis experiments, the data were subsequently fitted with as a second-order threading and first-order dethreading (Figure 35).

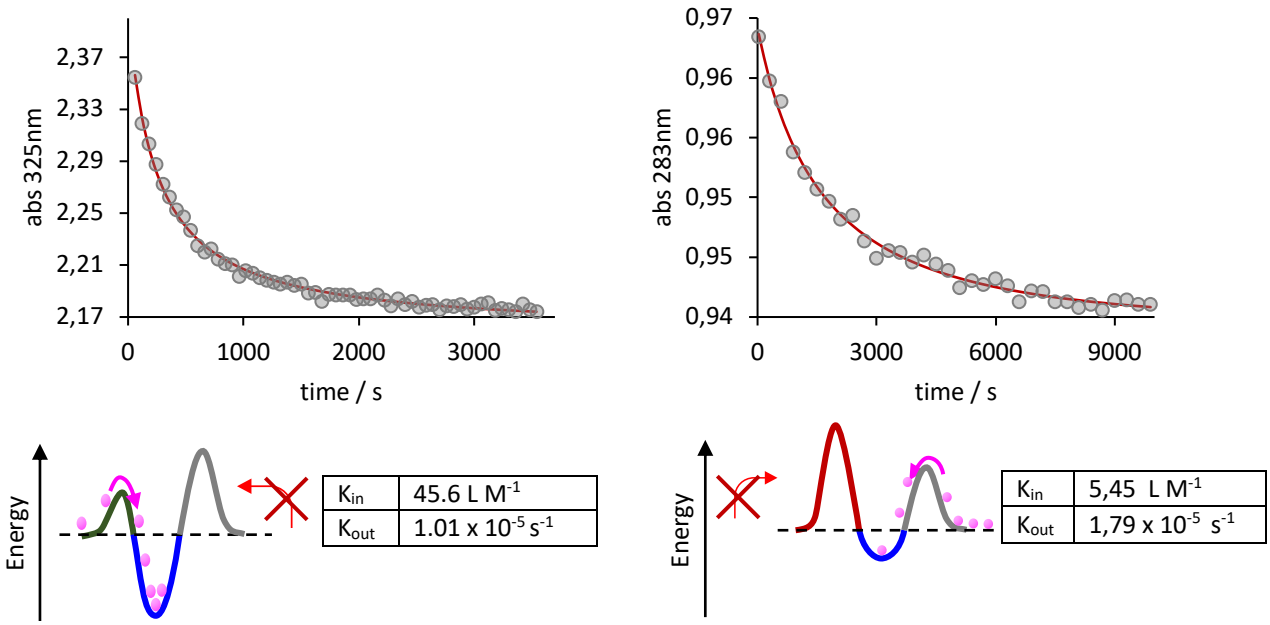

Figure 35 Time-dependent absorption spectra changes observed upon mixing 0,1 mM DN24C8 with 0,1 mM E-axle (left) and Z-axle (right). The full line represents the data fitting according to a kinetic model consisting of a second-order threading and an opposed first-order dethreading (CH_2Cl_2, r.t.).

The data reveal that, as for the previously studied system, the threading process relative to the E-axle is more than 6 times faster with the respect to the Z-axle. Consequently, this ratio between the kinetics values, allows to obtain the desired unidirectional transit of the ring along this asymmetric axle. As shown in the energy profiles (Figure 35), in fact, while the low kinetic barrier of the E-axle favors the threading process on the contrary, when the azobenzene is switched to the Z configuration, the correspondent barrier (represented in red) increases significantly acting as a closed gate for the ring.
Regarding the thermodynamic properties of the system UV-vis titrations experiments were performed. In this case the fluorescence signal of DN24C8 was exploited to investigate the formation of the complex.
During the complexation with the axle a quenching of the emission of the ring is observed, this is caused by an energy transfer from the naphthalene units in DN24C8 to the azobenzene moiety of the axle.
For this reason, the progressive fluorescence quenching of the emission signal of DN24C8 can be correlated with the formation of the pseudorotaxane.
In the next figures spectroscopic titrations are reported were a concentrated solution of 13 was progressively added to a solution of DN24C8 (Figure 36), after each addition the emission spectrum was recorded.

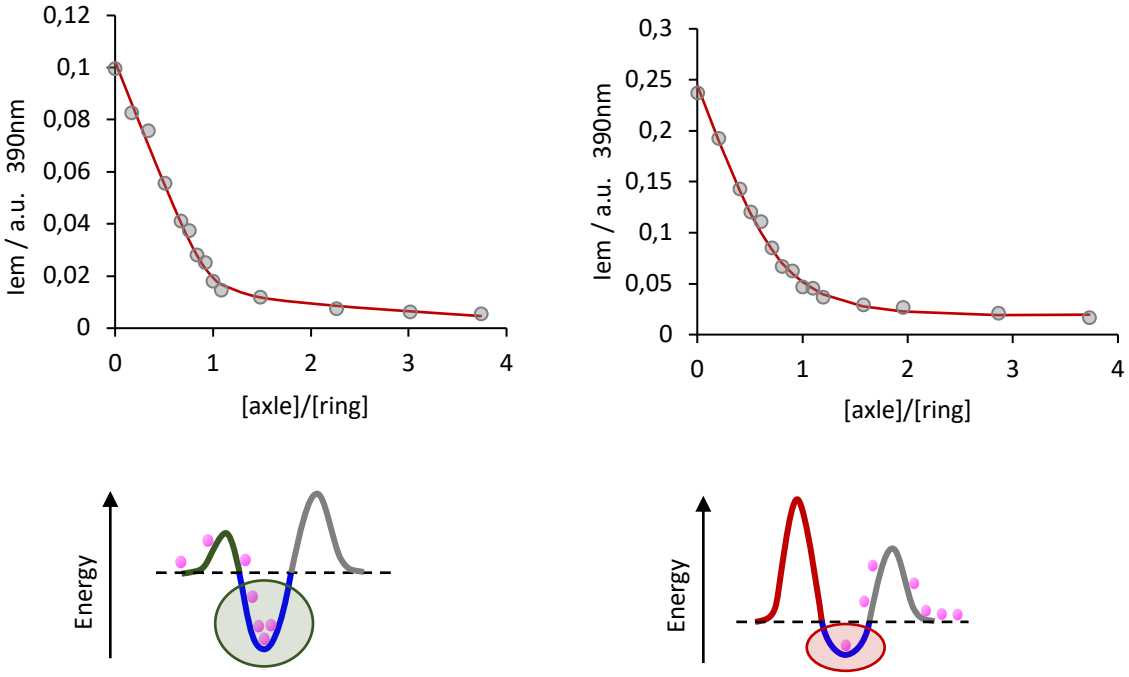

Figure 36 Titration curves, obtained from emission intensity values (λ_{exc} = 281 nm), observed upon addition of E-axle (left) and a Z-axle (right), to a 50 μM solution of DN24C8. The full line represents the data fitting according to a 1:1 binding model. (CH_2Cl_2, r.t.).

The titrations curves have been fitted at 390 nm in order to minimize the reabsorption contribute from the axle while, it was chosen to excite the solution at 281 nm because this represents an isosbestic point between the E and the Z-complex.
The calculated equilibrium constants were 4,5 x 10^6 $Lmol^{-1}$ for the E-complex and 3 x 10^5 $Lmol^{-1}$ for the Z-complex.

Remarkably, the results confirm the hypothesis of an enhanced stability of the E-complex and of a significant decrease in depth of the energy well upon the switching of the azobenzene unit. In fact, the equilibrium constant decrease by ca. one order of magnitude. As a consequence, the destabilization of the ring upon the photoisomerization step is obtained and reinforces the efficiency of the ratchet mechanism during the cycling operation of the pump. Summarizing, all the obtained data are promising results for the employment of the axle 13 as a new candidate for the molecular pump.
At this point the photoisomerization quantum yields of the azobenzene in the axle were examined (Figure 37).

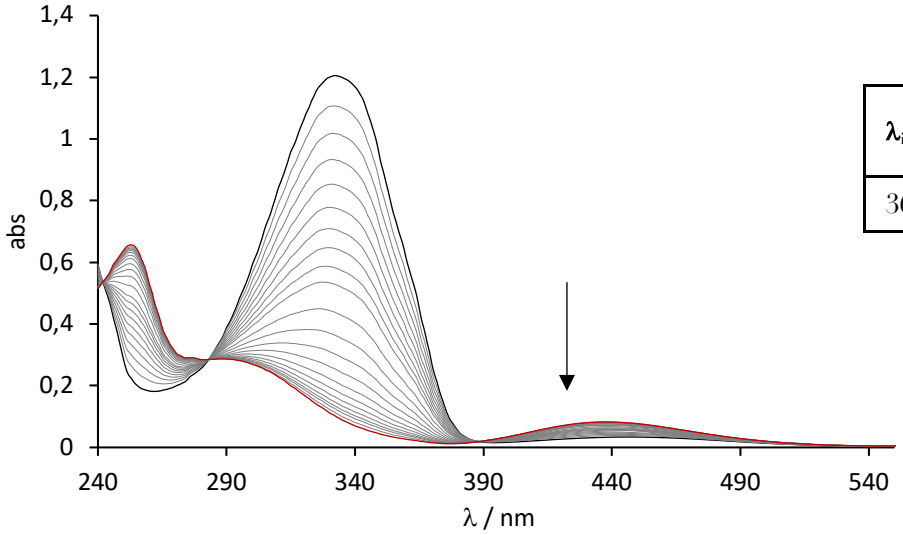

λ_{irr}	$\Phi_{E->Z}$	E/Z PSS%
365 nm	0.17	96%

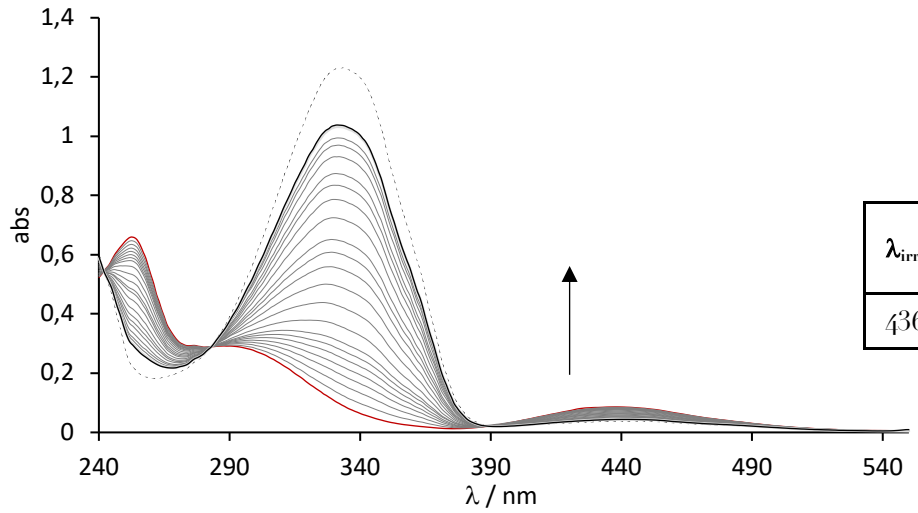

λ_{irr}	$\Phi_{Z->E}$	E/Z PSS%
436 nm	0.65	84%

Figure 37 Top: Absorption spectrum of 56 μM E-axle (black line), and spectral changes observed upon irradiation of the solution at 365 nm, showing the occurrence of the E→Z photoisomerization. Absorption spectrum of Z-axle (red line) **Bottom:** Absorption spectrum of 56 μM Z-axle (red line), and spectral changes observed upon irradiation of the solution at 436 nm, showing the occurrence of the Z→E photoisomerization. Absorption spectrum of the obtained PSS (black line). Absorption spectrum of the initial E-thread (dashed line). (CH_2Cl_2, r.t.).

The E→Z photoisomerization was obtained by irradiating a 56 μM solution of the free E-axle at 365 nm. Upon irradiation, typical spectral variations relative to the formation of Z azobenzene were observed and a stable PSS% (96% Z-axle) was reached.
The calculated quantum yield was 0,17, this value is comparable with the previously studied structures.
Furthermore, the opposite Z→E photoisomerization process was obtained by irradiating a 56 μM solution of the free Z-axle at 436 nm reaching a PSS% composition of ca. 84% E-axle. The calculated quantum yield valued in this case is 0,65.
Analogues irradiation experiments were performed with an associated axle solution maintaining equal experimental conditions.
Interestingly, the quantum yields values and the PSS% remained unchanged, this observation indicates that the presence of the ring has no noticeable effect on the efficiency of the photoswitching reactions.
Regarding the thermal back isomerization, the process was monitored by UV-vis spectroscopy in dark conditions (Figure 38).

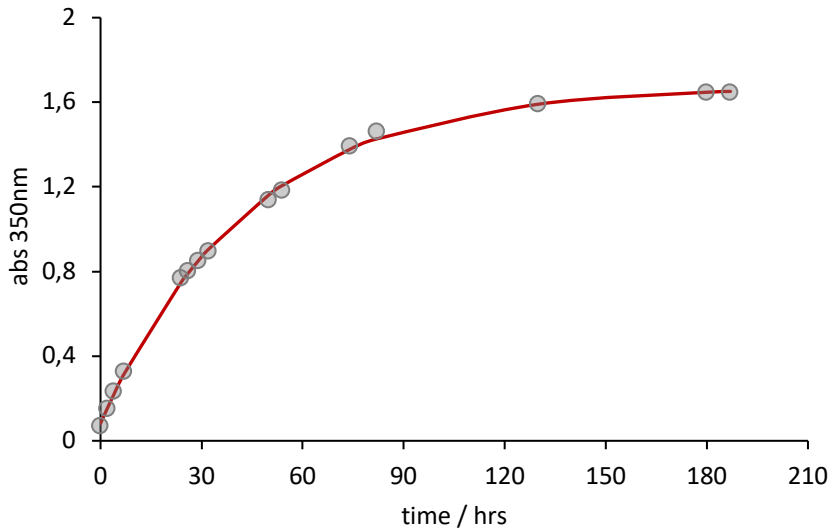

Figure 38 Time-dependent absorption changes at 350 nm observed on a 100 μM solution of Z-thread in the dark, highlighting the occurrence of the Z→E thermal isomerization. The red line represents the data fitting according to a first-order kinetic equation. (CH_2Cl_2, r.t.)

The thermal relaxation of the system is a relatively slow process which is usually completed in several days at room temperature. In this specific case, the azobenzene unit included in axle 13 shows a thermal return kinetic of 6,3 x 10^{-6} s^{-1} and it's completed in ca. 180 hours. Differently, for what concerns the associated axle the process results slightly slower with the respect to the free axle, in this case the calculated constant is 3 x 10^{-6} s^{-1}.
Finally, having extensively characterized the system from the thermodynamic and kinetic point of view; all the obtained parameters were very promising for the application as a photoactive molecular pump.
To investigate the cycling operation of the molecular pump, from a more informative and complete point of view, several experiments were conducted by means of NMR spectroscopy.

Differently from the UV-vis spectroscopy studies, which were performed in dichloromethane, in the case of NMR spectroscopy the employed solvent was a mixture of dichloromethane and acetonitrile in equal ratio 1:1. These conditions were chosen in order to have lower equilibrium constants allowing to observe the peaks relative to both the free and the associated axle. In fact a more polar solvent as MeCN decreases the binding strength between the ammonium and the crown ether, moreover, this ratio ensured the solubility of all the considered species even at the high concentration which is required for NMR experiments[111].

The experimental setup was adapted in order to include an optic fiber which was employed as light source and was incorporated directly inside the NMR tube.

This approach is extremely useful in this case as, differently from UV-vis spectroscopy, it allows to irradiate the system and at the same time to monitor the concentration of the components over time.

Two main experiments were conducted; in both cases the starting point was an equilibrated solution of the E-complex, subsequently a quick irradiation step with a high energy light input (λ_{irr}= 365 nm) was performed to reach an exhaustive E→Z conversion. At this point, in the first experiment the relaxation of the system was monitored in dark conditions for several hours. Contrarily, in the second investigation the operation of the pump was observed in continuous irradiations conditions (Figure 39).

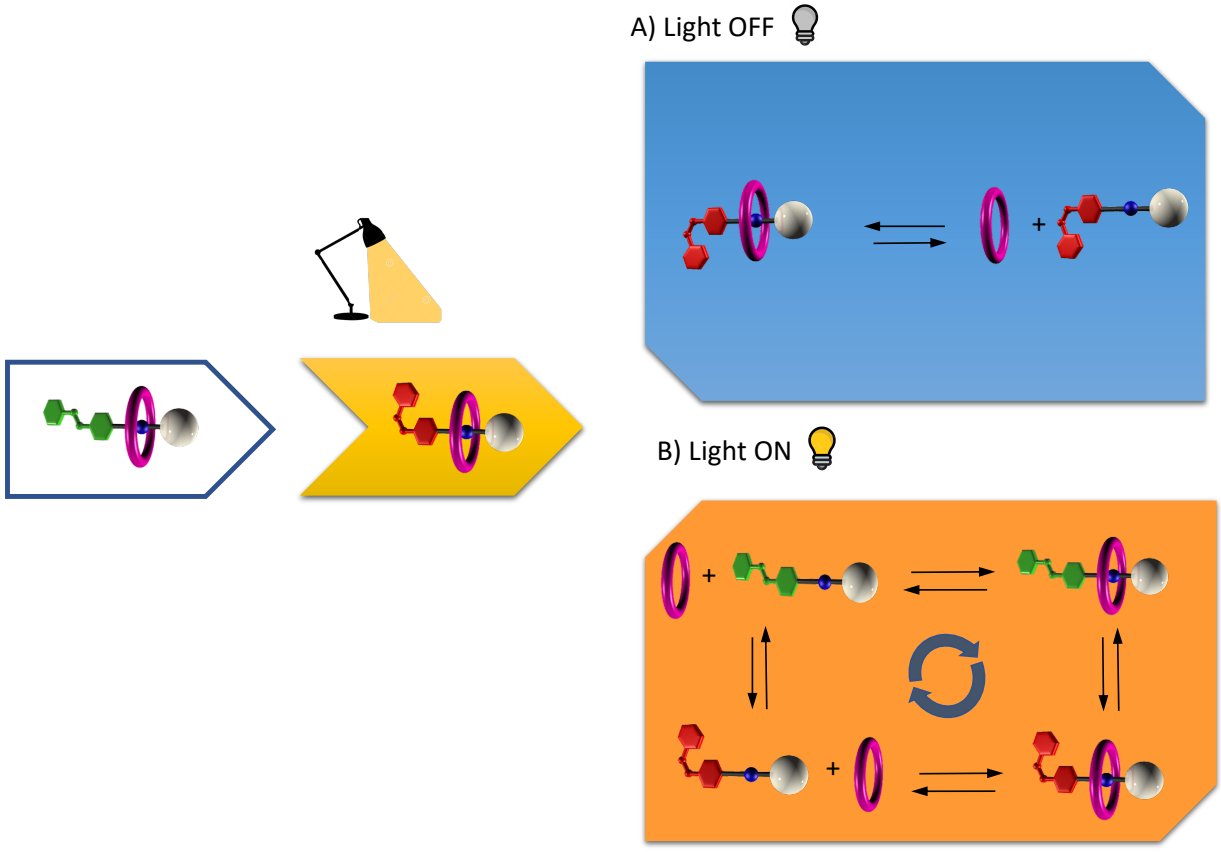

Figure 39 Schematization of the NMR investigations and the relative occurring processes.

The objective of these studies is to understand the differences between the behavior of the system in dark conditions, or in other words relaxing to the equilibrium and with light on conditions when the pump should operate out of equilibrium as explained before.
The data revealed a significant change in the 2 examined conditions, in the following figure for clarity reasons only the concentration of the Z-complex is reported (Figure 40).
During the first light off experiment (blue trace, Figure 40) the pump behaves as expected, in fact, as the equilibrium constant for the Z-complex is remarkably lower with the respect to the E-complex, the ring is supposed to dissociate over time. Moreover, the Z azobenzene will slowly convert back to the E isomer.
Differently, regarding the light on experiment the concentration of the Z-complex in this case is forced to maintain a constant value as long as the irradiation is kept (orange trace, Figure 40). Since the observed value is not compatible with the equilibrium regime concentration the system is considered to be cycling and operating out of equilibrium under continuous illumination conditions. The same considerations can be done to describe the behavior of all the other involved species.

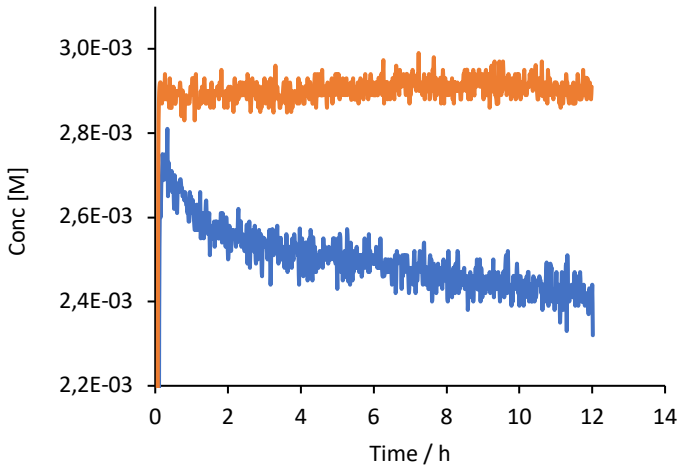

Figure 40 The light on experiment (orange trace) was performed by first irradiating at 100 % light power an equimolar solution of E-complex for 300 s, then lowering the light intensity to 40 %. The system was then left to operate in these conditions for 12 hours. The light off experiment (blue trace) was performed by first irradiating at 100 % light power an equimolar solution of E-complex for 300 s, then switching off the light. The system was then left to evolve toward equilibrium in the dark for 12 hours. (5 mM, CD_2Cl_2 : CD_3CN 1:1, 298K).

Concluding, in light of all the results, both from UV-vis and NMR spectroscopy, this system composed of the axle 13 and the DN24C8 ring, resulted to be a suitable and efficient prototype to be employed as a light effected molecular pump.

2.4 Towards the construction of "molecular reservoirs"

The aim of the development of the molecular pump is to introduce it as a module in bigger and more complex molecular architectures. In this way the pump would become a motor unit which can be exploited for different purposes.
One of the future applications of the described molecular pump involves the synthesis and characterization of an interesting device called molecular reservoir (Figure 41).

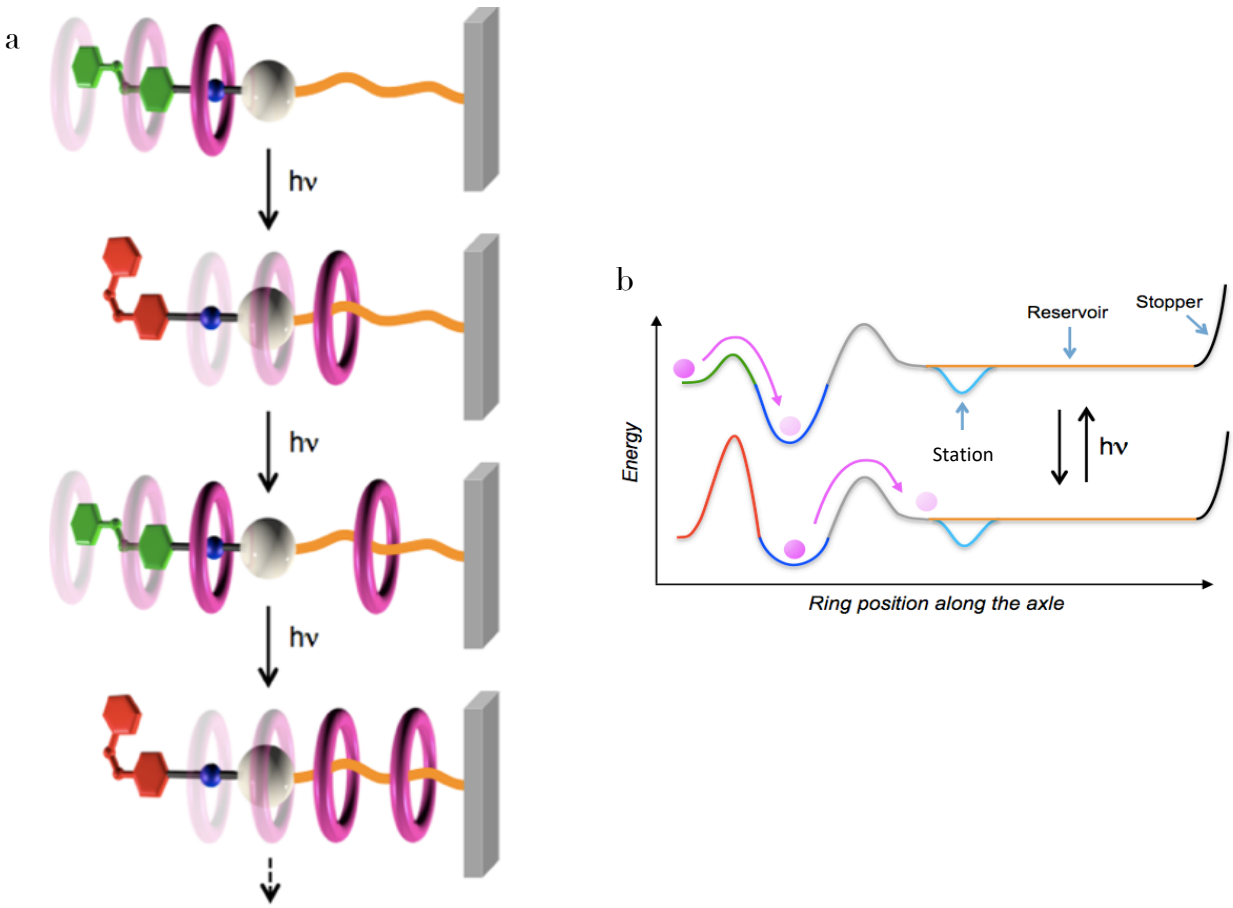

Figure 41 Operations scheme (a), potential energy curves (b).

This supramolecular assembly consists in a molecular pump motor moiety which has been modified by appending an alkyl chain of suitable length at the pseudostopper extremity (Figure 41 a). This chain comprises one or more stations for the ring and is designed in order to act as a reservoir, collecting molecular rings, pumped by light (Figure 41 b).
The study of this system is not trivial as it implies the calculation of several kinetic and thermodynamic parameters which are not always simple to separate from each other due to the structure of assembly.
A possible strategy to simplify this task is to conduct a previous analysis on a proper model compound consisting in the first part of the axle in order to proceed step by step. With this aim the axle 14 was synthetized and studied (Figure 42).

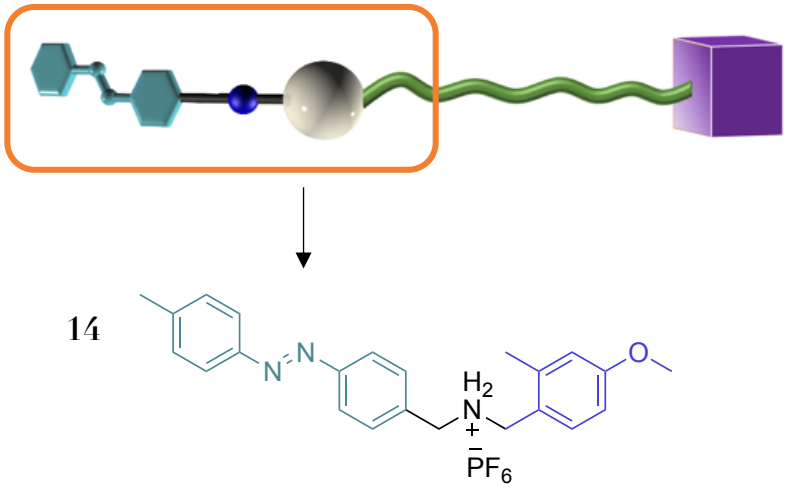

Figure 42 Structure of the model compound (axle 14)

The properties of axle 14 together with a macrocycle (DB24C8) were characterized by means of UV-vis and NMR spectroscopy. In the following figure the absorption spectrum of 14 is reported (Figure 43).

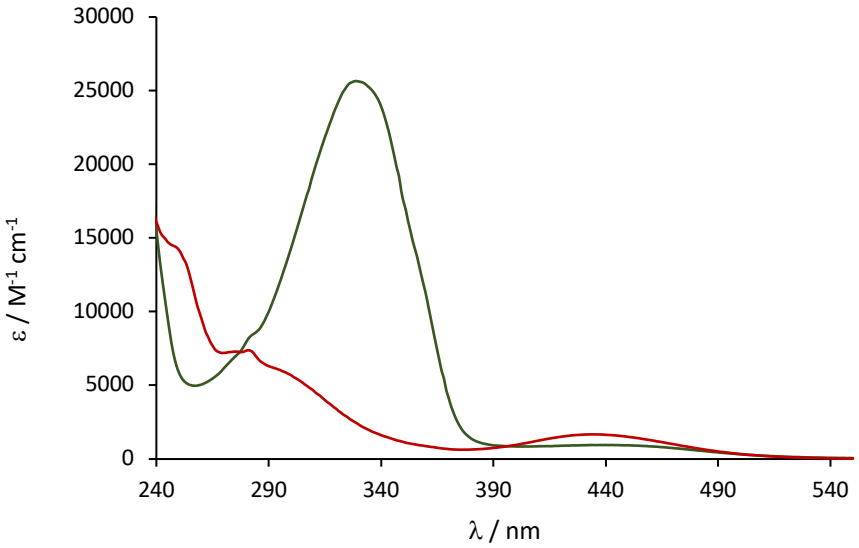

Figure 43 Absorption spectra of 14: E-axle (green line), Z-axle (red line), (CH_3CN, r.t.).

The data are in line with the previously presented axles, showing the two main absorption signals belonging to the azobenzene unit.
Subsequently, the kinetic behavior of 14 together with DB24C8 was characterized in acetonitrile solutions. The selection of the solvent was made in view of the parallel NMR study as explained before.
The equilibrium constant between the axle and DB24C8 is significantly lower in acetonitrile with the respect to dichloromethane consequently, in order to obtain a suitable association percentage it was necessary to increase the concentrations up to the mM range.

In these conditions, the threading process results almost instantaneous and so too fast to be monitored by means of a regular time-dependent UV-vis absorption experiment. Therefore, to overcome this experimental issue a stopped-flow apparatus, able to detect kinetics in the range of ns-s, was employed.

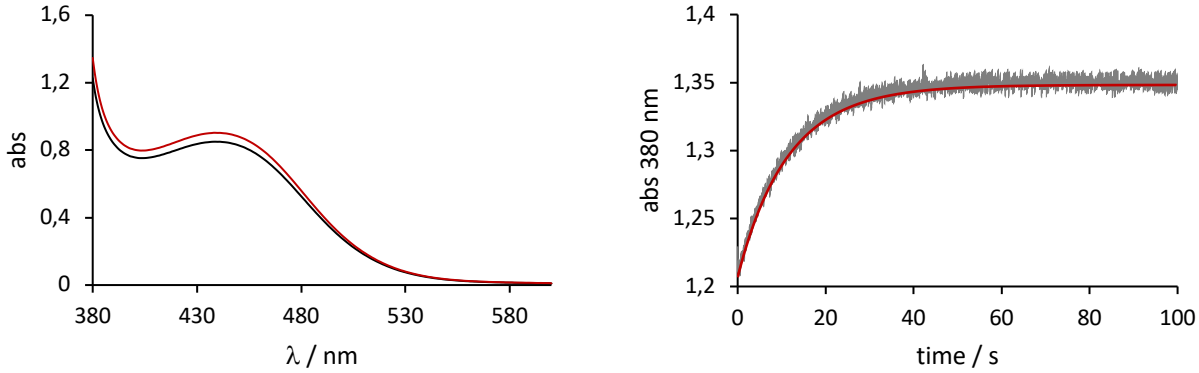

Figure 44 Left: Sum of the absorption spectra of 3 mM DB24C8 and 1 mM 14 E-axle (black line), and absorption spectrum of the mixture of the two compounds (red line). **Right**: kinetic trace and relative data fitting (red line) (CH_3CN, r.t.).

The spectral variations relative to the formation of the complex were first monitored with regular UV-vis absorption spectra. These data show that the spectrum relative to the mix of the component (ring and axle) results different from the correspondent sum of the spectra of the separated species. This observation indicates an effective formation of the pseudorotaxane (Figure 44 left).
Subsequently, the relative kinetic trace was obtained by rapid mixing of the components and the data were fitted with a mixed kinetic model: second order threading and first order dethreading (Figure 44 right). The calculated kinetic constants are k_{in} = 16.22 and k_{out} = 0.035.
The equilibrium constant for this complex is of 468 L mol^{-1}, such parameter was estimated by means of NMR experiments since at the UV-vis concentration regime it was impossible to obtain a proper titration profile to fit given the low association percentage.
At this point the photoisomerization of the azobenzene present in axle 14 was studied (Figure 45).

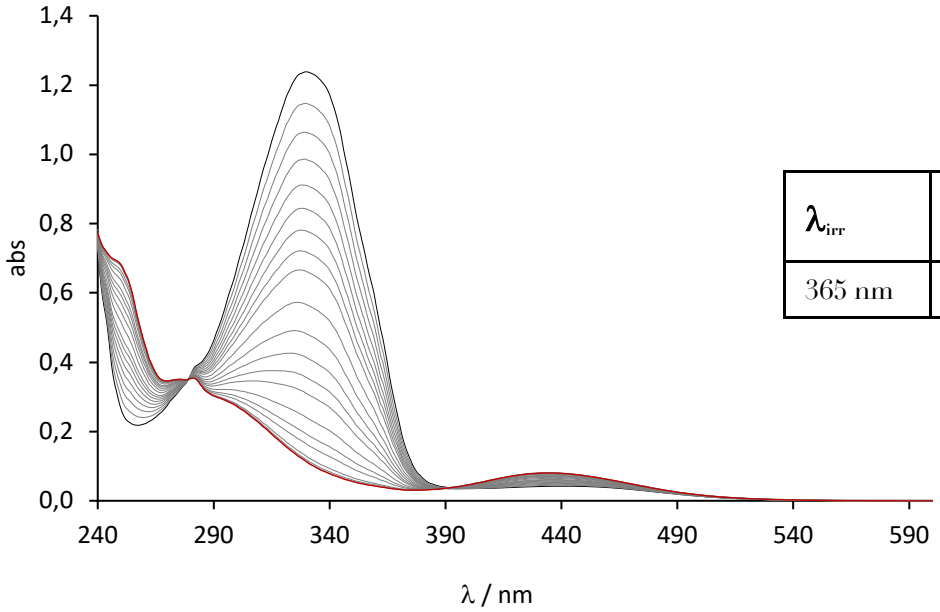

λ_{irr}	$\Phi_{E->Z}$	E/Z PSS%
365 nm	0.18	97%

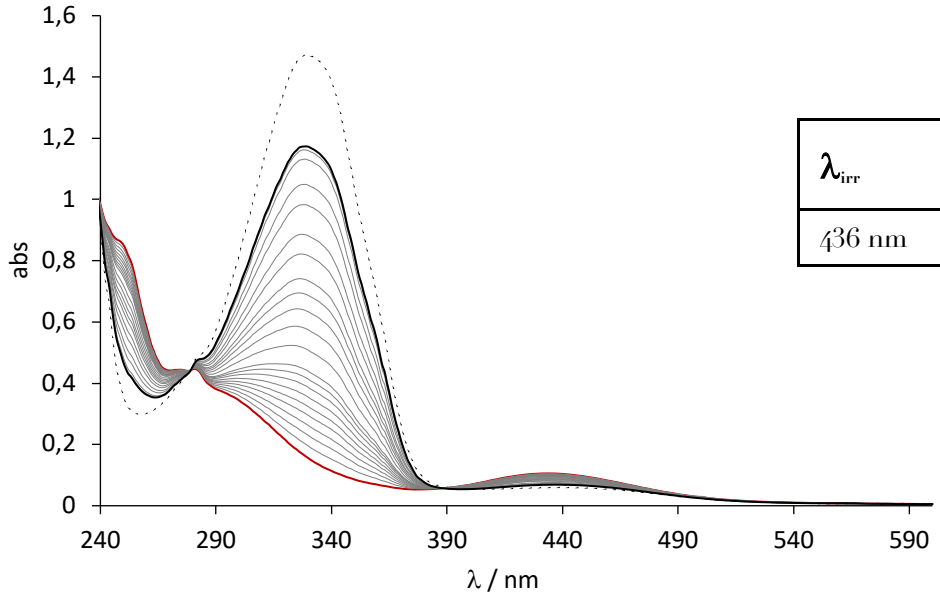

λ_{irr}	$\Phi_{Z->E}$	E/Z PSS%
436 nm	0.46	80%

Figure 45. Top: Absorption spectrum of 48 μM 4 E-axle (black line), and spectral changes observed upon irradiation of the solution at 365 nm, showing the occurrence of the E→Z photoisomerization. Absorption spectrum of Z-axle (red line) **Bottom:** Absorption spectrum of 48 μM 4 Z-axle (red line), and spectral changes observed upon irradiation of the solution at 436 nm, showing the occurrence of the Z→E photoisomerization. Absorption spectrum of the obtained PSS (black line). Absorption spectrum of the initial E-thread (dashed line). (CH_3CN, r.t.).

Other investigations are currently undergoing in order to understand the behavior of this supramolecular assembly under continuous irradiation conditions. Moreover, the developing of other molecular designs is also being examined.
Concluding, a nanodevice of this kind is of high interest because it would convert the luminous energy deriving from the incident photons into chemical energy in the form of molecular rings stored under a non-equilibrium condition.

2.6 Conclusions and future perspectives

In the presented projects a series of molecular designs for the development of a light-effected molecular pump have been investigated. To improve the efficiency of the pump several strategies were adopted, among them the substitution of the pseudostopper unit was studied. To this aim, a family of symmetric differently substituted dibenzylammonium axle compounds was synthetized and characterized by means of several techniques such as UV-vis and NMR spectroscopy. These structures were selected in order to include similar structures with possibly similar association and solubility features. Therefore, the thermodynamic and kinetic parameters of these guests with DB24C8 ring was carefully evaluated. Furthermore, with the significant contribution of computational studies the threading/dethreading of the axles and the relative conformation of the complex was investigated by means of metadynamics simulations, geometry optimizations and analysis of the relative transition states. In light of all the obtained results, it was possible to rationalize the behavior of the guests in two categories one in which the complex was efficiently formed and the second in which the threading was not achieved.
From the described group of compounds, the substituted benzylic unit present in axle 8, which showed suitable kinetic and thermodynamic features, was selected to be included in a second generation molecular pump. In this regard, axle 13 was synthetized and the correspondent supramolecular complex with DN24C8 was investigated. The new axle showed promising features to behave as motor maintaining the desired balance between the equilibrium and kinetic constants necessary to obtain the unidirectionality and the autonomy of the system. Moreover, to gain further about the operation of the pump the cycling operation under continuous illumination conditions were compared to the thermal relaxation of the device in the dark by means of a suitable NMR set-up. The data showed a significant difference in the two trend confirming the hypothesized functioning of the pump which, remarkably, is able to operate out of equilibrium upon continuous light stimulus.
In addiction axle 14 was as well characterized in vision of its future inclusion in a more complex architecture such as the described molecular reservoir. This device constitutes an interesting supramolecular transducer as it would be able to convert and store light into chemical energy collecting several rings which can subsequently be released in the dark. In this case, the obtained data were useful in order to elucidating specific parameters which can be difficult to be isolated while working with such a complex supramolecular assembly. The characterization of the designed molecular reservoir is currently undergoing by means of suitable NMR experiments.
In conclusion, the obtained results constitute a fundamental base for the projection of innovative devices and materials which relies on the fine tailoring of the molecular components properties. In this regards, additional architectures, including this light-activated molecular pump unit, are currently being investigated by the research group.
Among them, a catenane motor and functionalized liposomal membranes able to pump rings against a gradient have been designed and are now being studied in the research group.

3 A ROTAXANE ENDOWED WITH POINT AND MECHANICAL CHIRAL ELEMENTS

3.1 Aim of the project and introduction

Supramolecular assemblies such as rotaxanes and catenanes present many interesting properties. Since their structure is not based on covalent bonds, they show a significant freedom of motion being at the same time controlled and restricted by their mechanically interlocked arrangement. The combination of these two aspects can lead to remarkable results towards stereochemical applications.
Chiral elements comprised in MIMs (mechanically interlocked molecules) can be intrinsically present in the assembly even though the separated components are not chiral. This property is defined "mechanical chirality"[112] and it arises from the presence of a mechanical bond. For instance, considering a rotaxane, an oriented molecular axle unit can assume two different arrangements with respect to a molecular ring yielding two enantiomeric forms (Figure 46).

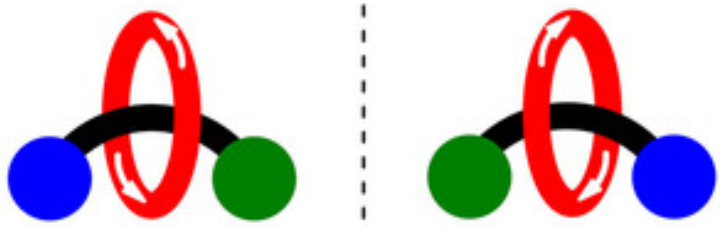

Figure 46 The mechanically planar enantiomers of a rotaxane consisting of oriented ring and axle components.

From the first examples regarding the synthesis of chiral supramolecular structures presented by Vögtle and co-workers[113], improved methodologies and synthetic procedures have been introduced[114] exploiting different strategies and leading to highly enantiopure products[115,116]. This branch of supramolecular chemistry offers interesting possibilities towards different applications such as chiroptical materials and enantioselective sensors[117–120]. Moreover, another widely explored field is constituted by switchable catalysis[121].
In biology, many important processes such enzymatic syntheses within cells frequently occur in parallel. To guarantee the necessary temporal and spatial to this reactions, and to avoid a negative affection caused by other reaction pathways, enzyme activity is often regulated by means of feedback loops and a variety of trigger-induced effects[122]. Differently, artificial catalysts are usually designed according only to the chosen reaction conditions. As such, the introduction of stimuli-responsive properties in artificial catalysis mechanism can add a "bio-like" level of control which is useful in the realization of otherwise impossible synthetic goals. Since MIMs, thanks to the presence of the mechanical bond, can be modified in order to obtain different arrangements in response to external inputs, a switchable catalyst projected with this strategy, could be able to accelerate or slow down a reaction depending on the presence of a specific analyte or to

change the stereochemical outcome of a reaction. Therefore, the employment of such supramolecular structures can be an advantageous strategy towards switchable catalysis. Different options are possible depending on the chosen switching mechanism. A common approach is to exploit a pH-driven switching of the system[123 125], the protonation/deprotonation of a rotaxane can in fact turn "on" or "off" specific sites of the assembly. Therefore, this allow to use selectively some building blocks in a pool of potential reactants, for instance, upon deprotonation is possible reversibly activate the widely used -NH_2^+- recognition motif which is dissociated from the macrocycle and to exploit it in catalytic processes.
Alternatively, a coordination-driven mechanism can be adopted to induce a switch in a rotaxane. Two main approaches are possible, the first includes the addition/removal of external ligands which can complex a metal ion present in the catalyst[126 129]; the second regards the addition/removal of metal ions that can coordinate a binding unit[130 133].
Regarding the project studied in this thesis, a novel rotaxane assembly was synthetized in collaboration with the group of Prof. P.G. Cozzi (University of Bologna).
The investigated structure presents a molecular ring unit constituted by an DB24C8 crown ether functionalized with an oxazoline group located on the benzyl moiety 5(δ). The axle unit 15(χ) includes a substituted benzyl as a stopper group, an ammonium center as a recognition site for the ring, a triazolium group and is terminated with a substituted oxazoline group (Figure 47).

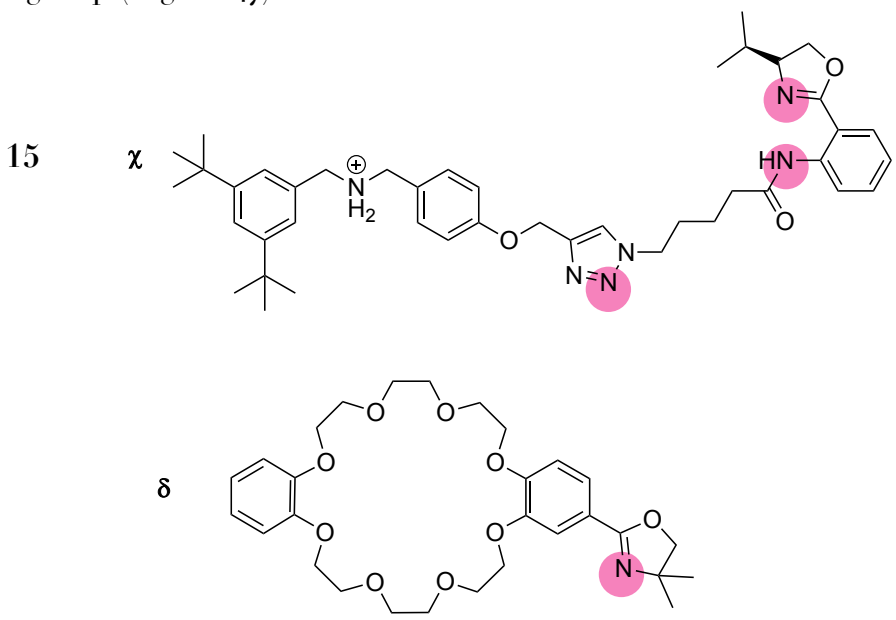

Figure 47 Structure of the rotaxane components: molecular axle 15(χ) and the macrocycle unit 15(δ). The highlighted pink circles represent the possible coordination sites for the Zn^{2+} ion.

The molecular design of this rotaxane was thought in order to show, besides the presence of the intrinsic mechanical chirality, an additional chiral element due to the presence of the oxazoline unit. Moreover, the activity of this assembly can be regulated by means of multiple inputs such as a pH-input, involving the possible deprotonation of the ammonium group, and a coordination-input which includes the exploitation of specific sites as ligands for a metal ion. Both of the latter leading to different arrangements and possibly, different properties of the rotaxane upon a suitable stimulus. As such, this

rotaxanes constitutes a promising assembly to be employed for switchable and possibly asymmetric catalysis.
With this aim, the coordination binding with the Zn^{2+} metal ion has been investigated by using a zinc triflate salt. Zn^{2+} usually shows a tetrahedral coordination geometry which implies that it can possibly coordinate a maximum of four ligands (Figure 48).

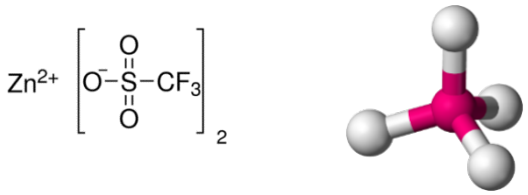

Figure 48 Zn^{2+} triflate salt and relative coordination geometry.

Considering the described rotaxane, the most probable coordination sites could be the ones highlighted in pink (Figure 47) furthermore, the protonated and the deprotonated assembly can present different coordination. When the ring is fixed on the ammonium the rotaxane will probably results in a monodentate ligand, however, upon deprotonation the macrocycle becomes more free to move along the axel and can possibly coordinate as well forming a bidentate ligand. To learn more about the formation and the arrangement of the coordination complex several experiments have been conducted by means of UV-vis spectroscopy and Circular dichroism (CD).

3.2 Investigation of pH and coordination inputs

Initially, the behavior of rotaxane 15 was investigated, in the following figure are reported the absorption spectra relative to the titration of the rotaxane with a solution of Zn^{2+} dissolved in acetonitrile (Figure 49).

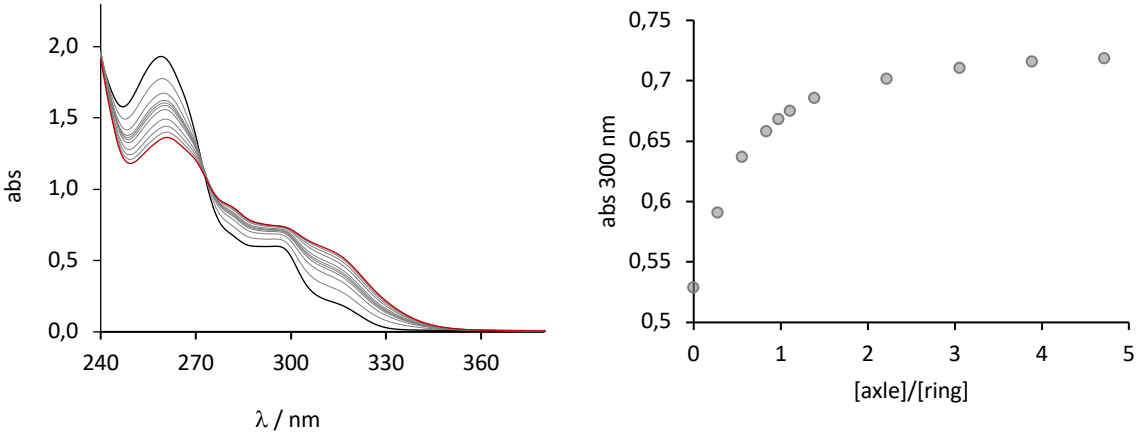

Figure 49 Absorption spectra observed upon titration of rotaxane 15 (7.41×10^{-5} M, MeCN) with a concentrated solution of $(CF_3SO_3)_2Zn$, the black line represents the initial spectrum of the rotaxane 15 while the red line represents the final spectrum in excess of Zn^{2+}(left). Correspondent titration curve reported at 300 nm (right).

The data show significant changes in the absorption spectrum of 15 upon addition of Zn^{2+}; moreover, the plateau reached after the addition of 1 equivalent of the metal ion suggests the formation of a 1:1 coordination complex. The circular dichroism spectrum of 15 presents two main bands corresponding to absorption range (240-350 nm) (Figure 50).

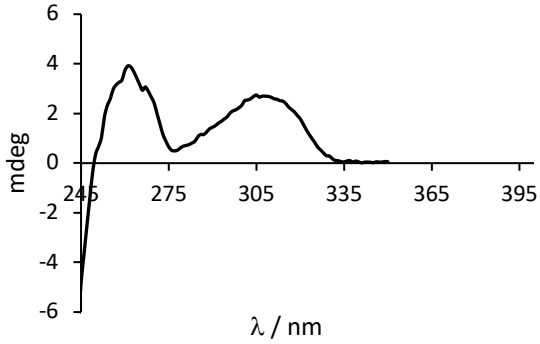

Figure 50 CD spectrum of 5 (7.41 x 10^{-5} M, MeCN)

CD spectra were also recorded in parallel on the same solution during the titration of 15 with the metal ion however, no remarkable variation has been observed.
To gain further on the behavior of the rotaxane 15 the deprotonation of the ammonium center located on the axle was investigated. Upon deprotonation the ring is possibly free to move along the axle as the ammonium group is no more a favored station.
The axle was then deprotonated with the P1-t-Bu-tris(tetramethylene) base and the process was monitored both by UV-vis and by CD spectroscopy (Figure 51).

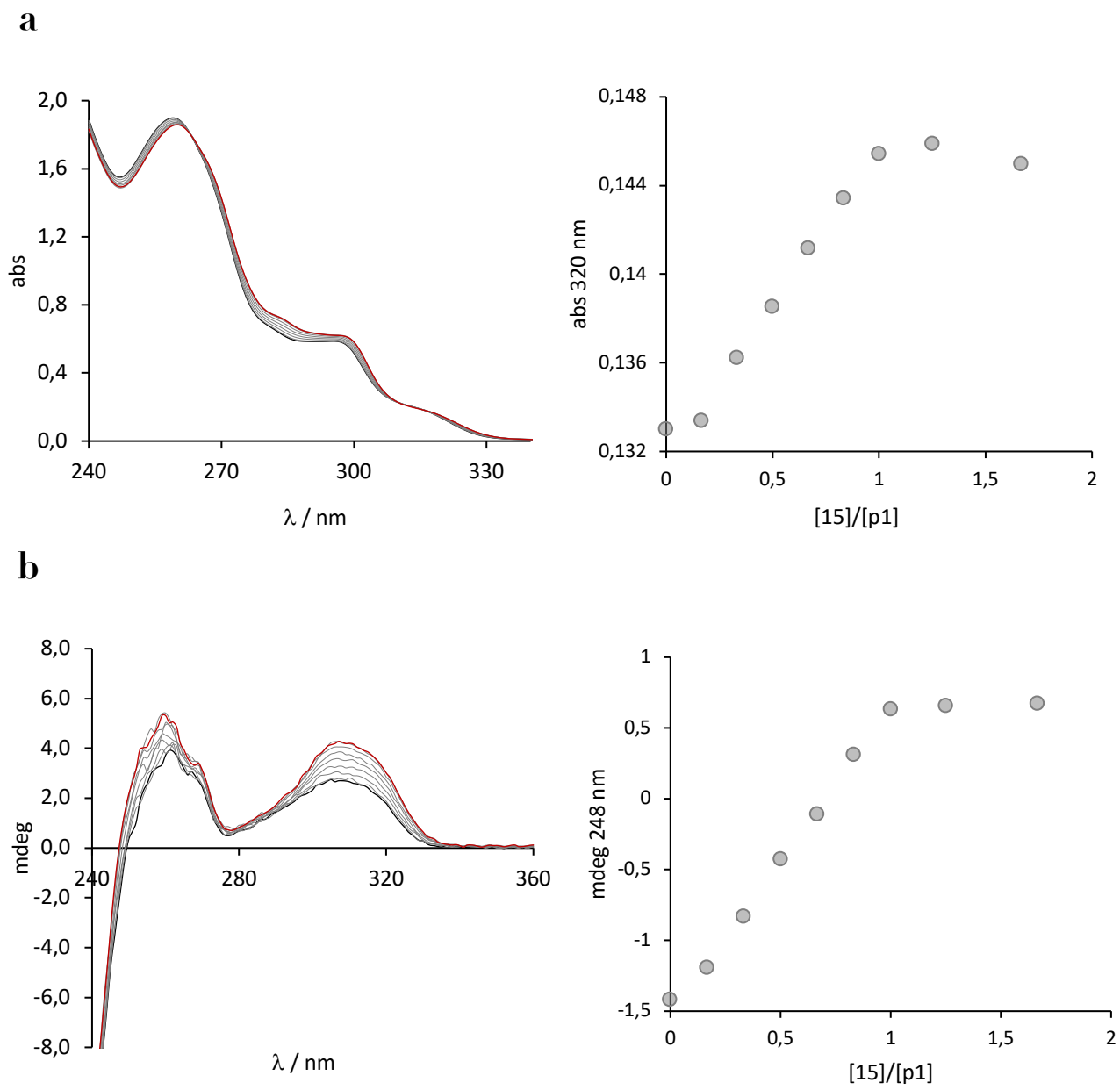

Figure 51 Absorption spectra observed upon titration of rotaxane 15 (7.41×10^{-5} M, MeCN) with a concentrated solution of P1 and correspondent titration profile at 320 nm. **b** Same experiment recorded by means of CD with correspondent plot at 248 nm.

The titration, performed by both techniques, shows a clear plateau after 1 equivalent confirming the complete deprotonation of the ammonium center. At this point the deprotonated rotaxane was then titrated with Zn^{2+}. In the next figure the titration experiment monitored by means of UV-vis spectroscopy is reported (Figure 52).

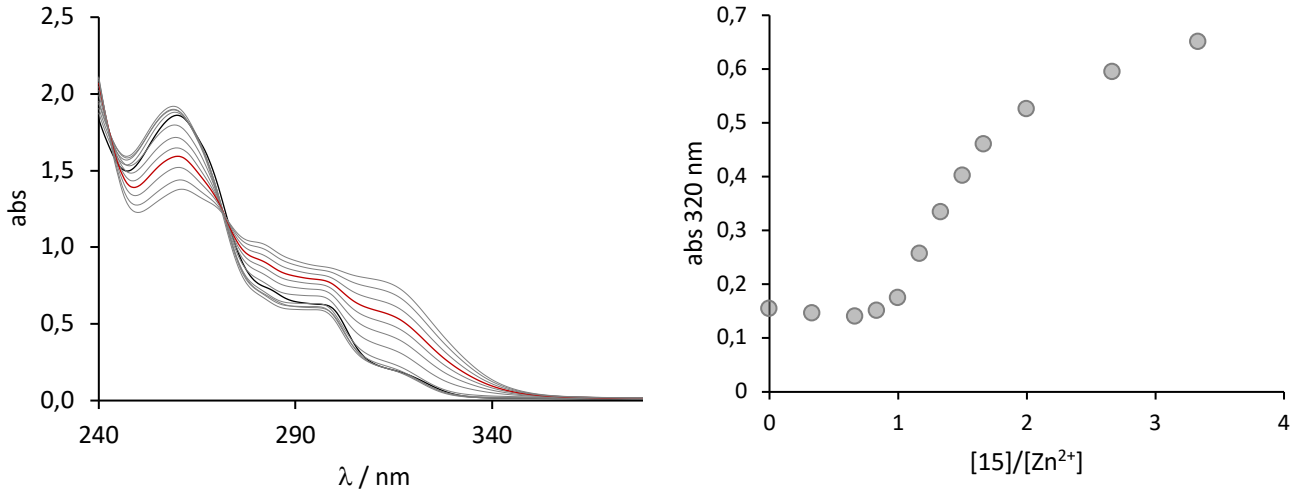

Figure 52 Absorption spectra observed upon titration of deprotonated 15 (7.41 x 10^{-5} M, MeCN) with a concentrated solution of $(CF_3SO_3)_2Zn$, the black line represents the spectrum of the deprotonated 15 while the red line represents the final spectrum in excess of Zn^{2+}(left). Correspondent titration profile reported at 320 nm (right).

The data suggest that in this case there could be 2 consecutive processes involving the coordination of 15 with Zn^{2+} as in the titration profile (Figure 52 right) is possible to observe 2 main changing in the slope of the curve the first at 1 equivalent and the second after 2 equivalents. These two trends could be hypothetically attributed to a different coordination arrangement by the metal. Conversely, no significant change has been detected from the parallel CD spectra.

3.3 Conclusions and future perspectives

The described rotaxane 15 has been characterized by means of UV-vis and CD spectroscopy. The coordination process with Zn^{2+} and the deprotonation of the ammonium station have been monitored; the data lead to conclude that both the protonated and the deprotonated axle comprised in 15 form a coordination complex with the metal probably with a different configuration. Regarding the next steps for this project, the precise coordination sites on the rotaxane will be determined by means of mono and bidimensional NMR experiments to understand more about the arrangements of the rotaxane coordinated with the metal ion.
Alternative structures for the rotaxane will also be developed to optimize the coordination stability and to substitute the -NH- group comprised in the axle which could not be stable upon the addition of a base. Moreover, the presence of this group could be a significant limitation for the rotaxane as it can form an intramolecular hydrogen bond with the nitrogen present in the axle oxazoline unit. These conditions lead to a closing of the structure on itself and consequently to the prevention of the coordination of the metal on that region of the rotaxane. With this aim, the substitution of this site with a simpler ether group will be investigated.
In conclusion a further interesting step will consist in the introduction of a second station by methylating the triazolium unit in the axle[123]. In this way, upon deprotonation of the

ammonium, the ring will move on this secondary recognition point providing a second stable state which will also possibly interact in a different way with the metal leading to a switchable coordination. Conveniently, a precise discrimination between the two states, corresponding to the two stations, will as well allow a clearer characterization of the rotaxane.

4 ENCAPSULATION OF PHOTOCHROMIC DIHYDROPYRENE WITHIN A COORDINATION CAGE

4.1 Aim of the project and introduction

Dihydropyrene (DHP) belongs to the category of diarylethene photoswitches[134,135]; this photochrome is constituted of a large π-conjugated system[136] that can be switched to the open form cyclophanediene (CPD) by irradiating in the visible range (Figure 53). This isomerization is reversible, as CPD can be converted back to DHP both photochemically and thermally[137].

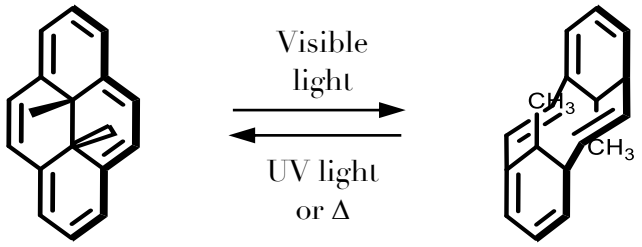

Figure 53 Schematization of the DHP photoswitching.

Differently from other photochromic compounds, such as azobenzenes and spiropyrans, DHP represents an uncommon case where the colored form is thermodynamically more stable with the respect to the colorless one, CPD[138].
One difficulty in the employment of this molecular switch, however, is its instability and poor fatigue resistance. The observed fatigue is considered to be the consequence of the reactivity of the biradical intermediate formed upon photocleavage of the central C C bond in the singlet excited state of DHP[139,140].
To render the photoswitching cycles more robust, the stabilization under confinement[141,142] upon encapsulation of DHP within the cavity of a coordination cage[143,144] was studied.
Reactive species such as radicals[145,146] and photochromes[147,148] can be protected upon confinement through a variety of different strategies[149,150].
Confined spaces can, for instance, create a hermetic seal around a reactive compound, which avoids or reduces interactions with the external environment[151,152].
By encapsulating DHP within a coordination cage, the objective was to protect the unstable intermediate from reacting with oxygen but also to prevent radical radical interactions which can cause a progressive decomposition[153].

4.2 Encapsulation of the guest and characterization of the inclusion complex

The employed coordination cage was an octahedral $Pd^{II}_6L_4$ cage (Figure 54). Cage 16 is composed by four aromatics panels connected by means of six Pd^{II} metal ions. This host, thanks to the high charge concentration, it's fully soluble in water and it presents two wide windows which allow the entrance of suitable molecular hosts.
Furthermore, cage 16 has been earlier shown to be significantly flexible. This feature is mainly due to the rotational freedom around the imidazole benzene bonds[25]. Cage 16 can thus adjust the shape of its cavity to the geometry of bound guest species.
Furthermore, the flexibility of cage 16 allows the cavity to dynamically adapt in upon the isomerization of encapsulated photoswitches such as spiropyran[25] and azobenzene[154].

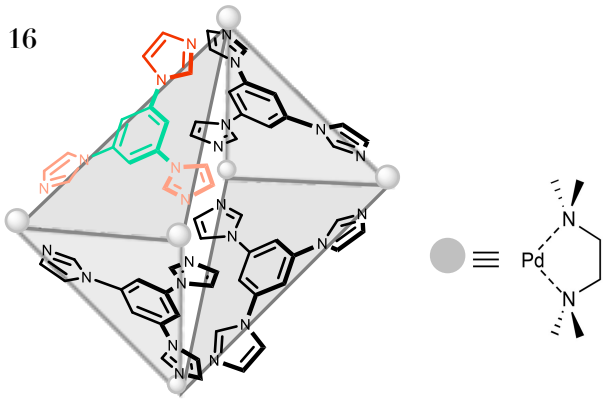

Figure 54 Structure of coordination cage 16.

DHP was encapsulated in cage 16 to investigate its properties upon confinement. To obtain the complex, an aqueous solution of 16 (1 mM) was stirred with an excess of solid DHP at room temperature for 24 hours. Subsequently, the undissolved DHP was eliminated by ultracentrifugation. The resulting supernatant was observed to be green, indicating the presence of encapsulated DHP.
In order to further characterize the complex 1D and a suite of 2D NMR experiments were conducted.
Initially, the ^{1}H NMR of DHP inclusion complex (DHP⊂16) was recorded (Figure 55). The data reveal that the aromatic peaks belonging to DHP (H_9, H_{10}, H_{11}) are significantly shifted upfield with the respect to the same signals of free DHP dissolved in chloroform. Moreover, the methyl group signal (H_{12}) is also shifted upfield from –4.24 to –6.44 ppm, these changes are probably caused by the shielding deriving from the aromatics panels on the cage.
By integrating signals from the cage and from the guest the stoichiometry ratio of the complex results 1: 1 furthermore, the complete disappearance of the signals relative to the empty cage (for instance H_1 e H_6) suggests a complete encapsulation yield.
All the signals present in ^{1}H NMR were fully assigned by means ^{1}H ^{1}H COSY and ^{1}H ^{1}H NOESY.

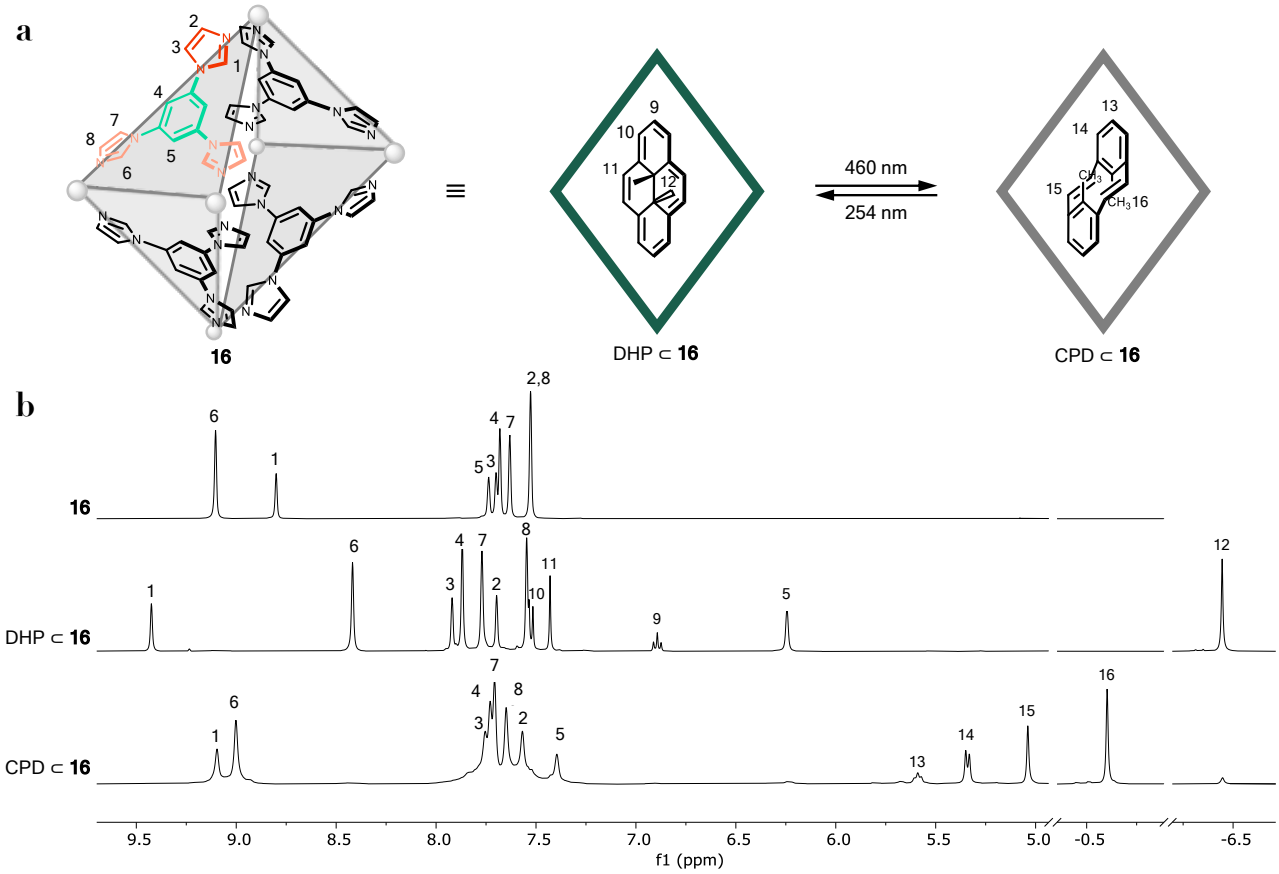

Figure 55. (a) Structural formula of cage 16, comprising signals numbering scheme reported in the NMR spectra. (b) Partial ^{1}H NMR spectra (400 MHz, D_2O) of empty cage 16, DHP⊂16, and CPD⊂16.

The ^{1}H DOSY experiment shows that all the signals present in the ^{1}H NMR diffuse with an equal rate; this data confirms the effective formation of the complex as the cage and the guest diffuse together through solution (Figure 56).
Same conclusions can be drawn either for CPD⊂16 inclusion complex, the relative data are not reported here for synthetic reasons.

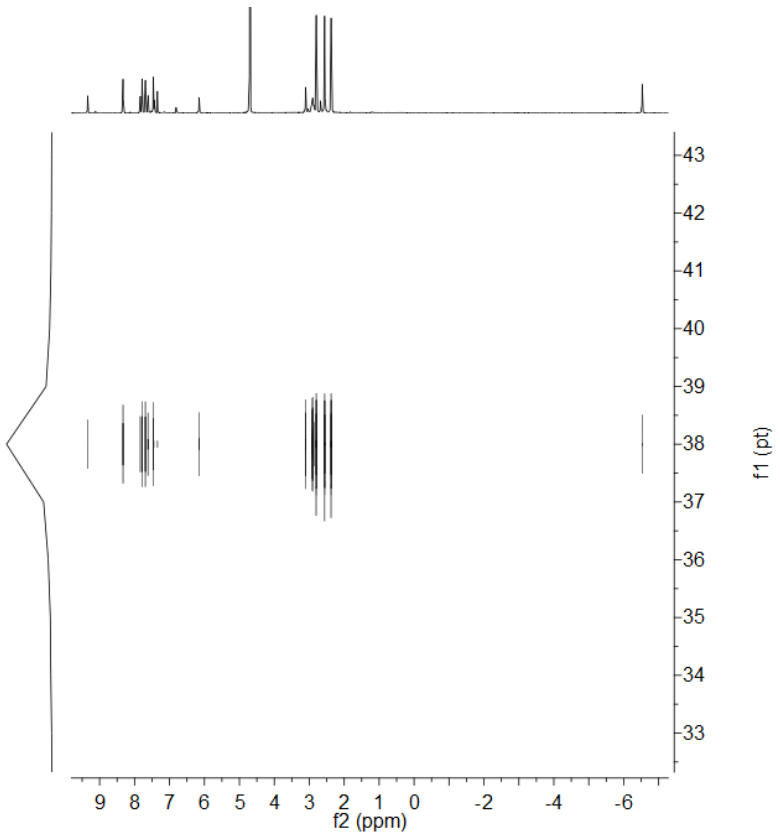

Figure 56 ^{1}H DOSY NMR spectrum (500 MHz, D_2O) of DHP⊂16. Adapted with permission[153].

The binding between cage 16 and DHP was monitored by means of UV-vis spectroscopy as well. An aqueous solution of 16 (0.62 mM) was titrated with a concentrated solution of DHP dissolved in acetonitrile (6.94 mM) (Figure 57).

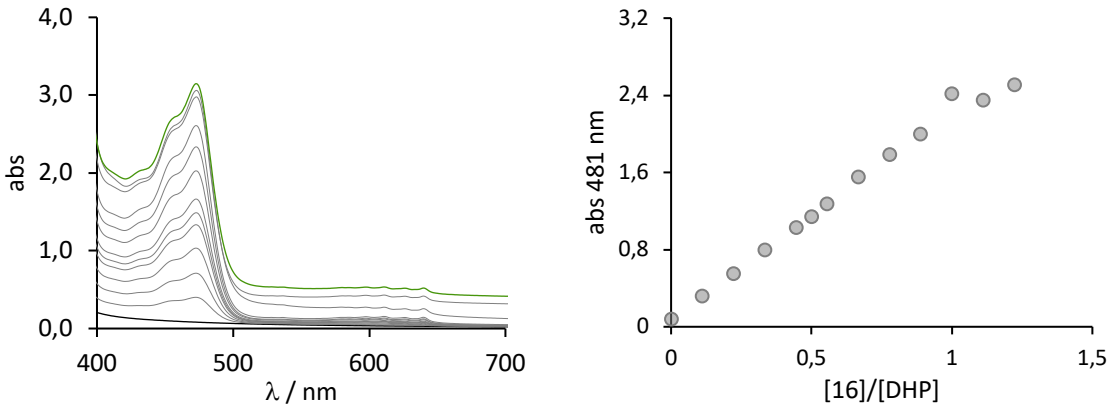

Figure 58 Absorption spectra observed upon addition of small aliquots of DHP solution to a solution of cage 16 (b) Correspondent titration curve.

The data suggest that the cage provides a complete encapsulation and dissolution of DHP in water until the addition of 1 equivalent is reached; this is confirmed by correspondent

increase of the absorbance band correspondent to DHP⊂16. After this point, since all the cage present in solution have been occupied, DHP cannot be encapsulated anymore and starts to precipitate due to its extremely low solubility in water. This is highlighted also by the significant increase of the baseline absorption value due to the presence of aggregated undissolved DHP.
DHP absorption features are significantly different depending on the polarity of the solvent. In more polar environments, for instance in acetonitrile, the maxima are located at 336 and at 376 nm, differently, in pentane they are located at 336 and 375 nm.
With the respect to the complex DHP⊂16 in water (λ_{max}= 346 and 383 nm), the spectrum of free DHP appears blue shifted by 10 nm. This difference is probably due to a remarkable interaction between the cage and the aromatic panels of cage 16.
Another experiment which was made in order to further understand the differences of the optical properties between free and encapsulated DHP was the DHP releasing from the cage (Figure 59).

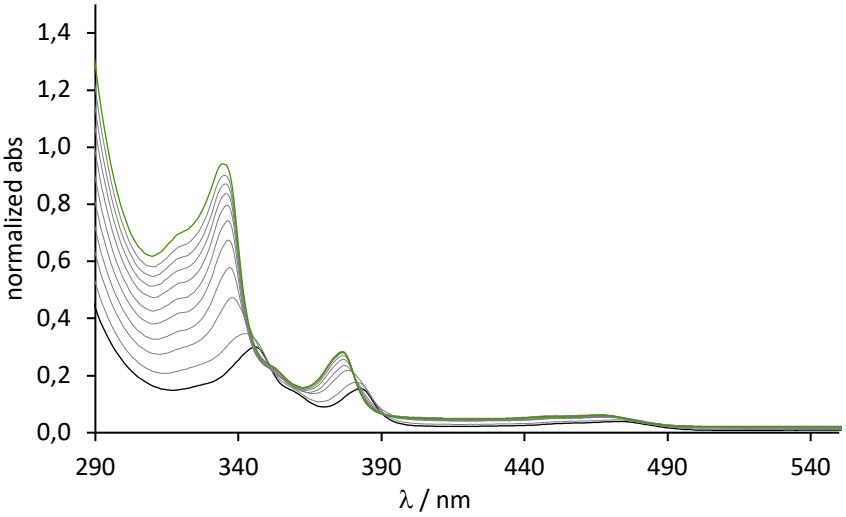

Figure 59 Normalized UV/vis absorption spectra following sequential additional of acetonitrile to an aqueous solution of DHP⊂16 (the black line represents no MeCN added while the green line represents 1500 µL of MeCN added).

During this experiment increasing amounts of acetonitrile (150 µL aliquots) where added to 1.5 mL of a 1 x 10^{-5} M aqueous solution of DHP⊂16 until a final volume of 3 mL was reached.
Upon each addition the solution was carefully stirred before recording an UV-vis absorption spectrum. The spectra were corrected by means of a factor which considers the ratio between the total volume present in the cuvette and the added volume for each point, in this way the absorption values are not affected by a decrease due to dilution.
The data show a remarkable increase in the absorbance associated with the addition of MeCN in the solution. This indicates the progressive realising of DHP from the cage cavity as the absorption coefficient is significantly higher for free DHP with the respect to the inclusion complex. Moreover, a progressive blue shift of the absorption maximum from 346 nm (typical of DHP⊂6) to 336 nm (typical of free DHP) was observed.

Unfortunately, there is no solvent which is able to dissolve DHP⊂16 and at the same time free DHP, this drawback renders the comparison of these two systems very complicated because, as explained above the properties can be significantly different upon a change in the conditions.

By analyzing the ^{1}H-^{1}H NOESY data the orientation of DHP located inside the cage cavity was studied. The data show a correlation between the middle part of the cage, correspondent to benzene units ($H_{4\text{-}8}$) and the methyl groups of DHP (H_{12}). The described signals are highlighted in purple and orange in figure 60.

Contrarily, no remarkable correlations are noticed between the aromatics signals of DHP ($H_{9\text{-}11}$) and any part of the cage. The same observation was found for the protons located at the upper and lower regions of the cage ($H_{1\text{-}3}$) and DHP.

In light of these data regarding DHP⊂16 in solution, is possible to hypothesize that DHP could be disposed such that the methyl groups of DHP can occupy the largest part of the cage, namely, the equatorial part.

Furthermore, the lack of other significant interactions suggest that the guest may be spinning within the cage cavity while the methyl units should stay relatively fixed in the equatorial pocket of the cage. The absence of a second set of signals relative to encapsulated DHP indicates the faster rate of this rotation with the respect to the ^{1}H NMR timescale.

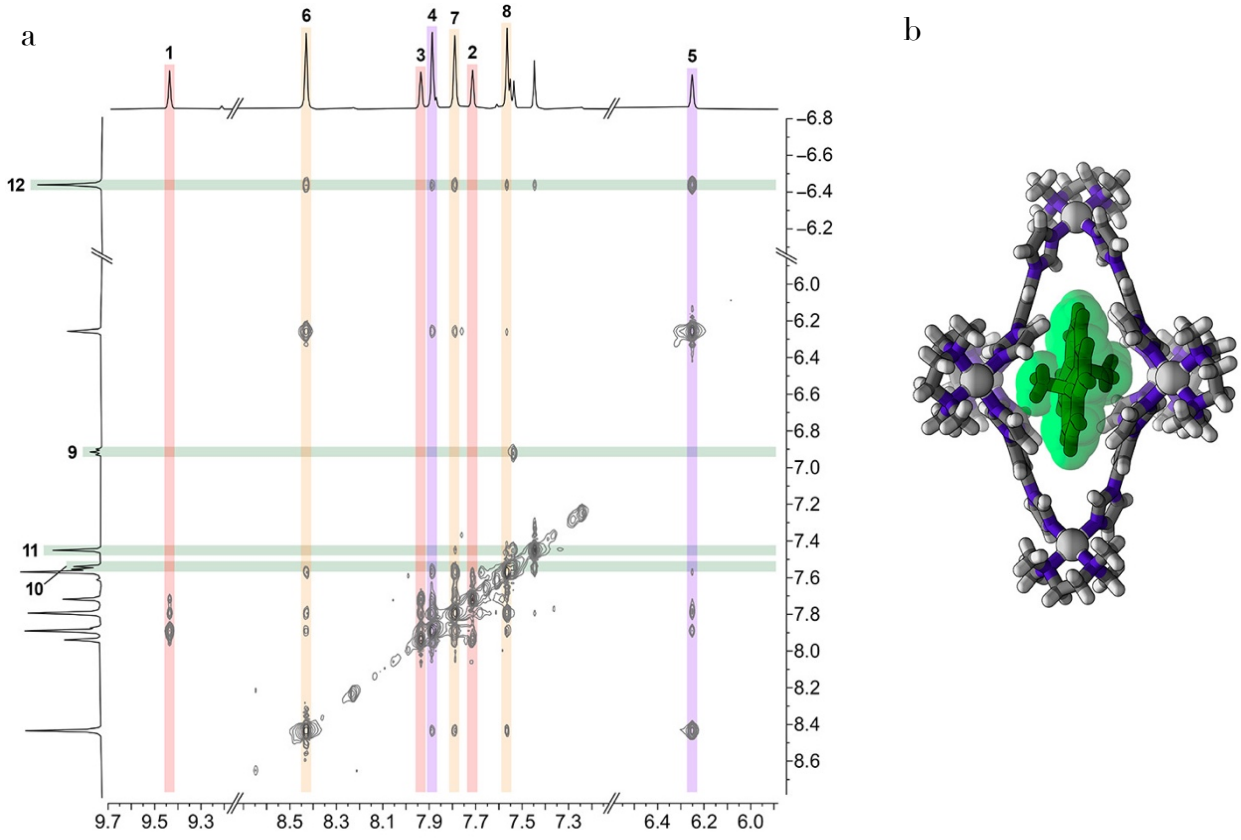

Figure 60 a) Partial ^{1}H ^{1}H NOESY spectrum (500 MHz, D_2O) of DHP⊂16. Signals highlighted in red, orange, and purple originate from 1's axial imidazole, equatorial imidazole, and benzene rings, respectively (see Figure 55). Signals highlighted in green originate from DHP. (b) Crystal structure of DHP⊂16 (major conformation). Adapted with permission[153].

Analogues signals and interactions were observed as well in the CPD⊂16 ^{1}H-^{1}H NOESY spectrum (Figure 61).

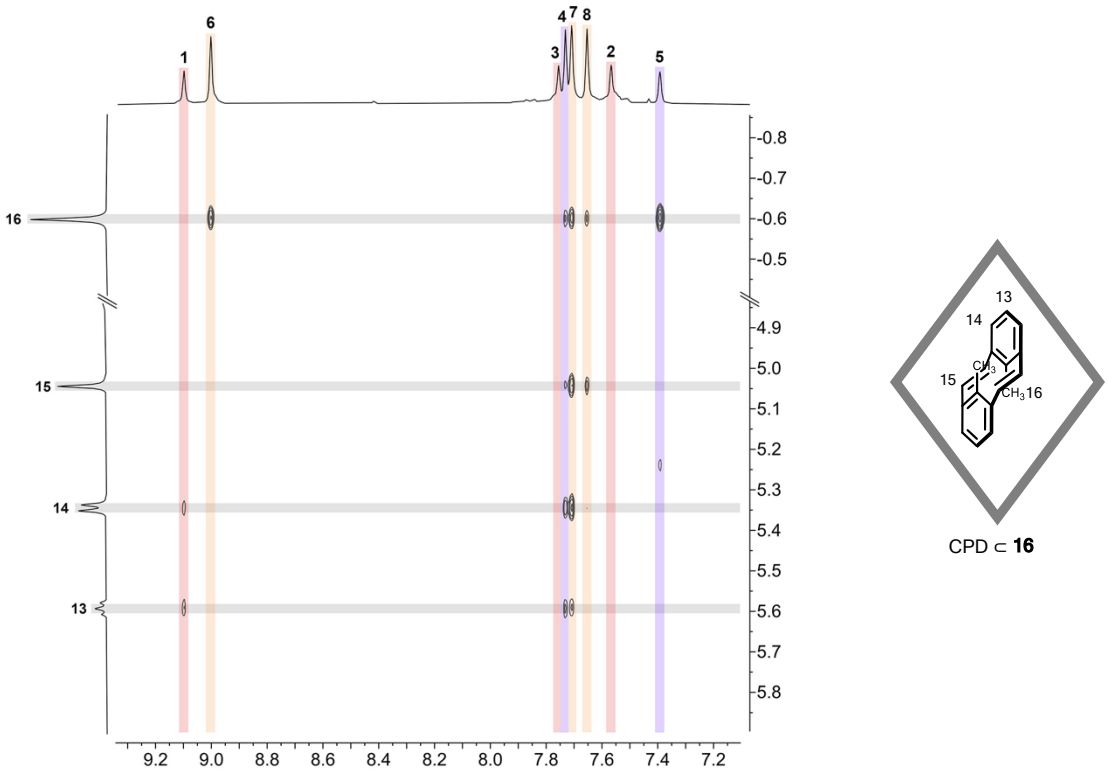

Figure 61 Partial 1H 1H NOESY NMR spectrum (500 MHz, D_2O) of CPD⊂16. Adapted with permission[153].

In the reported spectrum the strongest signals are attributed to correlation between the methyl groups of CPD and the equatorial region of the cage (i.e., interaction of H_{16} and H_5). The considered interactions result more intense with the respect to the correspondent ones in DHP⊂16, this is due to the different shape and volume occupied by the guest upon isomerization. In fact, CPD which constitutes the open isomer, is disposed more closely to the cage walls leading to stronger signals.
Furthermore, protons H_{13} and H_{14} interact with H_4 and H_7 located in equatorial and in the imidazole part of the cage.
Considering all these observations is possible to conclude that in this case CPD is disposed with a specific orientation with the upper part (H_{13} and H_{14}) facing the open window of the cage.
DHP inclusion complex characterization was conducted for the system at the solid state as well by studying the X-ray crystal structure.
Upon slowly evaporating of water from a solution of DHP⊂16 at room temperature the crystallization of the complex was achieved, and bright green crystals were obtained.
Interestingly, from the X-ray data it was possible to distinguish between two main guest orientations within the cage cavity.
The prevalent one, present in nearly the 66%, characterized by DHP disposed vertically inside the cage (Figure 62a) and the minor one in which DHP is oriented horizontally (34%) (Figure 62b).

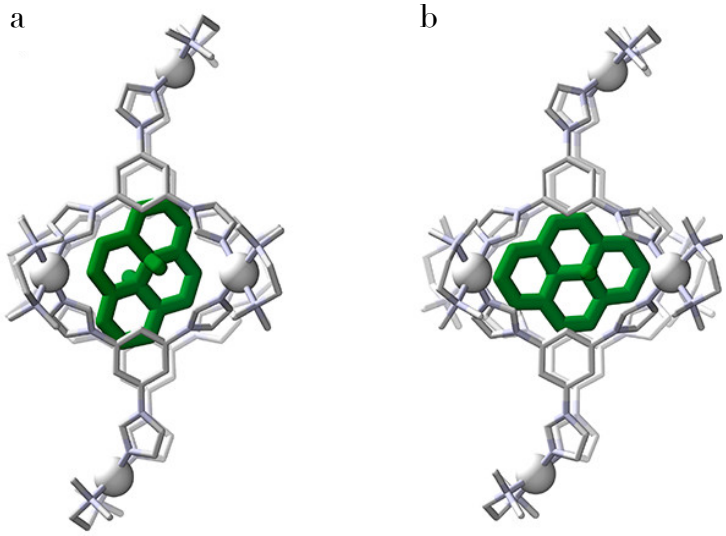

Figure 62 Side-views of the crystal structures of the major and minor conformers of DHP⊂16 showing the orientations of DHP within cage 16, vertical (a) and horizontal (b). Adapted with permission[153].

This observation is coherent with the previously reported ^{1}H ^{1}H NOESY data which suggested a significant freedom of the movements of DHP inside the cage confirming a nice agreement between the results in solution and at the solid state.
Furthermore, the significant degree of flexibility of the cage is highlighted from the X-ray solid state analysis. Upon comparison with the empty cage structure[154] is possible to observe that the cage is deformed vertically, in fact the distance between the two Pd^{2+} ions increases from 19.552 Å of the empty host up to 19.910 Å for DHP⊂16. More specifically, X-ray studies show an alternation of 2 complexes with slightly different structural properties namely with an increase of 15.9% and 18%. This distortion represents an already reported observation, however, this case is quite remarkable as the increase in the Pd-Pd distance is the largest ever reported.
Despite numerous attempts, the crystallization of CPD⊂16 was not achieved. In this case in fact, a stable crystal structure is more complicated to obtain because in solution as CPD tends to back isomerize to his close form DHP. However, considering of the good agreement between the NOESY and X-ray data for DHP⊂**1**, similar results are expected as well for the crystal structure of CPD⊂16.To solve this deal, a study for optimized experimental conditions is currently undergoing.

4.3 Guest exchange experiments

At this point, upon the investigation of the crystal structure of DHP⊂16, some analogies with the already studied complex of merocyanine (MC⊂16) were noticed (Figure 63).
A vertical elongation of the cage and the consequent increase in the Pd-Pd distance is present in both DHP⊂16 and MC⊂16 inclusion complexes, moreover, in both cases the guests are disposed vertically within the cage. Regarding the equatorial part of the cage, noticeably, the methyl groups of DHP and MC are both accommodated in middle larger region of the cage.

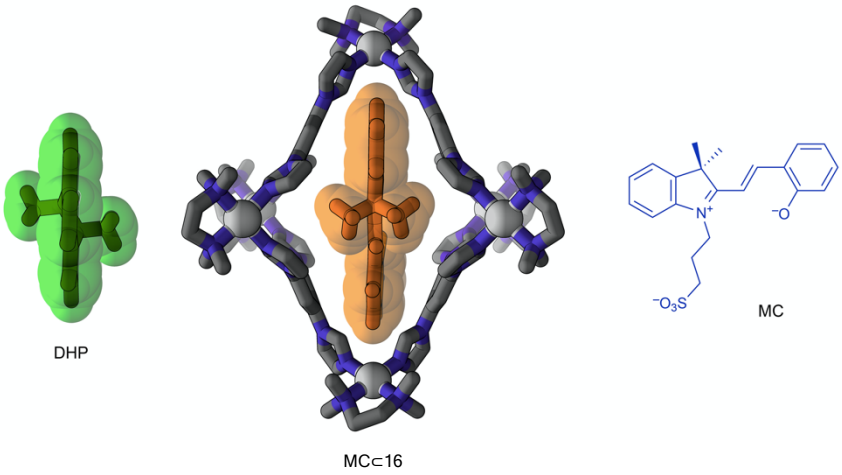

Figure 63 Comparison between free DHP and MC⊂16 (left), structural formula of MC (right). Adapted with permission[153].

Having observed these similarities, a guest exchange experiment was conducted. In the following investigation an excess of each compounds was added to a solution of the other guest as shown in next figure (Figure 64). The consequent equilibration was then monitored by recording absorption and emission spectra.

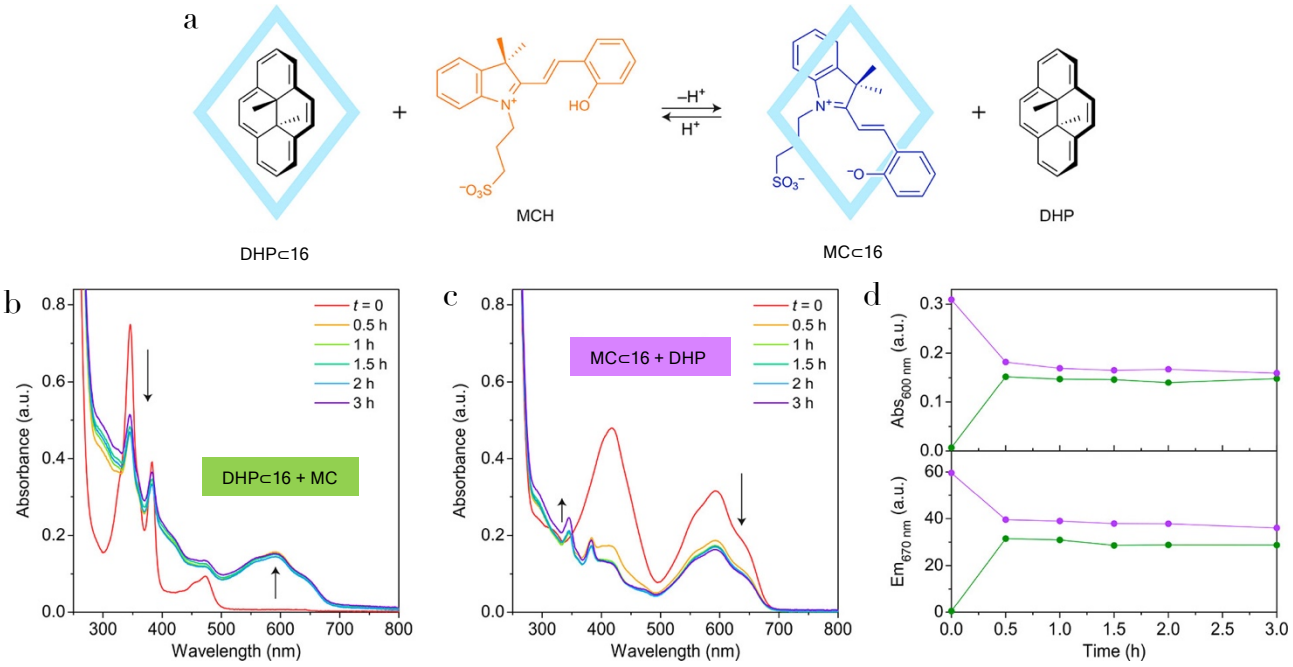

Figure 64 (a) Progressive guest exchange including DHP⊂16 and a sulfonated MC. (b) Changes of UV/vis absorption spectra upon mixing DHP⊂16 with an equimolar amount of free MCH. (c) changes of UV/vis absorption spectra upon mixing MC⊂16 with an equimolar amount of free DHP. (d) Plot of the absorbance at 600 nm (top; reported from parts b and c) and emission at 670 nm (range where encapsulated DHP does not absorb and emit) over time (λ_{exc} = 550 nm). Purple markers, MC⊂16 + DHP; green markers, DHP⊂16 + MCH. Adapted with permission[153].

In the first investigation, the increase of absorption at 600 nm corresponding to the MC maximum was monitored. In this case the exchange of the guests happened quite rapidly and was completed in ca. 30 min (Figure 64 b, d).
Contemporarily, the MC fluorescence spectrum was recorded and the emission value at 670 nm (where MC is the only emissive species) was monitored (Figure 64d).
In the second experiment free DHP was added to a MC⊂16, the exchange was slightly slower with the respect to the previous case, probably because of the poor solubility of DHP in water. Is important to underline that an equimolar amount of DHP and MC have been employed.
Remarkably, both experiments gave similar results, in fact, upon addition of the competitive guests, after the equilibration, the final composition of the system was approximately 1:1 with an equal amount of each guest being complexed by the cage.
The reported competition experiment is helpful also because it allows to roughly estimate the binding strength of the complex DHP⊂16. In fact, since DHP is insoluble in water the association constant between DHP and the cage is impossible to calculate directly.
However, having already calculated the K_{ass} relative to MC[25] which binds the cage relatively strongly with a $K_{ass} > 10^7$ M^{-1}, is possible to hypothesize that the K_{ass} for DHP is close to this value.
DHP and MC actually share several properties as molecular guests, both these compounds are highly conjugated and planar, moreover, they are characterized by an overall analogous geometry. In addition, both the compounds present as well protruding methyl units

oriented orthogonally with the respect to the aromatic structure. Considered all these correspondences, is therefore straightforward to infer that the energetic contribute for the cage to adapt and accommodate this guest is also comparable. More specifically, the complexes are stabilized by means of the π π stacking interactions which occur between the aromatic units of DHP and MC and the cage panels.

4.4 DHP photoisomerization reactions

After an extensive characterization of DHP⊂16 features by means of mono and bi-dimensional NMR techniques and by X-ray analysis, the photoisomerization of free and encapsulated DHP was investigated.
DHP⊂16 dissolved in water was irradiated at 460 nm with blue light. The irradiation was accompanied by a change in the color from green to a light brown. Significant variations were also present in the UV-vis spectrum of the complex (Figure 65).

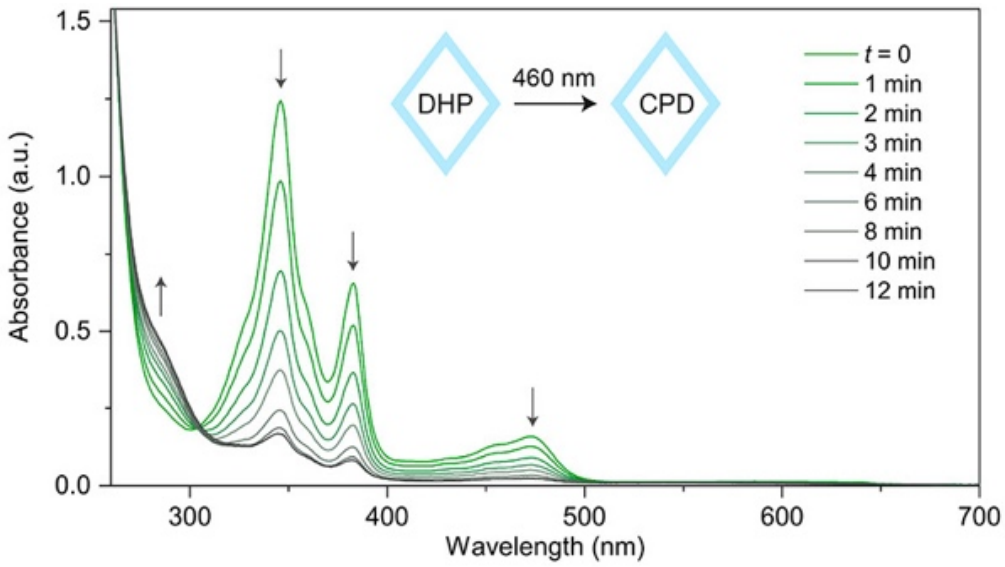

Figure 65 Uv-vis absorption spectra showing the occurrence of DHP⊂16 isomerization to CPD⊂16 (λ_{irr} = 460 nm). (H_2O, r.t.) Adapted with permission[153].

The absorption spectrum of DHP⊂16 shows the typical bands relative to the guests.
Upon irradiation, the results show a large decrease in the absorption bands typical of DHP (λ_{max}= 346, 383 and 470 nm) while the band below 300 nm is observed to increase. In this region also a strong absorption signal belonging the cage is present.
The same experiment was also performed for free DHP dissolved in MeCN and to compare the isomerization kinetic the two processes were monitored by recording a spectrum every 30 s under identical experimental conditions (Figure 66).

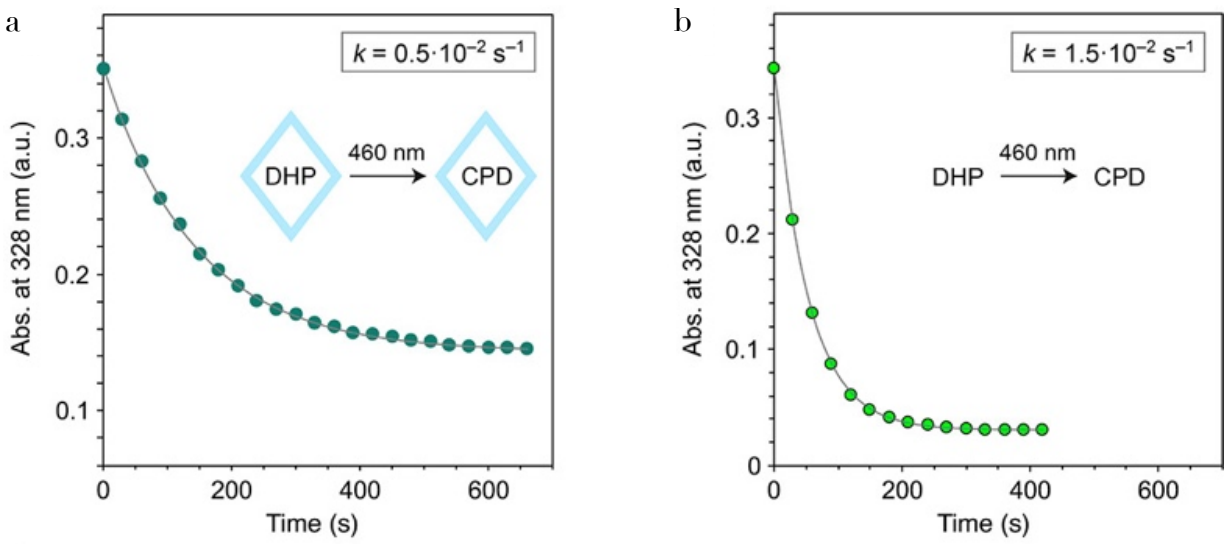

Figure 66 Kinetics of photoisomerization of DHP⊂16 to CPD⊂16 in water at 20 °C. (a) Kinetics of photoisomerization of DHP to CPD in acetonitrile at 20 °C (b). Experiments in (a) and (b) were conducted with equal irradiation conditions (λ_{irr} = 460 nm) under a pseudo-first-order regime ($A_{460} \ll 1$)[155]. Adapted with permission[153].

The reaction conducted in MeCN resulted to be approximately 3 times faster with the respect to the same process in water. This observation is unsurprising as even is the cage structure is quite flexible the change is the shape of the guest is still significant and the cage needs to adapt to this modification.

From these values is also possible to hypothesize that the photoisomerization quantum yield is decreased as well about 3 times. This is in line with an already reported case in which diarylethene was included within a highly ordered polymeric matrix[156].

The isomerization process was monitored also by means of NMR spectroscopy (Figure 67). The spectra show that, upon irradiation of a solution of DHP⊂16 (1 mM, D_2O) with blue light, the signals assigned to encapsulated DHP progressively decreased while signals from CPD started to appear.

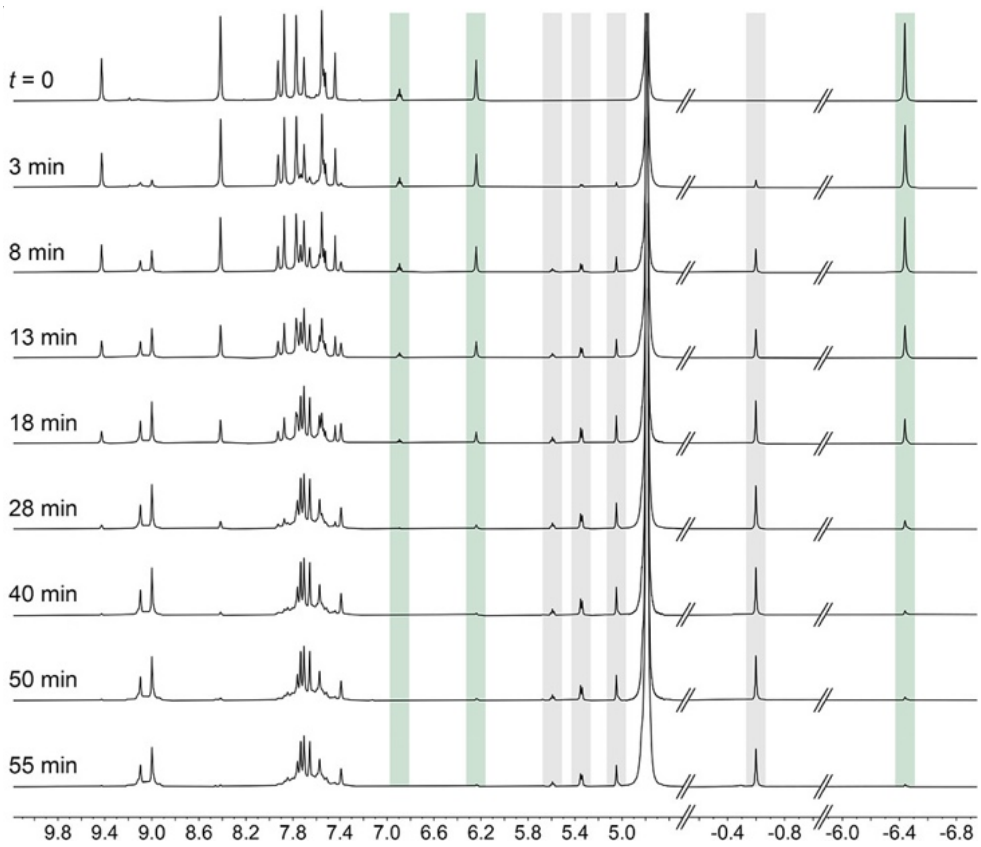

Figure 67 Partial ^{1}H NMR spectra (400 MHz, D_2O) of DHP⊂16 recorded after increasing irradiation time at 460 nm. Protons highlighted in green and gray are relative to DHP and CPD, respectively. Adapted with permission[153].

From this ^{1}H NMR data the molar composition of the analyzed solution was also calculated by integrating two clear and clean signals from the methyl units in DHP and CPD (i.e., H_{12} at -6,44 ppm and H_{16} at -0.6 ppm) (Figure 68).

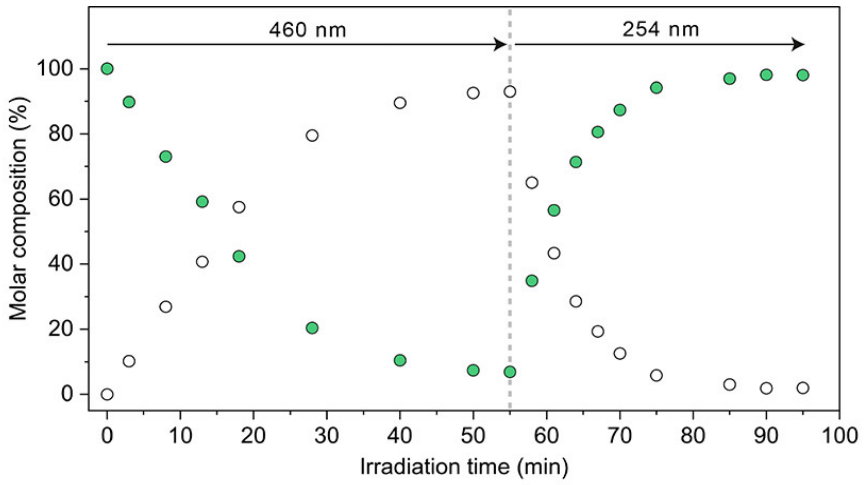

Figure 68 Molar composition of the DHP⊂16/CPD⊂16 (green and empty markers, respectively) as a function of 460 and 254 nm irradiation time. The data are calculated also from NMR spectra recorded immediately after irradiation. Adapted with permission[153].

The first PSS state comprising approximately 94 % of CPD⊂16 was reached after ca. 40 min of irradiation at 460 nm while the final PSS was achieved after approximately 80 min of irradiation comprising ca. the 98% of DHP⊂16.
Regarding the closing back reaction from CPD to DHP this process ca occurs not only by irradiating the system but also thermally.

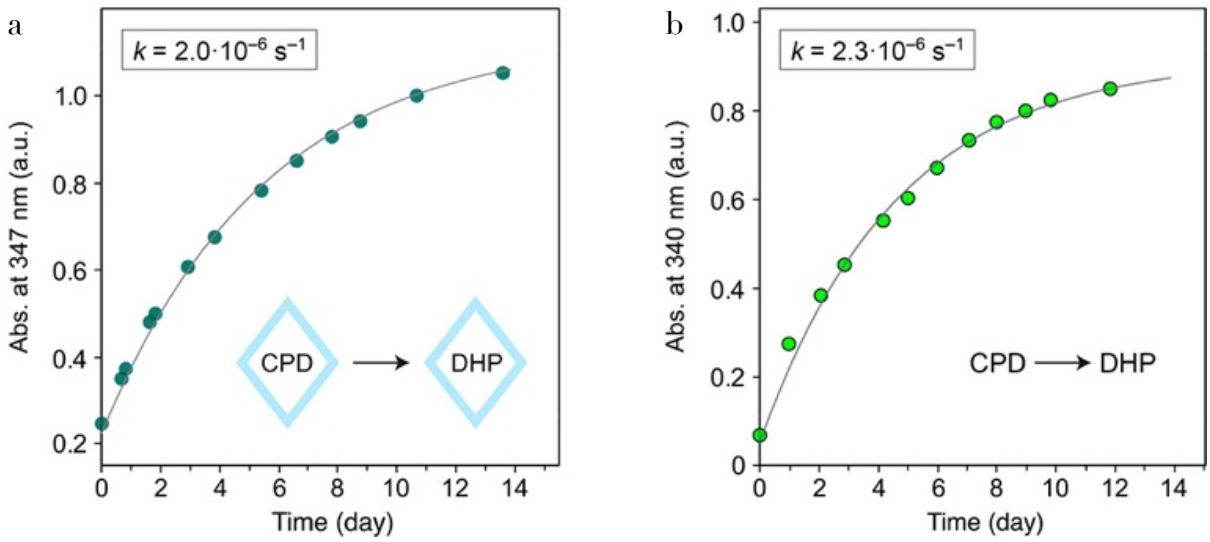

Figure 69 Kinetics of the thermal back-isomerization of CPD⊂**16** to DHP⊂**16** in water at 20 °C. (a) Kinetics of the thermal back-isomerization of CPD to DHP in acetonitrile at 20 °C (b). The data are consistent with first-order kinetics, as indicated by the gray lines (data fitting). Adapted with permission[153].

In the reported experiments, after an exhaustive irradiation at 460 nm encapsulated (Figure 69 a) and free DHP (Figure 69 b), the thermal back-isomerization was monitored in the dark at 20 °C by means of UV-vis spectroscopy.
In both the cases this process was relatively slow taking several days to be completed. However, upon the fitting of the absorption values at 347 nm (DHP⊂16) and at 340 nm (free DHP), the calculated kinetic constants resulted 2 x 10^{-6} s^{-1} and 2.3 x 10^{-6} s^{-1} respectively. The closing process resulted to be slightly faster for the free DHP suggesting that the closing reaction is slightly favored in the absence of the constriction due to the cage. On the other hand, the difference between these two values is negligible and the two values are fully comparable even under completely different conditions.
It is important to underline that the comparison between these two systems is not trivial as the solvent and the polarity of the environment can lead to extremely different effects on DHP.

4.5 Computational studies

Other interesting features of DHP⊂16 and CPD⊂16 were obtained with the contribute of atomistic molecular dynamic (MD) performed in collaboration with the group of Prof. Giovanni Pavan at the University of Southern Switzerland.
These simulations were carried out for both complex with explicit solvent (water). Regarding DHP⊂16 it was found that upon complexation of the guest the cage adapts to the shape of the guest. To quantify this effect two main parameters were considered, d_1 and d_2 which represents the distances between the axial Pd atom and the middle points of opposed edges in the equatorial region (Figure 70).
In the following figure the conformational free-energy surface (FES) is reported. Considering the empty cage 16^{157}, the gray area represents the area within 0,5 kcal/mol from the minimum. In addition, the green and cyan regions limit the free-energy minima of encapsulated DHP and CPD respectively.
As recently reported, such parameters are useful in order to understand the free-energy cost relative to the cage distortion after the binding of a guest.
The data indicate that the free-energy amounts for both DHP⊂16 and CPD⊂16 are approximately equal to 6 kcal/mol. This observation can be attributed to the relatively minimal conformational change upon the opening process from DHP to CPD.
Moreover, an analogous investigation has been conducted for different photochromic species such as arylazopyrazole (dark-blue) and tetra-o-methoxyazobenzene (violet). Coherently with the significant change in conformation related to the photoisomerization od these two compounds, a remarkable change in d_1 and d_2 parameters was observed.

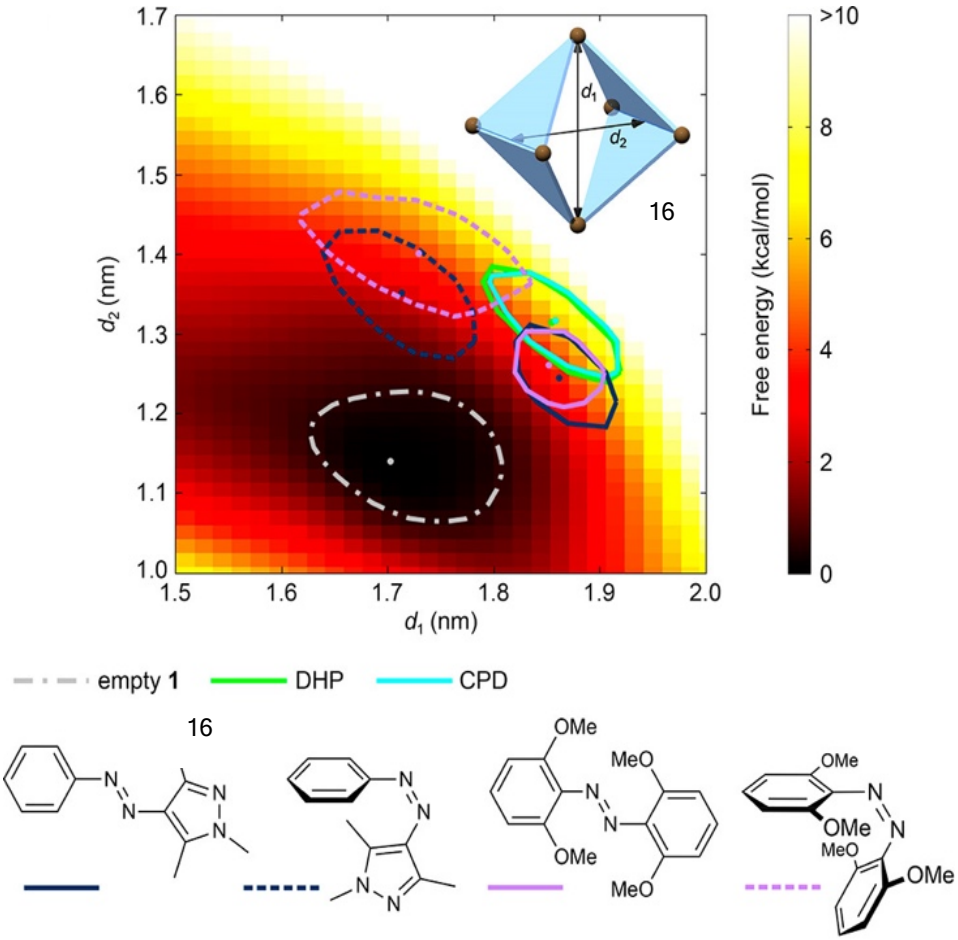

Figure 70 FES landscape of 16, plotted as a function of d_1 and d_2 (see inset). The location of the minimum-free-energy configuration of 16 is reported as a gray point; the dash-dotted line represents the region within 0.5 kcal/mol of the global minimum. Projected on the free-energy surface of 16 are energy minima (colored points) and regions within 0.5 kcal/mol of the minima (lines) of DHP⊂16, CPD⊂16, and four other, studied complexes including photochromic guests. Adapted with permission[153].

To gain further about the inclusion complexes arrangements a comparison between DHP⊂16 and CPD⊂16 was performed by means of MD simulations (Figure 71).

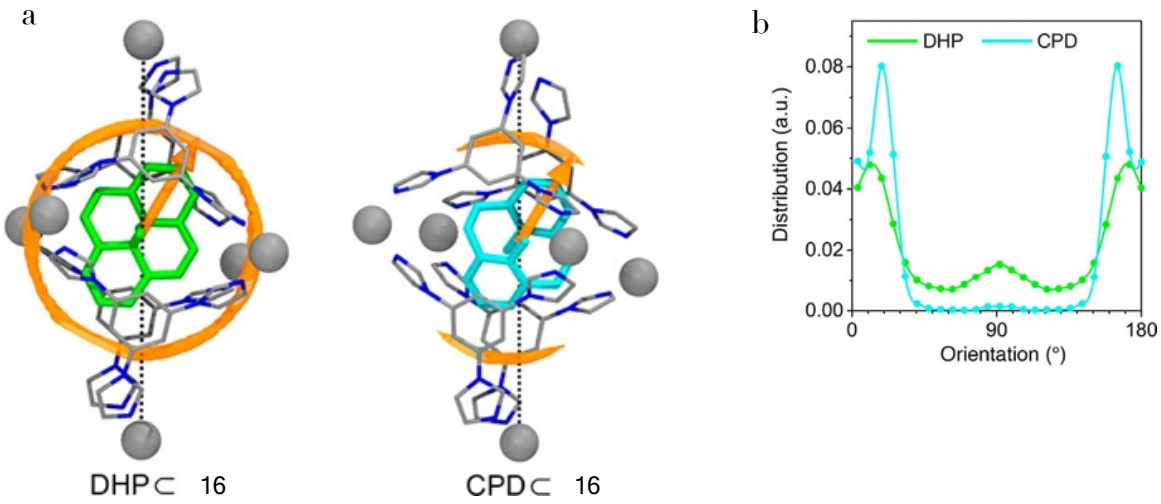

Figure 71 (a) Side-views of DHP⊂**16** and CPD⊂**16** with isosurfaces of the density of guest's orientation (shown in orange). (b) Normalized distributions of guest orientations within DHP⊂**16** and CPD⊂**16**. Adapted with permission[153].

From these results it was possible to learn more about the disposition and the dynamic of DHP and CPD within the cavity of cage 16. In the reported figure the orange arrows represent the vertical axes of DHP and CPD (i.e., the line connecting the 2 more separated carbon atoms). As such, a larger orange area implies a higher guest mobility in the cage cavity during the MD equilibration time.
Moreover, DHP results to be free to perform a complete rotation inside the cage (symbolized by the complete orange circle) in a gyroscope like way[158 161] such that the methyl units interact stably with the equatorial region of 16 .
This finding is not surprising considering the molecular structure of DHP, in fact, in this case the orthogonal disposition of the methyl groups causes the orientation of the planar aromatic part exactly along the longer axis of the cage (symbolized by the black dotted line connecting the two Pd atoms).
Contrarily, the bulkier CPD shows a remarkably higher limitation in its movements being mostly fixed in an almost vertical orientation (~30° of the long axis of the cage). This restriction is caused by the interactions between the cage panel and CPD methyl groups, as such, any rotation of the guests is limited.
Such data are also confirmed by the NOESY spectrum of CPD⊂16 which presents an interaction of cage 16 with all the protons of CPD.
Upon the calculation of the distribution of the guests orientations, the most stable disposition of DHP and CPD were individuated. For this calculation the angle between the cage axis (black dotted line) and the guest axis (orange arrow) was considered.
Regarding DHP it shows two maxima at 10° and 170° confirm the favored vertical orientation, however, a minor maximum at 90 indicates that a horizontal one is also possible.
Interestingly, these data are fully confirmed at the solid state by the X-ray analysis in which two main isomers were isolated. Furthermore, the results obtained for CPD suggest that the guest is almost fixed in its vertical disposition and any rotation is prevented.

4.6 Fatigue resistance evaluation

Another important point in the study of DHP⊂16 is the fatigue resistance parameter. In fact, as the main hypothesis describing DHP photoisomerization involves a radical intermediate[139], the fatigue resistance was investigated in order to compare free and encapsulated DHP. Since this parameter could be influenced by the occurrence of oxidative radical-radical decomposition processes, it was interesting to study the possible stabilizing role of the cage as a molecular host. In the next figure the fatigue resistance over 10 isomerization cycles is reported both for free DHP and for the complex.

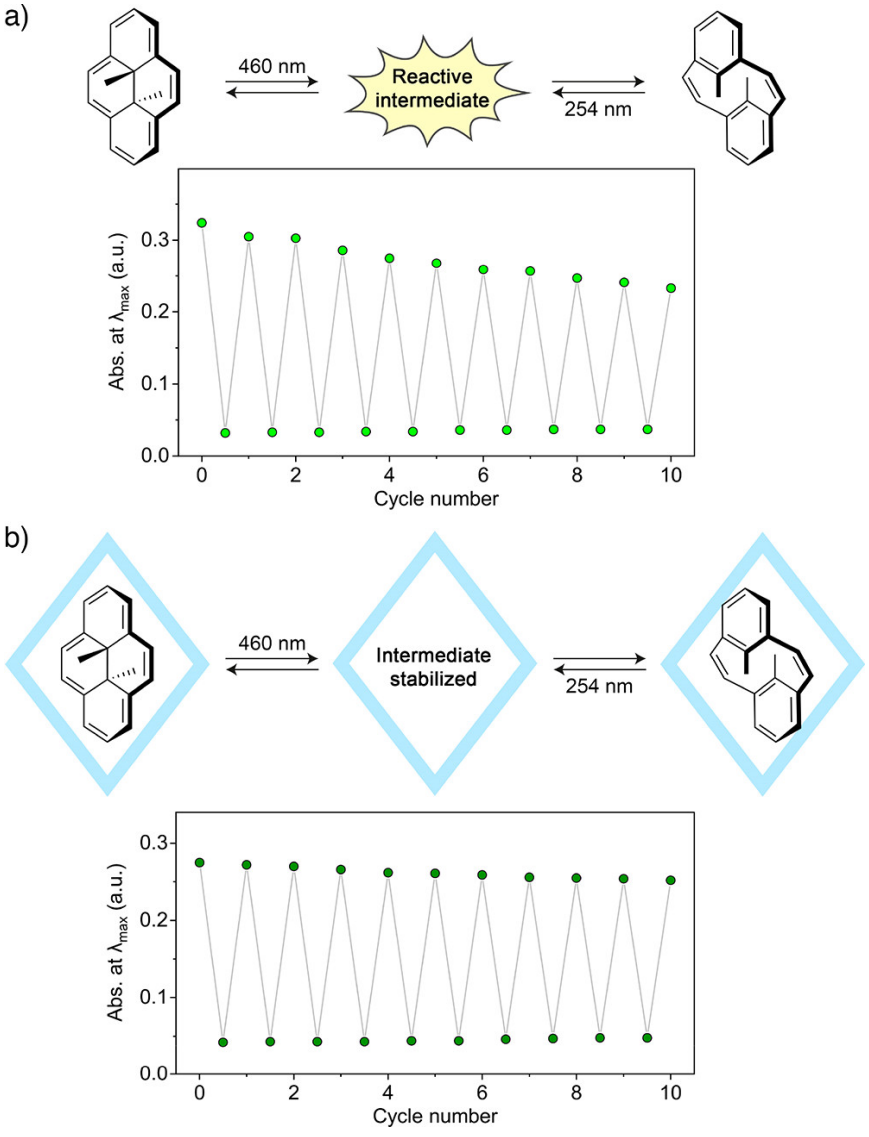

Figure 72 (a) Fatigue resistance of free DHP in pentane solution over 10 switching cycles. (b) Improved fatigue resistance of DHP⊂**16** in water over 10 switching cycles. Deoxygenated solvents were used. In each cycle, the samples were exposed to 10 min of blue light (λ = 460 nm) followed by 10 min of UV light (λ = 254 nm). Adapted with permission[153].

Since DHP is insoluble in water, the behavior of encapsulated DHP was compared to free DHP dissolved in pentane. Moreover, pentane is particularly suitable for this experiment because it is inert under these conditions and usually does not readily react with radical species.
For the comparison, two solutions of DHP⊂16 and DHP in pentane (at concentration in the μM range) were prepared and subsequently deoxygenated by bubbling nitrogen to minimize the contribute of oxygen.
The solutions were then irradiated in parallel, under the same irradiation conditions with blue light at 460 nm for 10 min and then with UV light at 254 nm, the spectral variations were monitored with UV-vis spectroscopy.
The data show a final lost in the DHP absorption intensity of 28% for free DHP (Figure x a) and of 8% for DHP⊂16.
Remarkably, these results confirm the hypothesis of the protecting role of the cage which not only minimize the contact of the guest with O_2 but also prevents the fatigue due to bimolecular radical-radical reactions.
To further investigate the fatigue resistance of DHP⊂16 the same experiment was performed as well in not deoxygenated water; in this case the observed fatigue was 13%.
The higher intensity lost is predictable considering the large open window present in the cage structure which can explain the access of oxygen.
Significantly, also in these conditions the cycling performances of complexed DHP remain better with the respect to the free DHP.

4.7 Conclusions and future perspectives

In this study the formation of an inclusion complex in aqueous solutions was achieved for both guest isomers, DHP and CPD.
The inclusion complex characterization was carefully conducted in solution by means of mono and bi-dimensional ^{1}H NMR spectroscopy which allowed to learn more about the host-guest interactions and the stoichiometry of the complex. UV-vis spectroscopy was also largely employed to monitor the guest isomerization processes.
Significantly, the cage resulted to be flexible and to readily adapt upon the guest isomerization. In fact, the guest photoswitching could be reversibly conducted in both directions obtaining stable PSSs and comparable isomerization kinetics with the respect to the free guest dissolved in organic solvents.
The complex was analyzed at the solid state as well, in fact, upon slow evaporation of water the crystal structure correspondent to DHP⊂16 was obtained. Interestingly, the X-ray data were coherent with the ^{1}H-NOESY observations confirming the hypothesis of a dynamic behavior of DHP inside the cavity of the cage.
Conformational free-energy surfaces and MD simulations were carefully analyzed and compared to previous studied inclusion complexes. The data were found to be interestingly in line with what observed experimentally both in solution and at the solid state.
Moreover, the encapsulation of DHP within cage 16 provided a significant stabilizing effect for the intermediate radical species involved in this isomerization.

The cage was observed to have an important role as it prevents bimolecular events and oxidative processes. Consequently, a reduction of the fatigue resistance over many switching cycles was achieved.
Importantly, the cage prevents DHP degradation but at the same time does not affect its photoswitching performances. The observed stabilization is significant also considering the relatively open structure of the cage framework which was found to allow rapid exchange kinetics for comparable guests (sulfonated MC).
Confined environment, has been usually employed to accelerate processes or to isolate transient species[162,163,164]. Interestingly, in this work a novel strategy is presented in fact, in this case, the final objective is to stabilize a reactive intermediate and to obtain a consequent improvement of the reaction yield.
Despite this system is limited to water, which favors the formation of the complex on account of the hydrophobic effect; in theory such approach can be also adopted in confined environments in different solvents. In this way, is also possible to minimize the generation of side products which often derives from reactive intermediates.

5 MATERIALS AND METHODS

5.1 Compounds and general methods

Commercial compounds and solvents were employed as received. Compounds 1-10 were synthetized and characterized via NMR by the group members Dr. Jessica Groppi and Dr. Stefano Corrà. Compounds 13 and 14 were synthetized and characterized via NMR by Dr. Jessica Groppi. Compound 15 were synthetized and characterized via NMR in the research group of Prof. P.G. Cozzi (University of Bologna). Cage 16 reported in chapter 4 was synthetized according to an already reported procedure[153] while the DHP was synthetized and characterized via NMR by the group of Prof. Joakim Andréasson (University of Chalmers).

5.2 UV-vis Spectroscopy

Absorption spectra were recorded with a cary 300 and with a Cary 50Bio (Varian) spectrophotometers, on air equilibrated solutions at room temperature if not otherwise stated. Circular dichroism spectra were recorded with a JASCO Type J-820 spectropolarimeter.
Regular 1 cm or 1 mm optical pathlength quartz cells were employed. For the determination of absorption changes upon association, specific spectrophotometric cells endowed with two sections separated by a quartz wall were used for a precise determination of the sum of the absorption spectra of the separated components (unmixed solutions) and the absorption spectrum of their complex (mixed solutions).
Emission spectra were recorded with a FS5 Edinburgh spectrofluorometer.
Irradiations experiments were performed with a Hanau Q400 or Helios Italquartz Polymer 125 medium pressure Hg lamp (respectively 150 and 125 W).
The flux of incident photons, calculated by ferrioxalate actinometry in its micro version[165], was usually 1.0 Å x 10^{-7} Einstein min^{-1} at 365 nm, and 2.4Å x 10^{-7} Einstein min^{-1} at 436 nm.
Kinetic and titration experiments were elaborated by means of the global analysis software SPECFIT[166]. The fittings were performed according to a mixed order model comprising a second order threading or association and first order dethreading or dissociation (equation 1).

$$\text{Host} + \text{Guest} \leftrightarrows [\text{Host} \supset \text{Guest}] \qquad 1$$

For photoirradiation experiments reported in section 2.3, a Prizmatix Mic-LED 460 nm (~1.0 $mW.cm^{-2}$ at the sample) light-emitting diode (LED) was used as a blue light source, and a UVGL-25 Compact UV Lamp (~0.7 $mW.cm^{-2}$ at the sample) by UVP (4-Watt) as a UV light source.

5.3 Other techniques

^{1}H NMR spectra were recorder on a 300 MHz spectrometer (Bruker Advance III-300), a 500 MHz spectrometer (Bruker Advance III HD-500), and a 400 MHz spectrometer (Bruker Advance III-400), respectively. ^{1}H DOSY, ^{1}H ^{1}H COSY, and ^{1}H ^{1}H NOESY spectra were

recorded on a 500 MHz spectrometer (Bruker Avance III HD 500). Unless stated otherwise, all NMR experiments were performed at a constant temperature of 298 K. ^{1}H chemical shifts (δH) are expressed in parts-per-million (ppm) and reported relative to residual solvent resonances (1.94 ppm for CD_3CN, 2.51 ppm for $(CD_3)_2SO$, 4.79 ppm for D_2O, and 7.26 ppm for $CDCl_3$). ^{1}H DOSY NMR spectra were recorded with temperature and gradient settings that were calibrated prior to the measurements. The diffusion coefficient of the solvent was employed as a calibration standard.

Activities report

First year

- Attendance of the "IP management" course.
- Attendance of the "Scientific writing" course.
- Participation in the conference "Giornate della chimica dell'Emilia Romagna" with a poster contribution (Bologna, 1-12-17).
- Participation in the school of electrochemistry "Enerchem" with a poster and an oral contributions (Firenze, 20/24-2-18).
- Participation in the conference "Roma Supramol 2018 giornata dei dottorandi" with an oral presentation (Roma, 25/27-05-18).
- Participation in the conference "Congresso nazionale di Chimica inorganica" with an oral presentation (Bologna, 10/13-11-18).

Second year

- Attendance of the "Complementi di chimica inorganica"course.
- Attendance of the "Complementi di chimica fisica"course.
- Participation in the school "VIII Ciamician Photochemistry School: From Fundamentals to Applications" (Bologna, 10/14-06-19).
- Participation in the conference "UK-IT Joint Meeting on Photochemistry 2019" with an oral presentation (Lipari, 24/26-06-19).
- Participation in the conference "Gordon Research Conference on Photochemistry" with a poster contribution (Easton USA, 14/19-07-19).

Third year

- Participation in the "Virtual Conference on Molecular Capsules: from Design to Application" (22/23-03-20).
- Visiting period abroad at the Weizmann institute of science (Israel) from September 2019 to February 2020 in the group of Professor Rafal Klajn (Organic chemistry department).

List of publications

- M. Baroncini, M. Canton, L. Casimiro, S. Corra, J. Groppi, M. La Rosa, S. Silvi and A. Credi, *Eur. J. Inorg. Chem.*, 2018, **2018**, 4589 4603.

- J. Groppi, L. Casimiro, M. Canton, S. Corra, M. Jafari-Nasab, G. Tabacchi, L. Cavallo, M. Baroncini, S. Silvi, E. Fois and A. Credi, *Angew. Chemie Int. Ed.*, 2020, **59**, 14825 14834.
- M. Canton, A. B. Grommet, L. Pesce, J. Gemen, S. Li, Y. Diskin-Posner, A. Credi, G. M. Pavan, J. Andreasson and R. Klajn, *J. Am. Chem. Soc.*, 2020, **142**, 14557 14565.

REFERENCES

1. Feynman, R. P. There's plenty of room at the bottom. *Eng. Sci.* **23**, 22–36 (1960).
2. Balzani, V., Credi, A. & Venturi, M. The Bottom-Up Approach to Molecular-Level Devices and Machines. *Chem. - A Eur. J.* **8**, 5524–5532 (2002).
3. Lehn, J. M. From supramolecular chemistry towards constitutional dynamic chemistry and adaptive chemistry. *Chem. Soc. Rev.* **36**, 151–160 (2007).
4. Goodsell, D. S. *The machinery of life*. (Copernicus Books, 2009).
5. Cram, D. J. & Cram, J. M. Host-Guest Chemistry. *Science* vol. 183 803–809.
6. Pedersen, C. J. Cyclic Polyethers and their Complexes with Metal Salts. *Journal of the American Chemical Society* vol. 89 2495–2496 (1967).
7. Suzuki, K. *et al.* Design and Synthesis of Calcium and Magnesium Ionophores Based on Double-Armed Diazacrown Ether Compounds and Their Application to an Ion Sensing Component for an Ion-Selective Electrode. *Anal. Chem.* **67**, 324–334 (1995).
8. Olsen, G., Ulstrup, J. & Chi, Q. Crown-Ether Derived Graphene Hybrid Composite for Membrane-Free Potentiometric Sensing of Alkali Metal Ions. *ACS Appl. Mater. Interfaces* **8**, 37–41 (2016).
9. Dave, S. R., Kaur, H. & Menon, S. K. Selective solid-phase extraction of rare earth elements by the chemically modified Amberlite XAD-4 resin with azacrown ether. *React. Funct. Polym.* **70**, 692–698 (2010).
10. Schmidt, B. V. K. J. & Barner-Kowollik, C. Dynamic Macromolecular Material Design—The Versatility of Cyclodextrin-Based Host–Guest Chemistry. *Angewandte Chemie - International Edition* vol. 56 8350–8369 (2017).
11. Zhou, J., Chemistry, H. R.-P. & 2010, undefined. Cyclodextrin functionalized polymers as drug delivery systems. *pubs.rsc.org*.
12. Uekama, K., Hirayama, F. & Irie, T. *Cyclodextrin Drug Carrier Systems*. *ACS Publications* https://pubs.acs.org/sharingguidelines (1998).
13. Shuang, Y., Liao, Y., Wang, H., Wang, Y. & Li, L. Preparation and evaluation of a triazole-bridged *bis* (□-cyclodextrin) bonded chiral stationary phase for HPLC. *Chirality* **32**, 168–184 (2020).
14. Ménand, M. *et al.* Solid-State Hierarchical Cyclodextrin-Based Supramolecular Polymer Constructed by Primary, Secondary, and Tertiary Azido Interactions. *Angew. Chemie* **126**, 7366–7370 (2014).
15. Tamesue, S., Takashima, Y., Yamaguchi, H., Shinkai, S. & Harada, A. Photoswitchable supramolecular hydrogels formed by cyclodextrins and azobenzene polymers. *Angew. Chemie - Int. Ed.* **49**, 7461–7464 (2010).
16. Jeon, W. S. *et al.* Complexation of ferrocene derivatives by the cucurbit[7]uril host: A comparative study of the cucurbituril and cyclodextrin host families. *J. Am. Chem. Soc.* **127**, 12984–12989 (2005).
17. Lagona, J., Mukhopadhyay, P., Chakrabarti, S. & Isaacs, L. The cucurbit[n]uril family. *Angewandte Chemie - International Edition* vol. 44 4844–4870 (2005).
18. Kim, K. *et al.* Functionalized cucurbiturils and their applications. *Chem. Soc. Rev.* **36**, 267–279 (2007).
19. Böhmer, V. Calixarenes, Macrocycles with (Almost) Unlimited Possibilities.

Angewandte Chemie International Edition in English vol. 34 713–745 (1995).
20. Arduini, A. *et al.* Towards controlling the threading direction of a calix[6]arene wheel by using nonsymmetric axles. *Chem. - A Eur. J.* **15**, 3230–3242 (2009).
21. Baldini, L., Casnati, A. & Sansone, F. Multivalent and Multifunctional Calixarenes in Bionanotechnology. *European Journal of Organic Chemistry* vol. 2020 5056–5069 (2020).
22. Cram, D. J. Molecular container compounds. *Nature* vol. 356 29–36 (1992).
23. Vriezema, D. M. *et al.* Self-assembled nanoreactors. *Chemical Reviews* vol. 105 1445–1489 (2005).
24. Fujita, M. *et al.* Self-assembly of ten molecules into nanometre-sized organic host frameworks. *Nature* **378**, 469–471 (1995).
25. Samanta, D. *et al.* Reversible chromism of spiropyran in the cavity of a flexible coordination cage. *Nat. Commun.* **9**, 1–9 (2018).
26. Yoshizawa, M., Tamura, M. & Fujita, M. AND/OR bimolecular recognition. *J. Am. Chem. Soc.* **126**, 6846–6847 (2004).
27. Ibukuro, F., Kusukawa, T. & Fujita, M. A thermally switchable molecular lock. Guest-templated synthesis of a kinetically stable nanosized cage [23]. *Journal of the American Chemical Society* vol. 120 8561–8562 (1998).
28. Wyler, R., de Mendoza, J. & Rebek, J. A Synthetic Cavity Assembles Through Self-Complementary Hydrogen Bonds. *Angew. Chemie Int. Ed. English* **32**, 1699–1701 (1993).
29. M Yoshizawa, J. K. M. F. Functional molecular flasks: New properties and reactions within discrete, self-assembled hosts. *Angew. Chem. Int. Ed.* **48**, 3418–3438 (2009).
30. Heinz, T., Rudkevich, D. M. & Rebek, J. Pairwise selection of guests in a cylindrical molecular capsule of nanometre dimensions. *Nature* **394**, 764–766 (1998).
31. Niu, Z., Huang, F. & Gibson, H. W. Supramolecular AA-BB-type linear polymers with relatively high molecular weights via the self-assembly of bis(m -phenylene)-32-crown-10 cryptands and a bisparaquat derivative. *J. Am. Chem. Soc.* **133**, 2836–2839 (2011).
32. Allwood, B. L., Spencer, N., Shahriari-Zavareh, H., Stoddart, J. F. & Williams, D. J. Complexation of Paraquat by a bisparaphenylene-34-crown-10 derivative. *J. Chem. Soc. Chem. Commun.* 1064–1066 (1987) doi:10.1039/C39870001064.
33. Song, N. *et al.* Stimuli-responsive blue fluorescent supramolecular polymers based on a pillar[5]arene tetramer. *Chem. Commun.* **50**, 8231–8234 (2014).
34. Schierbaum, K. D. *et al.* Molecular recognition by self-assembled monolayers of cavitand receptors. *Science (80-.).* **265**, 1413–1415 (1994).
35. Nishioka, Y., Yamaguchi, T., Yoshizawa, M. & Fujita, M. Unusual [2+4] and [2+2] cycloadditions of arenes in the confined cavity of self-assembled cages. *J. Am. Chem. Soc.* **129**, 7000–7001 (2007).
36. Kang, J. & Rebek, J. Acceleration of a Diels-Alder reaction by a self-assembled molecular capsule. *Nature* **385**, 50–52 (1997).
37. Taguchi, T., Isozaki, K. & Miki, K. Enhanced catalytic activity of self-assembled-monolayer-capped gold nanoparticles. *Adv. Mater.* **24**, 6462–6467 (2012).
38. Chen, S. *et al.* A metal-organic cage incorporating multiple light harvesting and

catalytic centres for photochemical hydrogen production. *nature.com*.
39. Feng, X. *et al.* Metal-Organic Framework Stabilizes a Low-Coordinate Iridium Complex for Catalytic Methane Borylation. *J. Am. Chem. Soc.* **141**, 11196 11203 (2019).
40. Roberts, J. M. *et al.* Urea metal-organic frameworks as effective and size-selective hydrogen-bond catalysts. *J. Am. Chem. Soc.* **134**, 3334 3337 (2012).
41. Sawano, T. *et al.* Metal-Organic Frameworks Stabilize Mono(phosphine)-Metal Complexes for Broad-Scope Catalytic Reactions. *J. Am. Chem. Soc.* **138**, 9783 9786 (2016).
42. Wu, S. *et al.* Supramolecular Nanotubules as a Catalytic Regulator for Palladium Cations: Applications in Selective Catalysis. *Angew. Chemie - Int. Ed.* **56**, 11511 11514 (2017).
43. Wang, Q.-Q. *et al.* Self-assembled nanospheres with multiple endohedral binding sites pre-organize catalysts and substrates for highly efficient reactions. *nature.com* 11 (2016) doi:10.1038/NCHEM.2425.
44. Chu, Z. *et al.* Supramolecular Control of Azobenzene Switching on Nanoparticles. *J. Am. Chem. Soc.* **141**, 1949 1960 (2019).
45. Sato, S. Minimal nucleotide duplex formation in water through enclathration in self-assembled hosts. *nature.com* (2009) doi:10.1038/nchem.100.
46. Cram, D. J., Tanner, M. E. & Thomas, R. The Taming of Cyclobutadiene. *Angew. Chemie Int. Ed. English* **30**, 1024 1027 (1991).
47. Mal, P., Breiner, B., Rissanen, K., Science, J. N.- & 2009, undefined. White phosphorus is air-stable within a self-assembled tetrahedral capsule. *science.sciencemag.org* doi:10.1126/science.1108944.
48. Pluth, M. D., Bergman, R. G. & Raymond, K. H. Acid catalysis in basic solution: A supramolecular host promotes orthoformate hydrolysis. *Science (80-.).* **316**, 85 88 (2007).
49. Kaphan, D. M., Levin, M. D., Bergman, R. G., Raymond, K. N. & Toste, F. D. A supramolecular microenvironment strategy for transition metal catalysis. *Science (80-.).* **350**, 1235 1238 (2015).
50. Pluth, M. D., Bergman, R. G. & Raymond, K. N. Supramolecular catalysis of orthoformate hydrolysis in basic solution: An enzyme-like mechanism. *J. Am. Chem. Soc.* **130**, 11423 11429 (2008).
51. Juríček, M. *et al.* Induced-fit catalysis of corannulene bowl-to-bowl inversion. *Nat. Chem.* **6**, 222 228 (2014).
52. De Oteyza, D. G. *et al.* Direct imaging of covalent bond structure in single-molecule chemical reactions. *Science (80-.).* **340**, 1434 1437 (2013).
53. Lee, T. *et al.* Chemistry inside molecular containers in the gas phase. *nature.com*.
54. Tu, M. *et al.* Reversible Optical Writing and Data Storage in an Anthracene-Loaded Metal Organic Framework. *Angew. Chemie Int. Ed.* **58**, 2423 2427 (2019).
55. Vidal, D., Olivo, G. & Costas, M. Controlling Selectivity in Aliphatic C–H Oxidation through Supramolecular Recognition. *Chem. - A Eur. J.* **24**, 5042 5054 (2018).
56. Mochizuki, S., Kitao, T. & Uemura, T. Controlled polymerizations using metal-organic frameworks. *Chemical Communications* vol. 54 11843 11856 (2018).
57. Jana, A. *et al.* Functionalised tetrathiafulvalene- (TTF-) macrocycles: recent trends

in applied supramolecular chemistry. *Chemical Society Reviews* vol. 47 5614–5645 (2018).
58. Klosterman, J. K., Yamauchi, Y. & Fujita, M. Engineering discrete stacks of aromatic molecules. *Chemical Society Reviews* vol. 38 1714–1725 (2009).
59. Biedermann, F., Elmalem, E., Ghosh, I., Nau, W. M. & Scherman, O. A. Strongly fluorescent, switchable perylene bis(diimide) host-guest complexes with cucurbit[8]uril in water. *Angew. Chemie - Int. Ed.* **51**, 7739–7743 (2012).
60. Balzani, V., Credi, A., Ferrer, B., Silvi, S. & Venturi, M. Articial molecular motors and machines: Design principles and protype systems. *Topics in Current Chemistry* vol. 262 1–27 (2005).
61. Schliwa, M. & Woehlke, G. Molecular motors. *Nature* vol. 422 759–765 (2003).
62. Sauvage, J.-P. & Dietrich-Buchecker, C. *Molecular Catenanes, Rotaxanes and Knots Edited by*.
63. Denis, M. & Goldup, S. M. The active template approach to interlocked molecules. *Nature Reviews Chemistry* vol. 1 1–17 (2017).
64. Baroncini, M. *et al.* Photoactive Molecular-Based Devices, Machines and Materials: Recent Advances. *Eur. J. Inorg. Chem.* **2018**, 4589–4603 (2018).
65. Balzani, V. *et al.* Switching of pseudorotaxanes and catenanes incorporating a tetrathiafulvalene unit by redox and chemical inputs. *J. Org. Chem.* **65**, 1924–1936 (2000).
66. Armaroli, N. *et al.* Rotaxanes incorporating two different coordinating units in their thread: Synthesis and electrochemically and photochemically induced molecular motions. *J. Am. Chem. Soc.* **121**, 4397–4408 (1999).
67. Badjic, J. D. *et al.* Operating molecular elevators. *J. Am. Chem. Soc.* **128**, 1489–1499 (2006).
68. Parisi, G. Brownian motion. *Nature* vol. 433 221 (2005).
69. Goodsell, D. S. *The Machinery of Life*. *The Machinery of Life* (Springer New York, 2009). doi:10.1007/978-0-387-84925-6.
70. Schill, G. *et al. A Molecular Shuttle*. *J. Chem. Soc., Perkin Trans. 1* vol. 113 https://pubs.acs.org/sharingguidelines (1991).
71. Bacljić, J. D., Balzani, V., Credi, A., Silvi, S. & Stoddart, J. F. A Molecular Elevator. *Science (80-.).* **303**, 1845–1849 (2004).
72. Koumura, N., Zijistra, R. W. J., Van Delden, R. A., Harada, N. & Feringa, B. L. Light-driven monodirectional molecular rotor. *Nature* **401**, 152–155 (1999).
73. Feringa, B. & Browne, W. Molecular switches. (2011).
74. Astumian, R. D. Design principles for Brownian molecular machines: How to swim in molasses and walk in a hurricane. *Physical Chemistry Chemical Physics* vol. 9 5067–5083 (2007).
75. Baroncini, M., Silvi, S. & Credi, A. Photo- And Redox-Driven Artificial Molecular Motors. *Chemical Reviews* vol. 120 200–268 (2020).
76. Corra, S., Curcio, M., Baroncini, M., Silvi, S. & Credi, A. Photoactivated Artificial Molecular Machines that Can Perform Tasks. *Adv. Mater.* **32**, 1906064 (2020).
77. Aprahamian, I. The Future of Molecular Machines. *ACS Cent. Sci.* **6**, 347–358 (2020).
78. Jones, R. Soft machines: nanotechnology and life. (2004).
79. Schäfer, C. *et al.* An Artificial Molecular Transporter. *ChemistryOpen* **5**, 120–124

(2016).
80. Chen, J., Wezenberg, S. J. & Feringa, B. L. Intramolecular transport of small-molecule cargo in a nanoscale device operated by light. *Chem. Commun.* **52**, 6765 6768 (2016).
81. Qiu, Y., Feng, Y., Guo, Q. H., Astumian, R. D. & Stoddart, J. F. Pumps through the Ages. *Chem* vol. 6 1952 1977 (2020).
82. Morth, J. P. *et al.* Crystal structure of the sodium-potassium pump. *Nature* **450**, 1043 1049 (2007).
83. McTernan, C. T., De Bo, G. & Leigh, D. A. A Track-Based Molecular Synthesizer that Builds a Single-Sequence Oligomer through Iterative Carbon-Carbon Bond Formation. *Chem* **6**, 2964 2973 (2020).
84. Ragazzon, G., Baroncini, M., Silvi, S., Venturi, M. & Credi, A. Light-powered autonomous and directional molecular motion of a dissipative self-assembling system. *Nat. Nanotechnol.* **10**, 70 75 (2015).
85. Qiu, Y. *et al.* A precise polyrotaxane synthesizer. *Science (80-.).* **368**, 1247 1253 (2020).
86. Astumian, R. D. Kinetic asymmetry allows macromolecular catalysts to drive an information ratchet. *Nat. Commun.* **10**, 1 14 (2019).
87. García-López, V. *et al.* Molecular machines open cell membranes. *Nature* **548**, 567 572 (2017).
88. Chen, J. *et al.* Artificial muscle-like function from hierarchical supramolecular assembly of photoresponsive molecular motors. *Nat. Chem.* **10**, 132 138 (2018).
89. Iwaso, K., Takashima, Y. & Harada, A. Fast response dry-type artificial molecular muscles with [c2]daisy chains. *Nat. Chem.* **8**, 625 632 (2016).
90. Li, Q. *et al.* Macroscopic contraction of a gel induced by the integrated motion of light-driven molecular motors. *Nat. Nanotechnol.* **10**, 161 165 (2015).
91. Dattler, D. *et al.* Design of Collective Motions from Synthetic Molecular Switches, Rotors, and Motors. *Chemical Reviews* vol. 120 310 433 (2020).
92. Foy, J. T. *et al.* Dual-light control of nanomachines that integrate motor and modulator subunits. *Nat. Nanotechnol.* **12**, 540 545 (2017).
93. Wang, J. & Feringa, B. L. Dynamic control of chiral space in a catalytic asymmetric reaction using a molecular motor. *Science (80-.).* **331**, 1429 1432 (2011).
94. Vlatkovic, M., Bernardi, L., Otten, E. & Feringa, B. L. Dual stereocontrol over the Henry reaction using a light- and heat-triggered organocatalyst. *Chem. Commun.* **50**, 7773 7775 (2014).
95. Pizzolato, S. F. *et al.* Central-to-Helical-to-Axial-to-Central Transfer of Chirality with a Photoresponsive Catalyst. *J. Am. Chem. Soc.* **140**, 17278 17289 (2018).
96. Štacko, P. *et al.* Locked synchronous rotor motion in a molecular motor. *Science (80-.).* **356**, 964 968 (2017).
97. Uhl, E., Thumser, S., Mayer, P. & Dube, H. Transmission of Unidirectional Molecular Motor Rotation to a Remote Biaryl Axis. *Angew. Chemie Int. Ed.* **57**, 11064 11068 (2018).
98. Berná, J. *et al.* Macroscopic transport by synthetic molecular machines. *Nat. Mater.* **4**, 704 710 (2005).
99. Ryabchun, A., Li, Q., Lancia, F., Aprahamian, I. & Katsonis, N. Shape-Persistent Actuators from Hydrazone Photoswitches. *J. Am. Chem. Soc.* **141**, 1196 1200 (2019).

100. Eelkema, R. *et al.* Nanomotor rotates microscale objects. *Nature* **440**, 163 (2006).
101. Gadsby, D. C. Ion channels versus ion pumps: The principal difference, in principle. *Nature Reviews Molecular Cell Biology* vol. 10 344 352 (2009).
102. Astumian, R. D. Microscopic reversibility as the organizing principle of molecular machines. *Nature Nanotechnology* vol. 7 684 688 (2012).
103. Astumian, R. D. Thermodynamics and kinetics of a Brownian motor. *Science (80-.).* **276**, 917 922 (1997).
104. Cheng, C., McGonigal, P. R., Stoddart, J. F. & Astumian, R. D. Design and Synthesis of Nonequilibrium Systems. *ACS Nano* vol. 9 8672 8688 (2015).
105. Astumian, R. D. *et al.* Non-equilibrium kinetics and trajectory thermodynamics of synthetic molecular pumps. *Materials Chemistry Frontiers* vol. 4 1304 1314 (2020).
106. Casimiro, L. *et al.* Photochemical investigation of cyanoazobenzene derivatives as components of artificial supramolecular pumps. *Photochem. Photobiol. Sci.* **17**, 734 740 (2018).
107. Groppi, J. *et al.* Precision Molecular Threading/Dethreading. *Angew. Chemie Int. Ed.* anie.202003064 (2020) doi:10.1002/anie.202003064.
108. Ashton, P. R. *et al.* Dialkylammonium Ion/Crown Ether Complexes: The Forerunners of a New Family of Interlocked Molecules. *Angew. Chemie Int. Ed. English* **34**, 1865 1869 (1995).
109. Ashton, P. R. *et al.* Hammett correlations "beyond the molecule." *J. Chem. Soc. Perkin Trans. 2* 2117 2128 (1998) doi:10.1039/a802406e.
110. Raymo, F. M., Houk, K. N. & Stoddart, J. F. The mechanism of the slippage approach to rotaxanes. Origin of the "all- or-nothing" substituent effect. *J. Am. Chem. Soc.* **120**, 9318 9322 (1998).
111. Baroncini, M., Silvi, S., Venturi, M. & Credi, A. Photoactivated directionally controlled transit of a non-symmetric molecular axle through a macrocycle. *Angew. Chemie - Int. Ed.* **51**, 4223 4226 (2012).
112. Evans, N. H. Chiral Catenanes and Rotaxanes: Fundamentals and Emerging Applications. *Chem. - A Eur. J.* **24**, 3101 3112 (2018).
113. Yamamoto, C., Okamoto, Y., Schmidt, T., Jager, R. & Vogtle, F. Enantiomeric resolution of cycloenantiomeric rotaxane, topologically chiral catenane, and Pretzel-shaped molecules: Observation of pronounced circular dichroism. *J. Am. Chem. Soc.* **119**, 10547 10548 (1997).
114. Kameta, N., Hiratani, K. & Nagawa, Y. A novel synthesis of chiral rotaxanes via covalent bond formation. *Chem. Commun.* **4**, 466 467 (2004).
115. Bordoli, R. J. & Goldup, S. M. An efficient approach to mechanically planar chiral rotaxanes. *J. Am. Chem. Soc.* **136**, 4817 4820 (2014).
116. Jinks, M. A. *et al.* Stereoselective Synthesis of Mechanically Planar Chiral Rotaxanes. *Angew. Chemie - Int. Ed.* **57**, 14806 14810 (2018).
117. Kameta, N., Nagawa, Y., Karikomi, M. & Hiratani, K. Chiral sensing for amino acid derivative based on a [2]rotaxane composed of an asymmetric rotor and an asymmetric axle. *Chem. Commun.* 3714 3716 (2006) doi:10.1039/b607251h.
118. Lim, J. Y. C., Marques, I., Félix, V. & Beer, P. D. Enantioselective Anion Recognition by Chiral Halogen-Bonding [2]Rotaxanes. *J. Am. Chem. Soc.* **139**, 12228 12239 (2017).
119. Corra, S. *et al.* Chemical On/Off Switching of Mechanically Planar Chirality and

Chiral Anion Recognition in a [2]Rotaxane Molecular Shuttle. *J. Am. Chem. Soc.* **141**, 9129 9133 (2019).
120. Ishiwari, F., Nakazono, K., Koyama, Y. & Takata, T. Induction of Single-Handed Helicity of Polyacetylenes Using Mechanically Chiral Rotaxanes as Chiral Sources. *Angew. Chemie - Int. Ed.* **56**, 14858 14862 (2017).
121. Blanco, V., Leigh, D. A. & Marcos, V. Artificial switchable catalysts. *Chem. Soc. Rev.* **44**, 5341 5370 (2015).
122. Traut, T. *Allosteric regulatory enzymes*. *Allosteric Regulatory Enzymes* (Springer US, 2008). doi:10.1007/978-0-387-72891-9.
123. Blanco, V., Carlone, A., Hänni, K. D., Leigh, D. A. & Lewandowski, B. A rotaxane-based switchable organocatalyst. *Angew. Chemie - Int. Ed.* **51**, 5166 5169 (2012).
124. Blanco, V., Leigh, D. A., Marcos, V., Morales-Serna, J. A. & Nussbaumer, A. L. A switchable [2]rotaxane asymmetric organocatalyst that utilizes an acyclic chiral secondary amine. *J. Am. Chem. Soc.* **136**, 4905 4908 (2014).
125. Beswick, J. *et al.* Selecting reactions and reactants using a switchable rotaxane organocatalyst with two different active sites. *Chem. Sci.* **6**, 140 143 (2015).
126. Wiester, M. J., Ulmann, P. A. & Mirkin, C. A. Enzyme mimics based upon supramolecular coordination chemistry. *Angewandte Chemie - International Edition* vol. 50 114 137 (2011).
127. Yoon, H. J., Kuwabara, J., Kim, J. H. & Mirkin, C. A. Allosteric supramolecular triple-layer catalysts. *Science (80-.).* **330**, 66 69 (2010).
128. Masar, M. S. *et al.* Allosterically Regulated Supramolecular Catalysis of Acyl Transfer Reactions for Signal Amplification and Detection of Small Molecules. (2007) doi:10.1021/ja071516.
129. Gianneschi, N. C., Cho, S.-H., Nguyen, S. T. & Mirkin, C. A. Reversibly Addressing an Allosteric Catalyst In Situ: Catalytic Molecular Tweezers. *Angew. Chemie Int. Ed.* **43**, 5503 5507 (2004).
130. Foy, J. T., Ray, D. & Aprahamian, I. Regulating signal enhancement with coordination-coupled deprotonation of a hydrazone switch. *Chem. Sci.* **6**, 209 213 (2015).
131. De, S., Pramanik, S. & Schmittel, M. A Toggle Nanoswitch Alternately Controlling Two Catalytic Reactions. *Angew. Chemie Int. Ed.* **53**, 14255 14259 (2014).
132. Schmittel, M., De, S. & Pramanik, S. Reversible ON/OFF nanoswitch for organocatalysis: Mimicking the locking and unlocking operation of CaMKII. *Angew. Chemie - Int. Ed.* **51**, 3832 3836 (2012).
133. Kita, M. R. & Miller, A. J. M. Cation-modulated reactivity of iridium hydride pincer-crown ether complexes. *J. Am. Chem. Soc.* **136**, 14519 14529 (2014).
134. Bohne, C. & Mitchell, R. H. Characterization of the photochromism of dihydropyrenes with photophysical techniques. *Journal of Photochemistry and Photobiology C: Photochemistry Reviews* vol. 12 126 137 (2011).
135. Boelke, J. & Hecht, S. Designing Molecular Photoswitches for Soft Materials Applications. *Advanced Optical Materials* vol. 7 (2019).
136. Garmshausen, Y., Klaue, K. & Hecht, S. Dihydropyrene as an Aromaticity Probe for Partially Quinoid Push Pull Systems. *Chempluschem* **82**, 1025 1029 (2017).
137. Ayub, K. *et al.* Suppressing the thermal metacyclophanediene to dihydropyrene isomerization: Synthesis and rearrangement of 8,16-dicyano[2.2]metacyclophane-

1,9-diene and evidence supporting the proposed biradicaloid mechanism. *J. Org. Chem.* **73**, 451–456 (2008).
138. Ayub, K., Li, R., Bohne, C., Williams, R. V. & Mitchell, R. H. Calculation driven synthesis of an excellent dihydropyrene negative photochrome and its photochemical properties. *J. Am. Chem. Soc.* **133**, 4040–4045 (2011).
139. Sheepwash, M. A. L., Mitchell, R. H. & Bohne, C. Mechanistic insights into the photochromism of trans-10b, 10c-dimethyl-10b, 10c-dihydropyrene derivatives. *J. Am. Chem. Soc.* **124**, 4693–4700 (2002).
140. Liddell, P. A. *et al.* Photonic Switching of Photoinduced Electron Transfer in a Dihydropyrene-Porphyrin-Fullerene Molecular Triad. *J. Am. Chem. Soc.* **126**, 4803–4811 (2004).
141. Grommet, A. B., Feller, M. & Klajn, R. Chemical reactivity under nanoconfinement. *Nat. Nanotechnol.* **15**, 256–271 (2020).
142. Yoshizawa, M., Klosterman, J. K. & Fujita, M. Functional molecular flasks: new properties and reactions within discrete, self-assembled hosts. *Angewandte Chemie - International Edition* vol. 48 3418–3438 (2009).
143. Cook, T. R. & Stang, P. J. Recent Developments in the Preparation and Chemistry of Metallacycles and Metallacages via Coordination. *Chemical Reviews* vol. 115 7001–7045 (2015).
144. Sepehrpour, H., Fu, W., Sun, Y. & Stang, P. J. Biomedically Relevant Self-Assembled Metallacycles and Metallacages. *J. Am. Chem. Soc.* **141**, 14005–14020 (2019).
145. Li, H. *et al.* Mechanical bond-induced radical stabilization. *J. Am. Chem. Soc.* **135**, 456–467 (2013).
146. Coles, M. S., Quach, G., Beves, J. E. & Moore, E. G. A Photophysical Study of Sensitization-Initiated Electron Transfer: Insights into the Mechanism of Photoredox Activity. *Angew. Chemie - Int. Ed.* **59**, 9522–9526 (2020).
147. Howlader, P., Mondal, B., Purba, P. C., Zangrando, E. & Mukherjee, P. S. Self-Assembled Pd(II) Barrels as Containers for Transient Merocyanine Form and Reverse Thermochromism of Spiropyran. *J. Am. Chem. Soc.* **140**, 7952–7960 (2018).
148. Mallo, N. *et al.* Photochromic switching behaviour of donor-acceptor Stenhouse adducts in organic solvents. *Chem. Commun.* **52**, 13576–13579 (2016).
149. Rizzuto, F. J., Ramsay, W. J. & Nitschke, J. R. Otherwise Unstable Structures Self-Assemble in the Cavities of Cuboctahedral Coordination Cages. *J. Am. Chem. Soc.* **140**, 11502–11509 (2018).
150. Sawada, T., Yoshizawa, M., Sato, S. & Fujita, M. Minimal nucleotide duplex formation in water through enclathration in self-assembled hosts. *Nat. Chem.* **1**, 53–56 (2009).
151. Yamashina, M., Sei, Y., Akita, M. & Yoshizawa, M. Safe storage of radical initiators within a polyaromatic nanocapsule. *Nat. Commun.* **5**, (2014).
152. Warmuth, R. o-Benzyne: Strained Alkyne or Cumulene? - NMR Characterization in a Molecular Container. *Angew. Chemie (International Ed. English)* **36**, 1347–1350 (1997).
153. Canton, M. *et al.* Improving Fatigue Resistance of Dihydropyrene by Encapsulation within a Coordination Cage. *J. Am. Chem. Soc.* **142**, 14557–14565 (2020).
154. Samanta, D. *et al.* Reversible photoswitching of encapsulated azobenzenes in

water. *Proc. Natl. Acad. Sci. U. S. A.* **115**, 9379–9384 (2018).
155. Logan, S. R. Does a Photochemical Reaction Have a Reaction Order? *J. Chem. Educ.* **74**, 1303 (1997).
156. Hou, L. *et al.* Engineering Optically Switchable Transistors with Improved Performance by Controlling Interactions of Diarylethenes in Polymer Matrices. *J. Am. Chem. Soc.* **142**, 11050–11059 (2020).
157. Pesce, L., Perego, C., Grommet, A. B., Klajn, R. & Pavan, G. M. Molecular Factors Controlling the Isomerization of Azobenzenes in the Cavity of a Flexible Coordination Cage. *J. Am. Chem. Soc.* **142**, 9792–9802 (2020).
158. Commins, P. & Garcia-Garibay, M. A. Photochromic molecular gyroscope with solid state rotational states determined by an azobenzene bridge. *J. Org. Chem.* **79**, 1611–1619 (2014).
159. Khuong, T. A. V., Nunez, J. E., Godinez, C. E. & Garcia-Garibay, M. A. Crystalline molecular machines: A quest toward solid-state dynamics and function. *Acc. Chem. Res.* **39**, 413–422 (2006).
160. Nawara, A. J., Shima, T., Hampel, F. & Gladysz, J. A. Gyroscope-like molecules consisting of PdX2/PtX2 rotators encased in three-spoke stators: Synthesis via alkene metathesis, and facile substitution and demetalation. *J. Am. Chem. Soc.* **128**, 4962–4963 (2006).
161. Lang, G. M. *et al.* Gyroscope-like complexes based on dibridgehead diphosphine cages that are accessed by three-fold intramolecular ring closing metatheses and encase Fe(CO)3, Fe(CO)2(NO)+, and Fe(CO)3(H)+ rotators. *J. Am. Chem. Soc.* **138**, 7649–7663 (2016).
162. Yoshizawa, M., Kusukawa, T., Fujita, M. & Yamaguchi, K. Ship-in-a-bottle synthesis of otherwise labile cyclic trimers of siloxanes in a self-assembled coordination cage [13]. *Journal of the American Chemical Society* vol. 122 6311–6312 (2000).
163. Lee, T. C. *et al.* Chemistry inside molecular containers in the gas phase. *Nat. Chem.* **5**, 376–382 (2013).
164. Iwasawa, T., Hooley, R. J. & Rebek, J. Stabilization of labile carbonyl addition intermediates by a synthetic receptor. *Science (80-.).* **317**, 493–496 (2007).
165. Montalti, M., Credi, A., Prodi, L. & Gandolfi, M. T. *Handbook of Photochemistry*. *Handbook of Photochemistry* (CRC Press, 2006). doi:10.1201/9781420015195.
166. Binstead, R. A. SPECFIT Spectrum Software Associates. 22 (1996).